A Diffuse-Interface Analysis of Two-Phase Thermo-Convective Instabilities

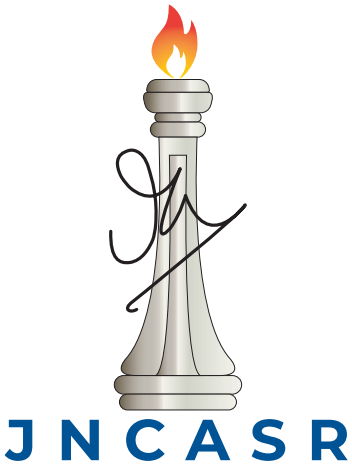

Saumyakanta Mishra

Engineering Mechanics Unit
Jawaharlal Nehru Centre for Advanced Scientific Research

This dissertation is submitted for the degree of
M. S. (Engg.)

August 2022

Declaration

I hereby declare that except where specific reference is made to the work of others, the contents of this dissertation are original and have not been submitted in whole or in part for consideration for any other degree or qualification in this, or any other university. This dissertation is my own work and contains nothing which is the outcome of work done in collaboration with others, except as specified in the text and Acknowledgements.

Saumyakanta Mishra
August 2022

CERTIFICATE

I hereby certify that the matter embodied in this thesis entitled "**A Diffuse-Interface Analysis of Two-Phase Thermo-Convective Instabilities"** has been carried out by **Mr. Saumyakanta Mishra** at the Engineering Mechanics Unit, Jawaharlal Nehru Centre for Advanced Scientific Research, Bengaluru, India under my supervision and that it has not been submitted elsewhere for the award of any degree or diploma.

Dr. Diwakar S. Venkatesan
(Research Supervisor)

Acknowledgements

Academically speaking, I would like to thank everyone who has given me advice and assistance during various stages of my time here. I want to start out by first acknowledging my thesis supervisor, Dr. Diwakar S. Venkatesan, for giving me an exciting problem to work on. I am grateful to him for introducing me to spectral methods, giving me complete freedom to explore the problem, and for his support throughout my master's. I thank my course instructors, Prof. Ganesh Subramanian, Prof. Meheboob Alam, Prof. K. R. Sreenivas, and Prof. Santosh Ansumali, for their courses. I would like to thank Prof. Subir K. Das for agreeing to be on my GSAC committee and for all the discussions during the project's initial phase.

I will always cherish the memories I shared with a few wonderful people I have met in JNC. It started with "Pinner dlans"; Nishant, for being a constant support and showing me the importance of writing good codes; Prateek, for showing me the power of being consistent, bearing with all my scientifically unscientific thoughts; Mahan, for various discussions on numerical schemes; Meha, for giving me one of the best pieces of advice. I thank all of you for being there for me.

During my stay at JNC, I made some terrific friends. Suryadev and Ritwik were the best batchmates that I could ask for. Rohan, thank you for sharing your true Odia spirit with me. I would like to acknowledge 105 lab folks, including Praveen, Akashay, and Subrat. I am glad I met Rafi, Vybhav, Akshay, Sabarish, Arun, and Pratik. I acknowledge my younger colleagues, Akhilesh, and Sangamesh, for their joyful conversations. Outside of EMU, I had some very good chit-chat with Abhijit, Anita, Madhulika, Gautam, Sinay, and Debendra. Thank you for making my life less mundane.

I am deeply thankful to Prof. Ranga Narayanan for long-hour discussions on the physics of the problem and for sharing some of his pearls of wisdom with me. Lastly, I must acknowledge my undergrad supervisor, Prof. Sudhansu S. Sahoo, for being a mentor and a friend.

Abstract

Two-phase flows are ubiquitous in natural and industrial settings. In the present work, we have developed a general 'one-fluid' diffuse-interface model suitable for various two-phase flow problems. The specific two-phase problem considered in the current work involves a binary fluid system, which poses a unique property of being miscible in each other depending on the system's temperature and is completely miscible above a particular temperature, called the upper critical solution temperature (UCST). Accordingly, we have developed a spectral collocation-based phase field model to study the onset characteristics of Rayleigh-Bénard convection in a two-layer binary fluid system. We have also considered the Marangoni effect (variation of surface tension) in addition to the pure buoyancy-driven instability to examine how the strength of surface tension gradient can alter the onset behavior of the system. We have observed that the strength of the Marangoni effect can expand or contract the oscillatory onset window observed in the case of pure buoyancy-driven convection. The solubility of the system acts in unison with the interfacial tension term and comes with its own dual role in making the onset of convection either oscillatory or stationary.

Table of contents

List of figures

List of tables

Chapter 1

Introduction

Buoyancy-driven flows are ubiquitous in geophysical fluid dynamics, ranging from Earth's molten core flow to atmospheric flow. They are also central to various transport processes in diverse industrial settings. Natural convection is essentially a buoyancy-driven flow that is instigated by density inhomogeneities in the presence of a gravitational field, mainly due to the variation in temperature or composition of the system. A typical example of the phenomena is the problem of Rayleigh-Bénard-Marangoni (RBM) convection, wherein fluid(s) is(are) subjected to adverse thermal gradient by sandwiching it(them) between two horizontal isothermal plates. The single-layer RB convection has been extensively studied since it serves as one of the model problems for understanding nonlinear physics, complex dynamics, pattern formation, and turbulence [72]. An extension of RB convection involving a multi-layer system also has many applications, like in the Earth's mantle and liquid encapsulation crystal growth. In a multi-layer setting, interfaces add further complexity to the problem. Common approaches to handling interfaces in a multiphase problem assume that the interface is of zero thickness. Necessary jump conditions across this zero-thickness interface maintain the continuity of different quantities like velocity, temperature, etc., and the associated fluxes.

It may be noted that the consideration of zero interface thickness is an idealization and does not often portray a realistic picture of the fluid configuration, particularly for systems closer to their critical (consolute) point. Here, the interface between the two fluids is a diffuse region wherein the properties change rapidly but smoothly. The idea of non-zero interface thickness was developed in detail by Rayleigh [59] and van der Walls [58]. An appropriate approach to realistically model fluid interfaces in a multiphase problem should involve non-sharp (diffuse) considerations, and in this regard, the widely-regarded 'phase-field model' serves as a potent tool. Here, the phase variable distinguishes between the phases involved and their interfaces. The current work uses a modified phase-field formulation approach

to understand the evolution of RBM convection in two-layer binary fluid systems. While detailed discussions on the phase-field model and its application to multiphase problems are reserved for subsequent chapters, a brief introduction of the Rayleigh-Bénard-Marangoni (RBM) convection phenomena is presented below.

1.1 RBM convection

1.1.1 RB convection in a single-layer problem

The Bénard problem mainly refers to the thermal instabilities that arise when a horizontal layer of fluid, confined between two plates, is heated from below, thereby creating an adverse thermal gradient that results in unstable stratification. As the name suggests, this instability was discovered by Bénard [6] in 1900. He observed hexagonal patterns in a thin layer of spermaceti heated from the bottom. In 1916, Rayleigh [53] put forward a theory for this instability wherein he identified buoyancy as the destabilizing force that instigates fluid motion, and kinematic viscosity and thermal diffusivity as the stabilizing factors. For sufficiently small temperature differences, thermal energy gets transferred via pure conduction from the lower to the upper plate, and no fluid motion is involved. The agitating fluid parcels start moving when the temperature difference exceeds a critical value. This process is called as the onset of convection. In other words, the competition amongst various factors yields a critical value that separates the flow and no-flow scenarios. Understanding how this criticality changes with different system parameters is often pertinent.

The overall mechanism behind the onset of convection can be explained as follows. Though the fluid density is uniform initially, the imposed temperature gradient creates a density stratification in the system. The fluid closer to the lower plate becomes lighter than the fluid above it. If one gives a small upward mechanical perturbation to this hot fluid particle, it will start to move upwards due to buoyancy. This action will further reinforce the buoyancy force acting on the particle as it experiences a colder ambiance during its ascent. To satisfy continuity, liquid from the neighborhood fills the original location of the agitating fluid. Thus, the fluid particles' shifting and relocating actions set the convection in motion. In the absence of any dissipative effects, this motion will continue indefinitely. However, no fluids are ideal, and a few fluid properties inhibit the growth of the perturbations through diffusion. For example, the kinematic viscosity tries to decelerate and diffuse the momentum of the agitated parcel. The thermal diffusivity attempts to equilibrate the fluid blob with its neighboring fluid particles thermally. In other words, due to the kinematic viscosity and the thermal diffusivity, the fluid blob loses the momentum and heat it initially carried. Therefore,

one can intuitively say that it is harder to set up convection in fluids having higher values of momentum and thermal diffusivities, *i.e.* one needs to maintain a higher temperature gradient in such fluids to start a convective motion.

From the above discussion, it is clear that the transition from a purely conductive state to a convective one depends on the magnitude of the temperature gradient and the dissipating entities like kinematic viscosity and thermal diffusivity. Essentially, the temperature gradient gives rise to unstable density stratification, and in the presence of the gravitational field, the destabilizing buoyant forces must outweigh the stabilizing dissipative forces for the onset of convection to occur via the continued growth of the initial disturbance imposed on the fluid particles. To quantify the relative importance of these opposite forces, one typically uses a non-dimensional number called the Rayleigh number (Ra), which gives the ratio between the buoyancy and the diffusive forces. Ra is defined as

$$Ra = \frac{g\beta\Delta\theta L^3}{\nu\kappa_T}, \tag{1.1}$$

where g is the magnitude of gravitational acceleration, β is the volumetric expansion coefficient of the fluid, and $\Delta\theta$ is the temperature difference between the top and bottom plate. L is the characteristic length-scale, typically the height of the fluid layer. ν and κ_T are the kinematic viscosity/momentum diffusivity and the thermal diffusivity of the fluid, respectively. Hence to instigate the instability, the magnitude of buoyant force must exceed the flow-inhibiting forces, *i.e.* $Ra >> 1$. Note that the Rayleigh number scales as L^3.

1.1.2 Marangoni convection in a single-layer problem

Another type of thermal instability occurs when a free surface replaces the upper rigid boundary. The length scale (L) of the problem is small such that the gravity-induced buoyancy has less influence on the convection onset characteristics. Here, the surface tension gradient plays a crucial role. With the imposed temperature gradient, any perturbation of the free surface exposes the trough to a higher temperature than the crest. This process creates a differential heating of the free surface, which incubates a gradient in the surface tension. As a result, the fluid particles from a lower surface tension region are pulled towards the higher surface tension region. Here again, the dissipating effects like momentum and thermal diffusivities try to inhibit this motion. Therefore, a threshold value of surface tension gradient is required to provoke convection in the system. The relative importance of the destabilizing gradient of interfacial tension to the stabilizing dissipative effects is given by a

non-dimensional number called the Marangoni number (Ma) written as

$$Ma = \frac{\sigma_\theta \Delta\theta L}{\mu \kappa_T}. \tag{1.2}$$

Here, σ_θ is the surface tension gradient with respect to temperature, and μ is the fluid's dynamic viscosity.

Thus for the onset of instability, Ma should be $>> 1$, *i.e.*, the inhibiting entities can no longer outweigh the driving surface-tension gradient force. The Marangoni number scales as L, and as we can see, the buoyancy-driven convection takes over the surface tension-driven convection as we increase the length scale of the problem under the gravitational influence.

1.1.3 RB convection in a two-layer problem

The two-layer counterpart of the RBM convection is rich in physics and is usually more complex. Typically, the lighter fluid is placed on top of the heavier fluid to maintain a stable stratification. Sometimes fluids of equal density are also considered. However, they should have different volumetric expansivity, preferably the top one with a higher value. An unstable stratification , *i.e.* denser fluid on the top leads to the classical Rayleigh-Taylor instability.

In a typical two-layer RB system, different modes of convection (Fig. 1.1) can be observed depending on the fluids' properties and the height ratios of the individual layers. The first mode is called the *lower dragging mode*, wherein the onset of buoyancy-driven convection primarily occurs in the lower layer of the system, and the upper layer is passively driven due to the continuity of velocity and shear stress at the fluid interface. The second one, called as the *upper dragging mode*, is a mirror image of the first kind. Here, the initial buoyancy-driven flow happens in the upper layer of the system, and the lower layer gets passively dragged. The third kind is called the *mechanical coupling mode*, wherein both layers undergo simultaneous excitation, and a proper mechanical continuity is maintained at the interface. The rotational orientation of the convection rolls is opposite in the layers. The fourth case, where the rolls rotate with the same orientation, is called the *thermal coupling mode*. Both layers undergo simultaneous excitation again, and the thermal continuity is maintained at the interface. Some idle rolls are formed in the vicinity of the interface to ensure mechanical continuity and avoid the high shearing region. The fifth case is more pertinent to the liquid-gas system and is called the *surface tension driven mode*. The buoyancy-driven instability occurs in the gaseous layer, and these convection rolls create an uneven temperature distribution on the fluid interface. This situation imposes a surface tension gradient on the interface, and the fluid particles from the lower surface tension region are pulled towards the region of higher surface tension, thereby forming a convective motion in the liquid layer. In this surface

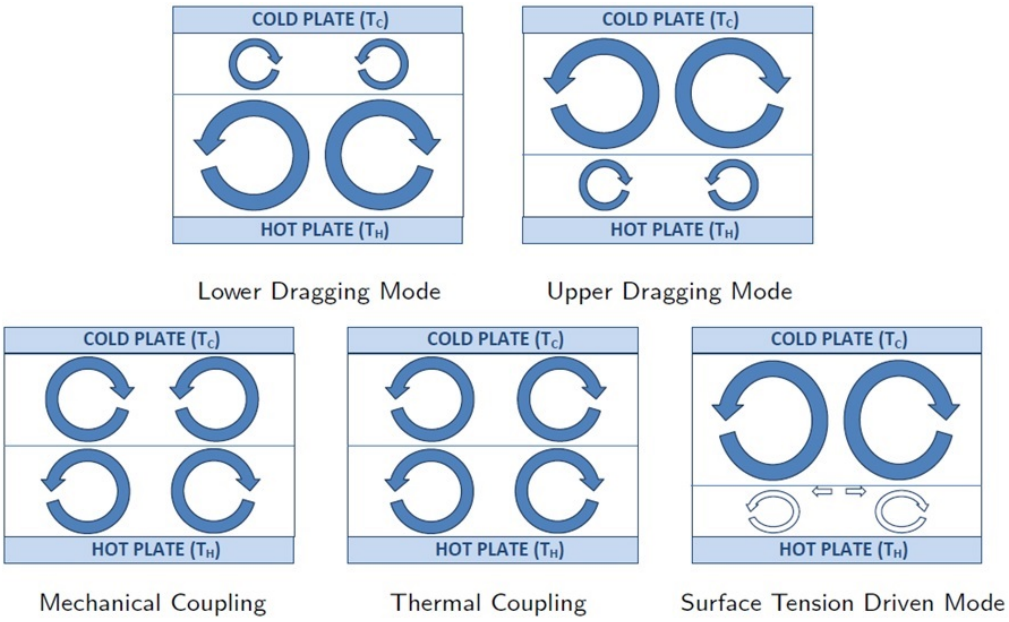

Fig. 1.1 Non-oscillatory modes of RB Convection

tension-driven mode, one can observe that the convection starts in the liquid layer due to the gradient in interfacial tension and not essentially due to the continuity of velocity and shear stresses.

Note that all the modes mentioned above can be categorised under the non-oscillatory modes of convection onset. An interesting scenario occurs when there is an equal propensity for the non-oscillatory mechanical coupling (MC) and thermal coupling (TC) modes to occur at some height ratios. This situation leads to the 'oscillatory mode of convection' wherein the system oscillates between MC and TC modes. The Lyapunov exponent at this flow onset condition is complex, *i.e.*, the imaginary part of the exponent is non-zero. From a dynamical system perspective, the oscillatory systems are essentially non-self-adjoint in nature. The underlying mathematical features of oscillatory convection are discussed in the next chapter.

1.2 Importance of multiphase/multilayer thermal instabilities

The need for the thorough characterisation of multi-layer convection arises both from the requirement of understanding natural phenomena and from relevant industrial applications. As mentioned earlier, the bi-layer thermal instabilities can be observed predominantly in the geophysical context, for example, in Earth's mantle convection [13]. As shown in Fig. 1.2, two types of hypotheses have been proposed in this regard: the whole mantle convection

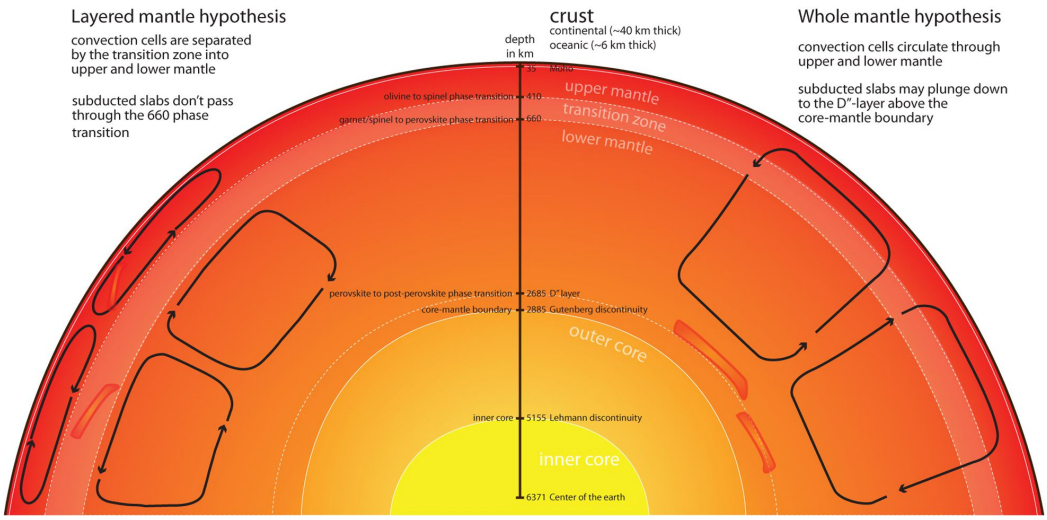

Fig. 1.2 Earth's mantle convection
(Credit: nationalgeographic.org)

theory and the layered mantle convection theory. The current study is more relevant to the latter viewpoint, wherein the convective rolls are observed in the upper and lower mantles, and there is an intermediate zone.

One of the industrial applications of the two-layer RB convection is in the process of liquid encapsulated crystal growth [33]. The encapsulation protects the core material from environmental effects. The basic idea of this process is to extract a high-quality crystal from the melt sandwiched between two liquids. The formation of crystals is effectuated by removing heat from the melt. However, this heat removal process can create a temperature gradient, which can induce convection inside the melt and deteriorate the quality of the crystal. Hence, understanding the convection onset behavior in such systems is essential to obtaining high-quality crystals.

1.3 Need for diffuse interface approach

As early as the 19^{th} century, the concept of a fluid interface being a region of rapid but smooth property change over a finite thickness was well recognised. Later in the same century, Rayleigh [59] and van der Walls [58] developed, in detail, the theory of non-zero thickness interfaces. As a fundamental fact of mixture thermodynamics, it is well known that there is limited miscibility between the so-called immiscible fluid components [39] even at low temperatures. As the temperature increases, the fluids become more soluble in one

another, and after a critical temperature, they form a single-well potential curve in the free energy vs. phase-parameter diagram.

For the sake of convenience, the conventional approach to modelling multiphase systems, via the sharp-interface approach, often assumes the interface to be a δ-function. Though this approximation works well within the limit of negligible miscibility (immiscible limit), it becomes ill-suited for fluid systems closer to their consolute point, a state beyond which the fluids are completely miscible. In such scenarios, the only viable option is to consider models that can account for the diffuse nature of the interface. The well-known 'Phase field model' is one such approach that implicitly considers the fluid interface to be diffuse in the 'one-fluid' framework. The current work uses the phase field model to understand the evolution of Rayleigh-Bénard-Marangoni (RBM) convection in two-layer binary fluid systems.

1.4 Overview of the thesis

In the present study, we attempt to computationally understand the onset characteristics of RBM convection in a two-layer binary fluid system. Binary fluids pose a unique property of being partially soluble in each other based on the temperature and are entirely miscible after a critical temperature, called the upper critical solution temperature (UCST) [8]. In order to capture this behaviour, we have employed the phase-field method with a modified free-energy formulation. Apart from its ability to model the diffuse interface structure, the additional benefit of using the phase-field method comes from its "one-fluid" formulation [50]. Note that the current implementation involves the Chebyshev pseudospectral approach, keeping in mind the stringent accuracy requirement for the stability problems. The need for obtaining a proper resolution of the interfacial gradients prohibits us from directly implementing the standard Gauss-Lobatto-Chebyshev (G-L-C) grid structure. To resolve this issue without losing accuracy, we have taken the help of an adaptively transformed Chebyshev grid system [67, 23]. Although the fluids considered are incompressible, their mixing region becomes non-solenoidal [17]. Thus, via the conventional approach, the problem becomes a Quasi-incompressible one [39] that is harder to solve since the chemical potential becomes a function of the pressure. Note that the pressure is presently determined by the kinematic condition and not by the thermodynamic constraints [3]. To overcome this issue, we have redefined the velocity field as the volume-averaged quantity [20, 1] instead of the typical mass-averaged value. This volume-averaged velocity field will be solenoidal throughout the domain, including the mixing region [20]. Thus by varying the parameter that controls the miscibility of the fluids, we have shown its importance and the way it affects the criticality of a typical RBM convection system.

The current thesis delves into the details of all the above activities via five chapters, including the current introduction chapter. In chapter 2, we begin with the historical development of RB convection. This is followed by the discussion on the occurrence of oscillatory modes in two-layer RBM systems. We subsequently introduce the different numerical methods/schemes that are currently in use to solve multiphase problems. In this context, we discuss the phase-field method in detail and show its appropriateness for the present problem of consideration.

In chapter 3, we initiate discussions about the modifications for making the phase-field model suitable for binary fluids. We provide a detailed description of the formulation, including the volume-averaging process. The linear stability problem is formulated via the spectral collocation procedure with appropriate mapping carried around the diffuse interface. We show the consistency of our approach by matching our results at a very small interface thickness with the results obtained from the *domain decomposition method (DDM)* (discussed in detail in Appendix A) for immiscible and sharp-interface limits. Finally, we discuss the RBM stability of binary fluids and how the miscibility factor affects the critical Rayleigh numbers and the window of oscillatory onset. All the analyses in Chapter 3 are performed ignoring the presence of Marangoni effects, which are dealt with in Chapter 4. The thesis ends with Chapter 5, which provides the summary and conclusions of the current work along with the scope for future extension.

Chapter 2

Literature review

As mentioned in the introduction chapter, the current work aims to understand the evolution of the Rayleigh-Bénard-Marangoni (RBM) convection in two-layer binary fluid systems. To this effect, the current chapter deals with an overview of the literature relating to RBM convection in single and multiple layers, followed by different multiphase simulation methods that can serve as tools to understand the binary fluid RBM convection problem. A brief overview of the works relating to binary fluids is also provided towards the end of this chapter. We now begin this chapter with a review of the literature describing the RBM convection in single-layer systems.

2.1 Rayleigh-Bénard-Marangoni (RBM) Convection in a single-layer system

The classical Bénard problem primarily refers to the thermal instabilities arising from unstable stratification in a heated fluid layer. The theory for this instability was formulated by Rayleigh [53] where he hypothesized that buoyancy is the driving force for the onset of convection here. Later, investigations by Block [9] and Pearson [48] revealed the surface tension to be the destabilizing force for the thin layer of fluid considered by Bénard in his experiments.

Note that the importance of surface tension fades away in comparison to buoyancy when the thickness of the fluid layer is increased. As mentioned in the previous chapter, two different non-dimensional numbers essentially govern the physics for these instabilities. For a relatively thicker layer of fluid, the onset of convective instability primarily depends on the Rayleigh number, which gives the relative importance of the destabilizing buoyancy effect over the stabilizing diffusive effects involving the heat diffusivity and the momentum diffusivity. Whereas for relatively thin layers, the onset of instability depends on the critical

values of the Marangoni number, which gives the relative importance of advective transport due to surface tension variations over the same diffusive effects. In 1964, Nield [43] shed light on the relative importance of driving forces with the layer height. Scriven and Sternling [60] investigated the effect of surface tension on cellular convection while neglecting buoyancy. They concluded that there is nothing called a critical Marangoni Number for the onset of stationary instability. However, further studies by Smith [63] confirmed the existence of a non-trivial critical Marangoni Number by considering the effect of gravity waves.

2.2 Rayleigh-Bénard-Marangoni (RBM) Convection in a two-layer system

Proceeding further, we move on to the two-layer systems where convective instabilities in two different, stably-stratified fluids are considered. The goal is to understand the diverse modes of convection that arise when such layers are subjected to destabilizing thermal gradients. Busse [13] focused on modelling Earth's mantle convection and concluded that the horizontal scale of convection in the lower mantle determines the horizontal scale of convection in the upper mantle owing to the larger thickness of the lower mantle. These phenomena are referred to as the lower or upper dragging mode (Johnson & Narayanan [32]), based on the layer which undergoes primary excitation. If both the layers have a propensity to undergo excitation, one can expect either a stationary mechanical or thermal mode of coupling between the layers. Interestingly, both MC and TC modes become equiprobable for some height ratios and a favourable combination of fluid properties. This often leads to the scenario of overstability, wherein the system oscillates between these modes as they cannot coexist simultaneously at any given instant. Rasenat *et al.* [52] proved the existence of such oscillatory instability, wherein a cyclic variation between the non-oscillatory mechanical and thermal coupling modes was observed. Gershuni and Zhukhovitskii [26] considered a two fluids system with a horizontal interface wherein the instability was set up when the fluids were heated from above.

Renardy and Joseph [56] performed a linear stability analysis for the RB convection in the two-layer setting. They found that the system of equations governing the onset of convection to be non-self-adjoint (possibility of finding complex eigenvalues) and showed that a Hopf bifurcation (a pair of travelling waves or a standing wave) could occur in fluids with different properties like dynamic viscosities and thermal expansion coefficient. They also concluded that the surface tension always gives a stabilizing effect for short wave disturbances. Renardy and Renardy [55] considered fluids with slightly different properties with slip boundary

conditions (shear stress vanishes at the boundaries) and concluded that the oscillatory modes are still possible for a specific type of perturbation.

Rasenat *et al.* [52] proposed that for an oscillatory onset to occur, there needs to be a competition between two different modes. They could be a bulk mode and an interfacial mode or two bulk modes. The first bulk mode essentially originates from the buoyancy-driven convection associated with adverse temperature gradients in a layer. Based on fluids' properties, this bulk mode competes with either an interfacial mode that tries to oppose the flow, to some extent, or another unstable bulk mode when the interfacial mode is highly stable.

Renardy [54] mainly concentrated on the second mechanism that applies to the case where the competition is between two bulk modes. Renardy [54] showed that for the case of infinite Prandtl numbers, the system will not be oscillatory when $\rho\beta\kappa_T \approx 1.0$, since the system will be self-adjoint for such a property combination (ρ: ratio of densities, β: ratio of coefficients of thermal expansion, κ_T: ratio of thermal diffusivities). Here, the leading eigenvalues are real. The following linearised form equation gives an idea on the eigenvalues of the system where the modes are proportional to $\exp(\lambda t + ikx)$.

$$\begin{aligned}\lambda\left[\int \kappa|\theta_1|^2 + \int \kappa_T|\theta_2|^2\right] = &-\int \kappa(k^2|\theta_1|^2 + |\nabla\theta_1|^2) - \int (k^2|\theta_2|^2 + |\nabla\theta_2|^2) \\ &+ \frac{\Lambda_2}{k^2 Ra}\left[\int |\nabla^2 v_1|^2 + \int \frac{\rho\beta\kappa_T}{\eta}|\nabla^2 v_2|^2\right] \\ &+ \frac{\Lambda_2}{k^2 Ra}(\rho\beta\kappa_T - 1)\frac{\partial\bar{v}_1}{\partial y}\frac{\partial^2 v_1}{\partial y^2}\bigg|_{y=I}\end{aligned} \tag{2.1}$$

As we can see, when $\rho\beta\kappa_T$ deviates from unity, the boundary term has a non-zero value and it results in the system being non-self-adjoint. Thus, one can expect the onset of oscillations when $\rho\beta\kappa_T$ deviates from unity.

Degen *et al.* [19] confirmed the above parameter by observing the onset of oscillatory convection for the silicon oil-water system with $\rho\beta\kappa_T = 0.375$ due to the formation of a cold spot at the top of the lower layer which results in the reversal of flow. Nepomnyashchy & Simanovskii [42] and Simanovskii & Nepomnyashchy [62] considered both buoyancy and thermocapillary effects and showed numerically that the oscillatory onset in silicon oil-water system is essentially due to the additional presence of thermo-capillarity. Diwakar *et al.* [22] showed that in addition to the favourable property combination for $\rho\beta\kappa_T$, the occurrence of oscillatory modes is also dependent on the closeness of the fluid height ratio to the critical height ratio at which the Rayleigh numbers of both the layers are equal. In the present work, we intend to understand how the above factors get modified in the context of a binary

fluid system that becomes miscible above a particular temperature. This requires a rigorous relook at the fundamental assumption of all the above works, *i.e.* the consideration of a sharp interface between the layers. To this effect, we now proceed to understand different multiphase flow formulations in the remaining part of the chapter.

2.3 Multiphase models

Numerical modeling of multiphase flows is a challenging task. Apart from the regular non-linearities of the simple fluid flow problem, multiphase flows are fraught with additional complexities arising from the hierarchy of scales involving different phases. As a result, the choice of using a particular multiphase modeling tool is often made based on the details of the problem that one is interested in studying. For example, the behaviour of a fine distribution of droplets in a spray can be emulated by a homogeneous model without paying much attention to the individual dynamics of the droplets and the associated interfacial heat and mass transfer. On the other hand, problems such as the dam-break or thin-film evaporation would require a detailed focus on the interfaces and the phenomena occurring in their vicinity.

Broadly, the multiphase methods can be classified as either moving-grid or fixed-grid based on the temporal action of the grid that is used to solve the problem. The grid for each fluid sub-domain is well defined in a typical moving-grid method. The grid points deform according to the fluid flow pattern, and the temporal evolution of the interface is obtained by following the discretized sub-domain boundaries. The issues with the moving-grid method primarily arise due to its inability to automatically handle phenomena like interfacial break-up and coalescence.

On the other hand, fixed-grid methods use special schemes to predict the multiphase flow dynamics on a non-deformable mesh. The fixed-grid methods can be further classified, either under the umbrella of "one-fluid" methods or under pure "multiphase" approaches like the Euler-Euler model. The latter, along with the population balance model, is quite effective in modeling dispersed systems like sprays, etc. Since the present problem involves segregated phases, the former "one-fluid" approach becomes a convenient means and is explained in the following sub-section.

In a typical *one-fluid* model formulation, we write a single set of governing equations for the entire domain and use markers to recognise the phases. The multiphase influence on the conservation equations is brought in by the spatio-temporal variations of mixture properties that are accounted for through the evolving marker function. The first model of this kind was the *marker-and-cell (MAC) method*, which was used by researchers in the Los Alamos National Laboratory in the 1960s. The MAC method was the first to simulate the dynamics

of an incompressible free surface flow [71]. The technique comes under the broad category of *interface-tracking* method since we track the tracer particles and define the interface by connecting them. However, usage of marker particles manifests computational issues primarily involving mass conservation. The method also does not automatically account for the interfacial break-up and merger. In order to overcome these issues, *interface-capturing* methods like the volume of fluid (VOF), the level-set method, and the diffuse interface (phase-field) method were later developed and are widely used in solving multiphase problems. In the case of the interface-capturing methods, an auxiliary variable is defined, which takes care of the phases and the interfaces involved in the system. We now briefly review these methods in the following subsections.

2.3.1 Volume of fluid (VOF)

The volume of fluid (VOF) method, introduced by Hirt and Nichols [29], is the most popular procedure among the 'one-fluid'models. The idea is to utilize an auxiliary function (F) that represents the exact fraction of the primary fluid within a computational cell. The spatio-temporal evolution of the phases is obtained by conserving 'F'using the advection equation.

$$\frac{DF}{Dt} = 0 \tag{2.2}$$

Note that F is a discrete function. Hence, the above advection equation is solved via special algebraic procedures or through geometric means involving the reconstruction of an approximate interface in the 'mixed' computational cells having F value between 0 and 1.

The algebraic VOF procedures compute the fluxes without needing interface construction and are easier to implement. However, the interface gets diffused when exposed to high-strain flows, and to avoid such distortion of the interface, an additional anti-diffusion term is usually incorporated into the volume fraction PDE. A few examples of such methods are *high-resolution interface capturing (HRIC)* technique (Muzaferija *et al.* [41]), *compressive interface capturing scheme for arbitrary meshes (CICSAM)* method (Ubbink and Issa [68]), *switching technique for advection and capturing of surfaces (STACS)* method (Darwish and Moukalled [18]), *bounded gradient maximization (BGM)* method (Walter and Wolgemuth [70]), *high-resolution artificial compressive formulation (HiRAC)* (Heyns *et al.* [28]).

The geometric VOF procedure, on the other hand, involves two steps, such as the interface reconstruction and the advection of the reconstructed interface by computing the material volumetric fluxes through the cell faces. The interface reconstruction step requires the estimation of the orientation and position of the interface within the computational cell. This also involves approximating the shape of the interface in each computational cell. In 1976,

Noh and Woodward [45] proposed the *simple line interface calculation (SLIC)* procedure in which the piecewise linear interfaces are positioned either vertically or horizontally based on the normal orientation. Unfortunately, such restricted orientations led to the formation of unrealistic 'jetsam'and 'floatsam'within the fluid domain. Later in 1982, Youngs [74] developed *piecewise linear interface calculation (PLIC)* in which the position of the interface is determined according to the normal vector calculated from the knowledge of volume fraction from the adjacent cells. Subsequently, many methods have been proposed to improve the robustness of the interface reconstruction step. A few examples are *least-squares VOF interface reconstruction algorithm (LVIRA)* (Puckett *et al.* [51]), *parabolic reconstruction of surface tension (PROST)* (Renardy and Renardy [57]), *spline-based interface reconstruction (SIR)* (López *et al.* [38]), *quadratic spline-based interface (QUASI) reconstruction* (Diwakar *et al.* [21]).

The advantages of the VOF method are its excellent volume conservation characteristics and the ability to handle topological changes in the fluid structures automatically. However, the technique is fraught with challenges, such as the non-uniqueness of the interface reconstruction process and the need for explicit geometric procedures.

2.3.2 Level-set method

In 1988, Osher and Sethian [47] introduced the level-set method. This method was extended to the case of two-phase flows by Sussman *et al.* [66]. Here, the interface is represented by a smooth auxiliary function [3] that denotes the signed distance of a grid point from the interface. Like VOF, no user intervention is required to account for the topological changes in the interface. Note that the level-set function 'ϕ'remains constant along particle paths, *i.e.*,

$$\frac{D\phi}{Dt} = 0 \tag{2.3}$$

In other words, the level-set value of a particle on the interface remains constant. The interface boundary $\mathscr{I}(t)$ is defined by $\{\mathbf{X}|\phi(\mathbf{X},t) = 0\}$. The region $\Omega(t)$ is bounded by $\mathscr{I}(t) : \{\mathbf{X}|\phi(\mathbf{X},t) > 0\}$ and its exterior is defined by $\{\mathbf{X}|\phi(\mathbf{X},t) < 0\}$ [46]. The momentum balance equation for the entire domain under consideration can be written as

$$\rho\frac{D\mathbf{u}}{Dt} = -\nabla p + \nabla\cdot(2\eta D) - \sigma\zeta\delta(\phi)\mathbf{n} \tag{2.4}$$

The surface tension is incorporated as a force concentrated on the interface. The properties of the fluids are expressed as the function of the level-set parameter. To ensure numerical consistency, the surface tension force is converted to a localized volumetric force in the

vicinity of the interface. Correspondingly, the Dirac-delta function in the surface tension forcing term is replaced by a smoothed or modified delta function $\delta_{\Delta X}$ [61]. A review paper by Sethian and Smereka [61] discusses the numerical issues of this method, like the spatial and temporal discretization schemes.

Son [64] developed a global mass correction method to ensure mass conservation in this approach. In order to improve the mass conservation, a dual-grid level-set method was introduced by Gada and Sharma [25], in which the momentum equations are solved using coarse grids, and the level-set equation is solved on a finer grid.

2.3.3 Front-tracking method

Unverdi and Tryggvason [69] introduced the front-tracking/distributed force model, where a few control points defined over the interface takes the place of the order parameter. Fluid properties like density, viscosity, etc., are varied smoothly across a thin region around the interface. Other desirable interfacial features, such as normals, curvatures, etc., are obtained from the connectivity information of the points.

Unverdi and Tryggvason [69] used this model to study the motion and interaction of multiple bubbles in two- and three-dimensional cases. In the second part, they studied the Rayleigh-Taylor instability in two- and three-dimensional cases. Nobari *et al.* [44] investigated the head-on-collision between two viscous droplets. A series of works by Juric and Tryggvason [35–37] applied this technique to the problems involving phase change, for example, vapor-bubble dynamics and film boiling. Notable issues with this approach include the evolution of spurious currents near the fluid interface when the capillary number is low. Also, this approach has no explicit means of enforcing mass conservation. Inguva *et al.* [30] have used a moving unstructured staggered mesh approach to address the above issues.

2.3.4 Phase-field method

All the above approaches essentially work with inherent sharp-interface consideration. Though the interface thickness would be of cell size, practically, one can approach the sharp interface limit by employing mesh refinement. Despite being popular, these methods are fraught with certain limitations that have been briefly discussed towards the end of the current section. We now delve into the alternate approach involving diffuse-interface consideration via the popularly known Phase-Field method.

Phase-field models offer a physically sound, systematic approach for investigating complex multiphase systems such as near-critical interfacial phenomena, phase separation under shear, microstructure evolution during solidification, etc. The basic idea here is to introduce

an order parameter or 'phase-field' which distinguishes between the bulk phases and the intervening interfaces. This order parameter varies rapidly but smoothly in the interfacial regions. One can choose any variable, such as density, composition, etc., as the order parameter based on the problem in hand [3].

Phase-field methods are built on the free energy of the fluid. Other methods focus on smoothening the surface tension forces over thin, numerically resolvable layers. Whereas in the phase-field formulation, the influence of interfacial phenomena is spread over a region spanning more than just a few cells. Note that the surface tension force is derived from the free energy expression using variational principles. The simplest model of the free energy density that gives two phases is [31]

$$f(\phi, \nabla\phi) = \alpha_1 \Psi(\phi) + \frac{1}{2}\alpha_2 |\nabla\phi|^2 \tag{2.5}$$

The first term is the free energy of the homogeneous phases. It is also called bulk energy and is responsible for the separation of the two phases. This term takes the form of a double-well potential in the bulk energy vs phase parameter diagram. Different forms of bulk energy expressions are used in practice to mimic this double-potential nature. $\Psi(\phi) = (\phi^2 - 1)^2$ [75, 15] is the most commonly used form, where $\phi = \pm 1$ represents the bulk phase fluids. Other varieties like $\Psi(\phi) = (\phi^2 - 1/4)^2$ and $\Psi(\phi) = (\phi^2 - 1/4)^{3/2}$, where $\phi_{bulkphase} = \pm 1/2$, have also been used in literature [31].

The second term is the gradient energy term. It provides the extra energy required for sustaining the interface between the two bulk phases. One of the crucial aspects of the phase-field method is determining the interface structure and its role in calculating the interfacial energy and the surface tension [31]. Note that the width of the interface is proportional to $\sqrt{\alpha_2/\alpha_1}$ while the surface tension is proportional to $\sqrt{\alpha_1\alpha_2}$. Bestehorn *et al.* [8] proposed a modified free energy functional to capture the miscibility to immiscibility transition in the context of a binary fluid system. The corresponding free functional density is given as

$$f(\phi, \nabla\phi) = \alpha_1 (r^q \phi^4 - r\phi^2) + \frac{1}{2}\alpha_2 r^p |\nabla\phi|^2 \tag{2.6}$$

where r is the parameter that controls the transition. We will discuss this equation and the role of r in detail in the next chapter. Bestehorn *et al.* [8] used the above-mentioned free energy expression for understanding miscibility-immiscibility transition in the context of Faraday instability.

Note that all the above mentioned models are valid only for isothermal systems. In case of a non-isothermal system, the temperature dependency will enter the free energy expression.

The general form of the free energy density functional can then be expressed as [2]

$$f(\phi, \boldsymbol{\nabla}\phi, \theta) = \alpha_1(\theta)\Psi(\phi, \theta) + \frac{1}{2}\alpha_2(\theta)|\boldsymbol{\nabla}\phi|^2 \tag{2.7}$$

Antanovskii [5] suggested the following form of free energy density in the context of capillarity

$$\begin{aligned} \rho f = {} & \rho_1(\theta) f_1(\theta)\phi + \rho_0(\theta) f_0(\theta)(1-\phi) \\ & + \frac{C(\theta)}{2a}[A(\theta, \phi)^2 + a^2|\boldsymbol{\nabla}\phi|^2] \end{aligned} \tag{2.8}$$

where $f_1(\theta)$ and $f_0(\theta)$ are the specific free energy of the fluid 1 and fluid 0 respectively.

The evolution of the phase-field parameter ϕ can be considered via two distinct partial differential equations (PDEs). For the non-conserved order parameter which involves the phase-change problems, one usually employs a second-order PDE called the Allen-Cahn equation that is given as

$$\frac{\partial \phi}{\partial t} + \boldsymbol{u} \cdot \boldsymbol{\nabla}\phi = \alpha_2 \nabla^2 \phi - \alpha_1 \Psi^{'}(\phi) \tag{2.9}$$

In two-phase flow situations, where the order parameter is conserved, a fourth-order PDE called as Cahn-Hilliard equation is generally used:

$$\frac{\partial \phi}{\partial t} + \boldsymbol{u} \cdot \boldsymbol{\nabla}\phi = \boldsymbol{\nabla} \cdot [\gamma \boldsymbol{\nabla}(\alpha_1 \Psi^{'}(\phi) - \alpha_2 \nabla^2 \phi)] \tag{2.10}$$

Note that there is no explicit specification of interfacial conditions in the phase-field model; it has to be built into the governing equations. The surface specification emanates from the free energy expression, as mentioned earlier. The phase-evolution PDE and the momentum equations are coupled to take care of the surface evolution. Usually, an additional term, either $-\phi\boldsymbol{\nabla}\mu$ or $\mu\boldsymbol{\nabla}\phi$, is added to the Navier-Stokes equation to take care of the interfacial forcing [31].

Mirjalili *et al.* [40] performed an unbiased comparison between the VOF and phase-field methods and concluded that "*it seems likely that whether the interfacial regions are filling the domain or confined in space, the accuracy of DI accompanied by its scalability and low cost allow for DI to outperform VOF in many practical simulations.*" The phase-field method shares many features with the level-set method, and hence, it can be viewed as a physically motivated level-set method [15]. Solving PDEs in a complex domain is more cumbersome and tedious using the level-set method, whereas the phase-field method comes handy [61]. The VOF, level-set, and front-tracking methods are sharp-interface methods and their phase

(or marker) evolution PDEs are hyperbolic in nature. Thus, there is a fair chance that the velocity field may not retain its smoothness when subjected to topological changes [61]. The diffuse-interface models do not suffer from such short-comings. Note that sharp-interface methods use approaches like the continuum surface force (CSF) method [12] to allow for the single-domain treatment of a multi-phase system.

From the above arguments, it is evident that the phase-field model gives us an advantage over the other existing models for carrying out the current study on binary fluids in the vicinity of their critical behaviour.

2.4 Application of phase-field model to different problems

Jacqmin [31] addressed the importance of choosing a proper diffuse interface width and how the wider interfaces can exacerbate problems like the curvature-dependent solubilities in the phase-field model. He introduced a higher-order scheme that allowed the use of thinner interfaces and gave an insight on choosing the mobility of the interface, which is related to the relaxation time of the interface.

Anderson *et al.* [4] developed a phase-field model for the solidification of a pure material by employing the principles of irreversible thermodynamics that included convection.

Borcia and Bestehorn [10] presented a phase-field formulation to study the Marangoni convection in a liquid-gas system and described the short and long wavelengths instabilities associated with it. Yue *et al.* [75] proposed a diffuse-interface model for micro-structured complex fluids using the energy-based variational formalism. Celani *et al.* [15] studied the onset of Rayleigh-Taylor instability for immiscible fluids in the limit of small Atwood number via the phase-field formulation. Guo and Lin [27] proposed a thermodynamically consistent model for thermo-capillary effects and discussed the migration in density-matched fluids. Bestehorn *et al.* [7] proposed a new free energy functional to capture the miscibility to immiscibility transition in the case of a binary fluid system and studied this transition in the context of Faraday instability.

2.5 Binary fluids

Before we conclude this chapter, we briefly examine some important works on binary fluids. In 1990, Joseph [34] experimented on miscible liquid droplets rising or falling in another liquid and observed the capillary-type effects. He also observed that density in the interfacial region changes due to the composition variations (and temperature if present), though not affected by the pressure variations. This investigation gave rise to a different class of fluids

called quasi-incompressible fluids. In the case of quasi-incompressible fluids, densities of the individual fluid components remain constant. However, density change occurs in the mixing region which gives rise to a non-solenoidal velocity field ($\boldsymbol{\nabla} \cdot \boldsymbol{u} \neq 0$) in the interfacial region. The pressure will still be determined from kinematics, not from thermodynamics. This notion of quasi-incompressibility was adopted into the diffuse-interface model by Lowengrub and Truskinovsky [39]. They also showed the importance of taking a physical quantity as a phase-field parameter. Typically, to achieve a solenoidal velocity field throughout the system, one has to consider fluids of equal density or impose an additional assumption of a slow diffusion process [17]. Note that the above studies have obtained the velocity field as a mass-averaged quantity.

In 2007, Ding *et al.* [20] adopted a different approach to defining the mean velocity field of the system and called it the volume-average velocity of the fluid components. The advantage of implementing this idea is that the velocity field is solenoidal ($\boldsymbol{\nabla} \cdot \boldsymbol{u} = 0$) throughout the system including the interfacial region(s). In fact, in the bulk part, this velocity is the same as the mass-average velocity; it differs only in the transition layers. Abels [1] used this idea to develop a frame-invariant phase-field model for incompressible fluids. He has discussed the choices for different order parameters.

2.6 Critical summary of the literature

From the above literature review, one can make the following observations:

1. The mechanism of onset of single layer R-B-M convection has been widely studied, and there is sufficient understanding of the phenomena.

2. However, the literature on multi-layer R-B-M convection is limited, particularly concerning the onset of oscillatory convection modes.

3. More importantly, we are unaware of any notable work that attempts to understand the R-B-M convection in the context of partially soluble binary fluid systems.

4. A detailed review of different numerical multiphase approaches reveals that the diffuse-interface (Phase-Field) model would be a suitable candidate for understanding the above phenomena.

5. Since the present consideration of binary fluids involves large density differences, it is imperative to use the volume-averaged velocity field so as to make the velocity field solenoidal throughout the domain.

2.7 Aim of the current work

The current work aims to develop a phase-field model to study the Rayleigh-Bénard-Marangoni (RBM) convection in a binary fluid system. We have considered the intermiscibility of the fluids with change in the temperature of the system. Most of the prior studies have neglected this factor of miscibility. This is important because, even at low temperatures, there is always limited miscibility between the fluid components in a given fluid mixture. First, we perform linear stability analyses to understand how the marginal Rayleigh number and the window of oscillatory onset of the instability get affected by solubility in a pure RB (neglecting the surface tension variation) setting. We then add the Marangoni effect (surface tension variation with temperature) to the above problem and understand the changes in the onset characteristics.

Chapter 3

Onset of Rayleigh-Bénard convection in a two-layer binary fluid system

3.1 Introduction

As indicated in the previous chapter, the present work aims to understand the onset of Rayleigh-Bénard-Marangoni convection in binary fluids that exhibit criticality with respect to miscibility. The focus is to particularly identify and understand the occurrence of oscillatory modes in such fluid combinations. It may be noted that the solubility and miscibility of the fluids are considered here to be functions of temperature only. The fluids exhibit partial miscibility below the so-called 'upper consolute' or 'upper critical solution temperature' (UCST) and are entirely miscible above it. Correspondingly, the current interest is focused on systems in the immiscible regime that are gradually approaching the UCST.

With the above-stated larger objective in mind, this chapter presents the details of analyses in the specific case of pure buoyancy-driven Rayleigh-Bénard (RB) convection where the thermo-capillary effect is precluded. The combined influence of all these effects is dealt with separately in the ensuing chapter.

The behavior of R-B convection in binary fluids is mimicked here using the phase-field modeling approach. The model essentially uses fixed grids (Eulerian approach) and a diffuse interface consideration between the fluids. The whole domain is represented as a single continuum with additional consideration of a phase evolution equation that calculates the phase distribution within the domain.

Note that the conventional procedure for understanding R-B-M convection typically involves the Boussinesq approximation, wherein the variation in fluids' densities is considered to be small. However, for the single domain consideration of the phase-field model

and the mass-averaged velocity system [39, 17], a non-solenoidal velocity field, which is proportional to the relative flux of the components, is obtained even for a small density variation. Eventually, the formulation and the solution procedure, as discussed in the preceding chapter, become very complicated. In order to overcome this issue, we have employed a volume-averaged velocity field, as suggested by Boyer [11] and Ding *et al.* [20], that results in a solenoidal velocity field while conserving the mass of the individual fluids.

Along with the above modification, the present approach utilizes spectral/pseudospectral discretization to accurately estimate the critical parameters. Note that the pseudospectral discretization typically demands the use of standard Gauss-Lobatto-Chebyshev (G-L-C) points which involve grid clustering in the vicinity of the domain extremities. While such a configuration is conducive for modelling single-phase systems or decomposed domains, the need for proper resolution of sharp gradients around the diffuse interface precludes its direct implementation for the "one-fluid" phase field model. One may attempt to find a work-around by using a large number of GLC points, but this may not always be practical. Hence, to resolve the diffuse interface better and to reduce the associated computational effort, we have implemented a strategy [67, 23] which maps the G-L-C points in the transformed domain to a cluster of points around the diffuse interface in the physical domain. Note that the current clustering around the mixing layer region is controlled by a scaling parameter, $\in$. The implementation of such a mapping in the present *one-fluid* context is explained in the latter part of the current chapter.

In this chapter, we perform detailed linear stability analyses to estimate the critical parameters for the onset of convection and identify the oscillatory/non-oscillatory states of the onset. As a check for consistency, the reproducibility of the results obtained from a sharp-interface based *domain decomposition approach (DDM)* is verified for infinitesimal interfacial thickness value. For this consistency test, the dimensionless diffuse interface width (ε/L) was maintained at 10^{-4}.

We now begin this chapter with a brief description of the problem statement and the various modifications carried out with regard to the convectional phase-field formulation for modelling R-B convection in the present context.

3.2 Phase-field modeling and the governing equations

It may be recalled from Chapter 2 that the free energy density for an isothermal two-fluid system is given as

$$f(\phi, \nabla\phi) = \alpha_1 \Psi(\phi) + \frac{1}{2}\alpha_2 |\nabla\phi|^2 \tag{3.1}$$

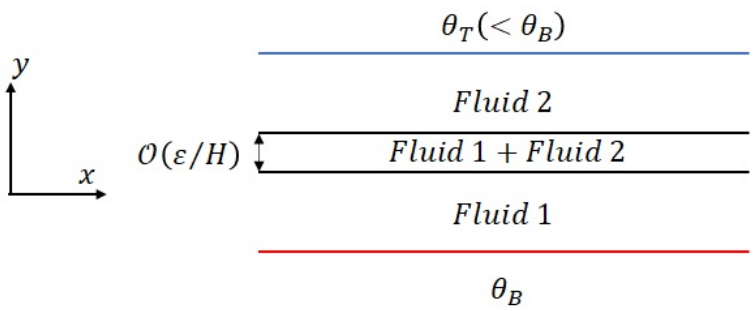

Fig. 3.1 Schematic of the problem under consideration

In the context of a non-isothermal system, one can use the free energy formulation suggested by Alt and Pawlow [2], and Antanovskii [5] as given below

$$F(\phi,\theta,\nabla\phi)=\int_{\Omega}\left[f_{bulk}(\phi,\theta)+\frac{1}{2}\alpha_2(\theta)|\nabla\phi|^2\right]d\boldsymbol{x} \tag{3.2}$$

where

$$f_{bulk}(\phi,\theta)=\rho c(\phi)\theta-\rho c(\phi)\theta\log\theta+\alpha_1(\theta)\Psi(\phi,\theta) \tag{3.3}$$

This formulation needs to be further modified for the present binary fluid consideration. The schematic of the current two-layer system is shown in Fig. 3.1. The lighter fluid is stacked over the heavier one to avoid the manifestation of the classical Rayleigh-Taylor instability. The system is considered to be infinite in the horizontal directions. The top and bottom walls are maintained at uniform temperatures, with the bottom being hotter than the top. The interface between fluids is diffuse, and its thickness diverges as the system approaches the UCST. Considering the change in miscibility of fluids (in each other) with temperature, the free energy functional of Eq. (3.2) can be modified as [8]

$$F(\phi,\theta,\nabla\phi)=\int_{\Omega}\left[f_{bulk}(\phi,\theta)+\mathscr{H}(r)\frac{\Lambda}{2}r^p|\nabla\phi|^2\right]d\underline{\mathrm{x}} \tag{3.4}$$

Recall that ϕ is a continuous parameter that helps distinguish between the bulk phases and the intervening interface and, in general, is called the order parameter. The above expression is similar to the classical Ginzburg-Landau free energy expression wherein Λ is the magnitude of the mixing free energy of the system. Here, r is an indicator of the system's state with regard to UCST.

The first term in the free energy expression refers to the bulk energy part *i. e.* it gives the energy for homogeneous phases and can be written in the form

$$f_{bulk}(\phi,\theta) = \rho c(\phi)\theta - \rho c(\phi)\theta\log\theta + \mathscr{H}(r)\frac{\Lambda}{4\varepsilon^2}r^q\phi^4 - \frac{\Lambda}{2\varepsilon^2}r\phi^2 \tag{3.5}$$

As we can see, the free energy expression for the uniform phases is the same as that of Besthorn *et al.* [8] with the addition of a few extra terms which account for the temperature non-uniformity in the system. Here, we have taken the internal energy as a linear function of ϕ. The third and fourth terms together can be interpreted as the mixing energy of the system. The mixing energy takes the form of a double-well potential below UCST and a single-well form above this critical temperature. This mixing bulk energy is responsible for the separation of fluids.

The gradient part of the free energy represents the weakly non-local interaction between the components [75] and is also responsible for the formation of the mixing layer between the two fluids [15]. The coefficient Λ is sensitive to the exact nature of the long-range interaction of intermolecular potential between the molecules in the system [14]. The structure of the interface is determined by the competition between these philic (gradient energy) and phobic (bulk mixing energy) effects [75].

The value of r provides detail about the base operating condition of the system. $r = 1$ indicates that the system is far below the upper consolute temperature of the liquids and its diminishing value, say $r = 0.1$, indicates the system's closeness to the UCST. Any negative value of r indicates that the system's temperature is above the UCST, wherein the components are completely miscible with no intervening interfaces, and hence, there will be no distinction between the phases. In the present case, r is defined as

$$r = \frac{\exp(-a\vartheta) - \exp(a\vartheta)}{\exp(-a\vartheta) + (Le)\exp(a\vartheta)} \tag{3.6}$$

where the reduced temperature "ϑ" is defined as $(\theta - \theta_{crit})/\theta_{crit}$. a is a positive constant, and Le is the Lewis number which gives the ratio of thermal diffusivity to the mass diffusivity of the components involved. Figure 3.2 gives an idea of how r varies with ϑ for $a = 10$, and $Le = 10$. As can be seen from the figure, r is equal to one when the system is far below the UCST, and it saturates to a value of $-\frac{1}{Le}$ when the system is above UCST. In the present consideration, 'r' provides a convenient means for modelling the immiscible to miscible phase transition through the use of the Heaviside step function $\mathscr{H}(r)$, which is zero for any negative value of r and is one for any non-negative of r.

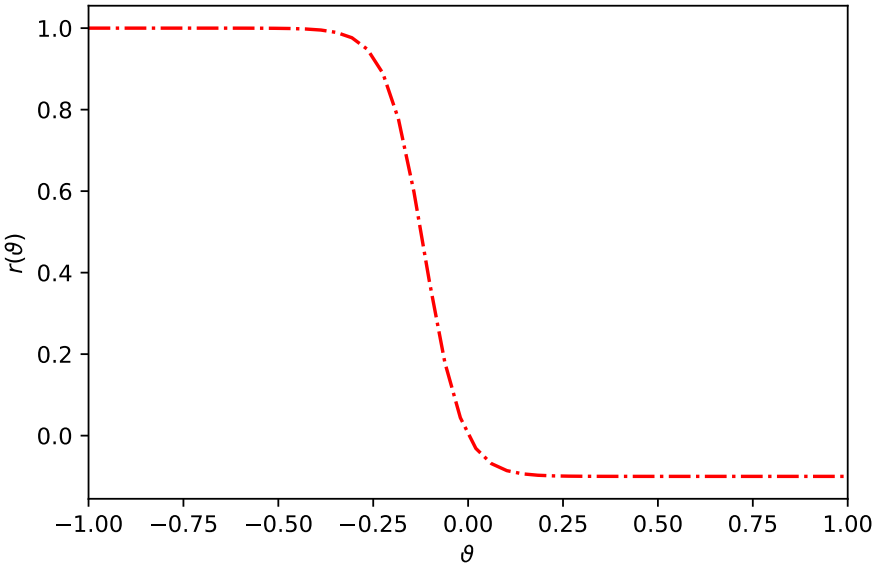

Fig. 3.2 Variation of r with ϑ

Obviously, the current R-B convection problem is non-isothermal, and the value of 'r' would be slightly inhomogeneous in the system. However, such inhomogeneity can be deemed insignificant in the present case as we are interested in the criticality corresponding to the onset of convection. From the Fig. 3.2, it is evident that r reduces from a value of one to $-\frac{1}{Le}$ in the range of ϑ between -0.375 and 0.125. For a typical binary fluid system like FC-72 and 1cSt Silicon Oil with UCST = 315.5 K, this ϑ range corresponds to a large change in the absolute temperature, and correspondingly, the rate of change of 'r' with temperature is meager. Interestingly, for a typical two-fluid configuration as considered by Degen *et al.* [19], the critical temperature difference is of the order of 1K. Note that such temperature difference values are also relatable to the Boussinesq approximation that becomes invalid for larger temperature differences. Thus, the percentage change in r corresponding to 1 K temperature difference is normally very small. Only when the system is very close to UCST, the inhomogeneity in r would become significant. Even in such scenarios, the inhomogeneity can be subdued by considering fluid layers of larger thickness that may result in smaller values of critical temperature difference. Thus, the consideration of constant r is a reasonable assumption for a large range of the problem's parametric space, making the complex problem at hand more tractable.

Note that the generalized chemical potential [3], μ, which is responsible for driving any change in the chemical composition of the system, is given as

$$\mu = \frac{\delta F}{\delta \phi} = \Lambda \left[\frac{\mathscr{H}(r) r^q \phi^3 - r\phi}{\varepsilon^2} - \mathscr{H}(r) r^p \nabla^2 \phi \right] \tag{3.7}$$

We have assumed $\rho_1 c_1 \approx \rho_2 c_2$ while deriving the above expression for the generalized chemical potential. As mentioned before, we will mainly focus on the immiscible or partially miscible cases where the value of r is positive, *i.e.* $0.1 \leq r \leq 1.0$. Hence, we will consider $\mathscr{H}(r) = 1$ for all further analyses.

The kinetic equation for the evolution of the conserved order parameter can be written as [49]

$$\frac{\partial \phi}{\partial t} = -\boldsymbol{\nabla} \cdot \boldsymbol{j}_\phi \tag{3.8}$$

Here, $\boldsymbol{j}_\phi$ is the flux of the order parameter and is given as $\boldsymbol{j}_\phi = -\gamma \boldsymbol{\nabla}(\delta F / \delta \phi) = -\gamma \boldsymbol{\nabla} \mu$ [3]. γ is the mobility of the diffuse interface and is assumed to be a constant [31]. Thus, a general form of phase evolution equation can be written as

$$\frac{\partial \phi}{\partial t} + \boldsymbol{u} \cdot \boldsymbol{\nabla} \phi = \boldsymbol{\nabla} \cdot \left[\gamma \boldsymbol{\nabla} \left\{ \Lambda \left(\frac{r^q \phi^3 - r\phi}{\varepsilon^2} - r^p \nabla^2 \phi \right) \right\} \right] \tag{3.9}$$

This is known as the Cahn-Hilliard (CH) equation. We have added the convective term to include the effects of fluid flow on the species transport [31]. At steady state, there is no bulk movement of the fluids; hence, the base state profile for the order parameter can be obtained by considering a trivial chemical potential, *i.e.* $\mu = 0$. The resulting equation for 'ϕ' can be expressed as

$$\Phi^b(y) = \pm r^{\frac{1-q}{2}} \tanh \left(\frac{y}{\sqrt{2}\varepsilon} r^{\frac{1-p}{2}} \right) \tag{3.10}$$

Figure 3.3 shows the variation of base 'ϕ' in the domain with decreasing 'r', *i.e.,* with increasing operating temperature. Evidently, the peak magnitude of 'ϕ' reduces in both the layers owing to the enhanced solubility of the phases. The interfacial width, being inversely proportional to $r^{\frac{p-1}{2}}$, also increases with the increase in temperature of the system. Here, the contribution of the gradient energy term decreases, and more material is introduced into the interfacial region, thereby creating a wider interface.

Note that proper care should be taken while including the interfacial forces in the momentum equations since we will not be using any explicit matching (jump) conditions at the fluids' interface. The classical concept of the surface tension is contained in the total (bulk+gradient) mixing energy of the system since this mixing energy represents the molecular interaction between the existing phases [75]. The generalized form of the non-viscous/reversible second

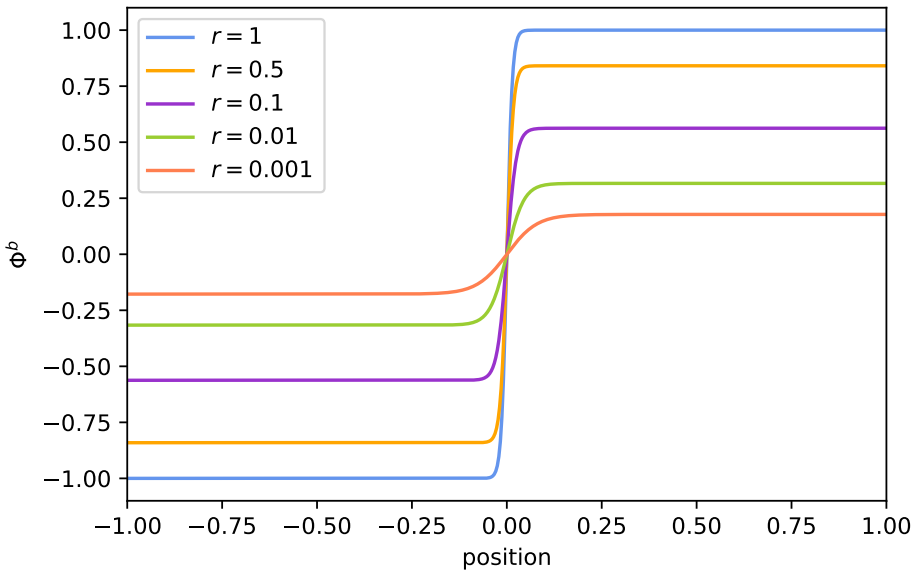

Fig. 3.3 Phase distribution with r

order tensor is given as [3, 73]

$$\boldsymbol{\tau}^{nv} = \mathscr{L}\boldsymbol{I} - \boldsymbol{\nabla}\phi\frac{\partial\mathscr{L}}{\partial(\boldsymbol{\nabla}\phi)} \tag{3.11}$$

where $\mathscr{L} = f_{mix}(\phi,\theta) + \mathscr{H}(r)\frac{\Lambda}{2}r^p|\partial\phi(x)|^2$ is the Lagrangian energy density.

One can account for the surface tension effects through an additional forcing term in the momentum equations. This surface tension force density can be modelled as a bulk stress term obtained as the divergence of the reversible part of the stress tensor acting over the interfacial width, which also inherently represents the Korteweg stress tensor. Thus, the modified Navier-Stokes equations are written as

$$\frac{\partial\rho\boldsymbol{u}}{\partial t} + \boldsymbol{\nabla}\cdot(\rho\boldsymbol{u}\boldsymbol{u}) = -\boldsymbol{\nabla}p + \boldsymbol{\nabla}\cdot\left[\eta\left(\boldsymbol{\nabla}\boldsymbol{u} + (\boldsymbol{\nabla}\boldsymbol{u})^+ - \frac{2}{3}\boldsymbol{\nabla}\cdot\boldsymbol{u}\boldsymbol{I}\right)\right] + \boldsymbol{\nabla}\cdot\left(\mathscr{L}\boldsymbol{I} - \boldsymbol{\nabla}\phi\frac{\partial\mathscr{L}}{\partial(\boldsymbol{\nabla}\phi)}\right) - \rho^{'}g\mathbf{1}_y$$

$$\frac{D\rho}{Dt} + \rho\boldsymbol{\nabla}\cdot\boldsymbol{u} = 0 \tag{3.12}$$

where $\rho^{'} = \rho - \rho_0$ and $\rho = \rho_1(1-\beta_1(\theta-\theta_0))(\frac{1+\phi}{2}) + \rho_2(1-\beta_2(\theta-\theta_0))(\frac{1-\phi}{2})$. ρ_0 is the original density field without any temperature effect. The last term in the Navier-Stokes equation accounts for the buoyancy effect and plays a crucial role in any natural convection problem. The details of its approximation are provided separately in the following section.

At steady state and in the absence of fluid motion, the Navier-Stokes (NS) equation will be reduced to the following form:

$$-\boldsymbol{\nabla} p - \rho^{'} g \mathbf{1}_y = 0 \tag{3.13}$$

Finally, the overall energy balance equation can be written as

$$\frac{\partial \rho c \theta}{\partial t} + \boldsymbol{\nabla} \cdot (\rho \boldsymbol{u} c \theta) + \mu \frac{D\phi}{Dt} + \mathscr{L} \boldsymbol{\nabla} \cdot \boldsymbol{u} = \boldsymbol{\nabla} \cdot (\kappa \boldsymbol{\nabla} \theta), \tag{3.14}$$

where κ is the thermal conductivity. In the subsequent representations of the energy balance equation, the viscous dissipation term will be neglected since it is very small as compared to the amount of heat stored/convected by the system [65, 24]. In the absence of any bulk movement of the fluid elements and at a steady state, the energy equation can be reduced to a simple conduction problem.

$$\boldsymbol{\nabla} \cdot (\kappa \boldsymbol{\nabla} \theta) = 0 \tag{3.15}$$

Note that the phase evolution equation obeys the no flux boundary condition owing to the consideration of impermeable no-slip walls at the top and bottom, as shown in Fig. 3.1.

$$\begin{aligned} \mathbf{1}_y \cdot \boldsymbol{\nabla} \phi &= 0 \ @ y = 0, H \\ \mathbf{1}_y \cdot \boldsymbol{\nabla} \mu &= 0 \ @ y = 0, H \end{aligned} \tag{3.16}$$

Since $\mu = \Lambda \left[\frac{r^q \phi^3 - r\phi}{\varepsilon^2} - r^p \nabla^2 \phi \right]$, we simplify the above equations to obtain

$$\frac{\partial \phi}{\partial y} = \frac{\partial^3 \phi}{\partial y^3} = 0 \ @ y = 0, H \tag{3.17}$$

The velocity conditions at the top and bottom no-slip boundaries are

$$\boldsymbol{u} = 0 \ @ y = 0, H \tag{3.18}$$

Both the walls in the current problem are maintained at constant temperatures; hence, the energy equation will obey the following boundary conditions.

$$\begin{aligned} \theta &= \theta_B \ @ y = 0 \\ \theta &= \theta_T \ @ y = H \end{aligned} \tag{3.19}$$

Since the phase-parameter ϕ acts as a marker for the phases and the interfaces, the various properties of the fluid mixture can be expressed as a linear function of ϕ as follows:

- Density : $\frac{\rho}{\rho_2} = \frac{1}{2}(1+\frac{\rho_1}{\rho_2}) + \frac{\phi}{2}(\frac{\rho_1}{\rho_2} - 1)$
- Dynamic viscosity : $\frac{\eta}{\eta_2} = \frac{1}{2}(1+\frac{\eta_1}{\eta_2}) + \frac{\phi}{2}(\frac{\eta_1}{\eta_2} - 1)$
- Thermal conductivity : $\frac{\kappa}{\kappa_2} = \frac{1}{2}(1+\frac{\kappa_1}{\kappa_2}) + \frac{\phi}{2}(\frac{\kappa_1}{\kappa_2} - 1)$
- Heat capacity : $\frac{\rho c}{\rho_2 c_2} = \frac{1}{2}(1+\frac{\rho_1 c_1}{\rho_2 c_2}) + \frac{\phi}{2}(\frac{\rho_1 c_1}{\rho_2 c_2} - 1)$

3.3 Boussinesq approximation

A typical process of understanding the onset of convection begins by invoking the Boussinesq approximation, which essentially means that the density variation can be neglected everywhere except in the buoyancy term that drives the motion [65, 24]. With this in mind, the continuity, the momentum, and the energy equations can be reduced to the following expressions:

$$\boldsymbol{\nabla} \cdot \boldsymbol{u} = 0 \tag{3.20}$$

$$\rho_0 \left[\frac{\partial \boldsymbol{u}}{\partial t} + \boldsymbol{u} \cdot \boldsymbol{\nabla} \boldsymbol{u} \right] = -\boldsymbol{\nabla} p + \boldsymbol{\nabla} \cdot \left(\eta \left(\boldsymbol{\nabla} \boldsymbol{u} + (\boldsymbol{\nabla} \boldsymbol{u})^{+} \right) \right) + \mu \boldsymbol{\nabla} \phi - \rho^{'} g \mathbf{1}_y \tag{3.21}$$

$$\rho_0 \left[\frac{\partial (c\theta)}{\partial t} + \boldsymbol{u} \cdot \boldsymbol{\nabla} (c\theta) \right] + \mu \frac{D\phi}{Dt} = \boldsymbol{\nabla} \cdot (\kappa \boldsymbol{\nabla} \theta) \tag{3.22}$$

where $\rho^{'} = \rho(\phi, \theta) - \rho_0$, and $\rho = \rho_1(1 - \beta_1(\theta - \theta_0))(\frac{1+\phi}{2}) + \rho_2(1 - \beta_2(\theta - \theta_0))(\frac{1-\phi}{2})$, and $\rho_0 = \frac{\rho_1 + \rho_2}{2}$.

In this simplified representation, the density change brought in by the mixing process is considered only in the buoyancy term and is ignored everywhere else. Unfortunately, such an approximation is limited by its applicability, *i.e.*, for fluids with minimal density disparity. However, in the current problem, the density values of the two fluids are not close; hence, directly implementing this approximation would lead to inconsistent results.

3.4 Partial non-Boussinesq/Boussinesq approximation

In order to overcome the above issue, we consider the effect of phase-mixing on the density field everywhere, not only in the body force term of the N–S equations. However, we will still neglect the temperature-induced density variations in all the terms except buoyancy.

Note that this thermal effect can be neglected as a leading order approximation. Here, the continuity equation takes the following form:

$$\frac{D\rho(\phi)}{Dt} + \rho(\phi)\boldsymbol{\nabla}\cdot\boldsymbol{u} = 0 \tag{3.23}$$

Since $\rho(\phi) = \rho_1(\frac{1+\phi}{2}) + \rho_2(\frac{1-\phi}{2})$, the velocity field is no more solenoidal; rather it carries an expansion part due to the density disparity of the two fluids which can be shown as [17]

$$\boldsymbol{\nabla}\cdot\boldsymbol{u} = -\frac{\rho_1 - \rho_2}{2\rho(\phi)}\frac{D\phi}{Dt} \tag{3.24}$$

The above equation shows that the expansion velocity is proportional to the density difference and the rate of phase evolution. The latter depends on the mobility of the phases and the chemical potential gradient inside the interfacial region. Thus, we can expect this non-solenoidal component of velocity to exist in the mixing layer between two incompressible fluids. Consequently, the momentum balance equation takes the following form to account for the contribution of the non-solenoidal velocity field.

$$\rho(\phi)\left[\frac{\partial\boldsymbol{u}}{\partial t} + \boldsymbol{u}\cdot\frac{\partial\boldsymbol{u}}{\partial\boldsymbol{x}}\right] = -\boldsymbol{\nabla}p + \boldsymbol{\nabla}\cdot\left(\eta\left(\boldsymbol{\nabla u} + (\boldsymbol{\nabla u})^{+} - \frac{2}{3}\boldsymbol{\nabla}\cdot\boldsymbol{uI}\right)\right) + \mu\boldsymbol{\nabla}\phi - \rho^{'}g\mathbf{1}_y \tag{3.25}$$

where $\rho^{'} = \rho(\phi,\theta) - \rho(\phi)$, and $\rho(\phi,\theta) = \rho_1(1-\beta_1(\theta-\theta_0))(\frac{1+\phi}{2}) + \rho_2(1-\beta_2(\theta-\theta_0))(\frac{1-\phi}{2})$, and $\rho(\phi) = \rho_1(\frac{1+\phi}{2}) + \rho_2(\frac{1-\phi}{2})$. This equation is based on the assumption that the second coefficient of viscosity (bulk viscosity) is independent of the rate of fluid compression.

The above consideration gives rise to the quasi-incompressibility condition, where both components are incompressible, and the pressure is kinematic while the velocity field is non-solenoidal [39]. Note that the analysis associated with quasi-incompressible fluids is very complicated since the chemical potential μ becomes a function of the kinematic pressure. Interestingly, one can avoid such complications by taking density-matched fluids in the system. Since we aim to study the R-B convection in a general two-fluid system, such considerations may not be appropriate. One has to then evolve an alternate approach to simplify the analysis. It is worthy to note here that the very definition followed for the velocity field has essentially created the non-solenoidal velocity in the mixing region. This leads us to ponder over alternate means for defining the velocity field such that it would be solenoidal throughout the domain. We now attempt to address this issue in the following section.

3.4.1 Incompressible approach

One may note that the mean velocity was implicitly defined as mass-averaged/barycentric velocity field [17] before.

$$\boldsymbol{u} = \frac{\tilde{\rho}_1 \boldsymbol{u}_1 + \tilde{\rho}_2 \boldsymbol{u}_2}{\rho} \tag{3.26}$$

where $\tilde{\rho}_1$ and $\tilde{\rho}_2$ are the densities of fluid 1 and 2, respectively, and $\rho = \tilde{\rho}_1 + \tilde{\rho}_2$ is the total density. With this mass-averaged velocity, the classical continuity equation, $\partial_t \rho + \boldsymbol{\nabla} \cdot (\rho \boldsymbol{u}) = 0$, is satisfied.

Solving the resulting continuity and momentum formulations in the present case requires more computation than its solenoidal counterpart.

In order to overcome this issue, we will now adopt a different approach as suggested by Boyer [11], Ding *et al.* [20], and Abels *et al.* [1]. The objective is to come up with a solenoidal velocity field throughout the system, including the interfacial region. Correspondingly, the velocity is now defined as a volume-averaged field instead of a mass-averaged one, *i.e.,*

$$\boldsymbol{u} = \frac{\tilde{\rho}_1}{\rho_1} \boldsymbol{u}_1 + \frac{\tilde{\rho}_2}{\rho_2} \boldsymbol{u}_2 \tag{3.27}$$

where ρ_1 and ρ_2 are the densities of the fluid 1 and 2, respectively, in the pure immiscible state. With the above form of velocity field, the mass conservation equations of the individual species involved, $\partial_t \tilde{\rho}_j + \boldsymbol{\nabla} \cdot (\tilde{\rho}_j \boldsymbol{u}_j) = 0$, are satisfied. This yields a solenoidal velocity field, as shown below.

$$\begin{aligned} \boldsymbol{\nabla} \cdot \boldsymbol{u} &= \boldsymbol{\nabla} \cdot \left(\frac{\tilde{\rho}_1 \boldsymbol{u}_1}{\rho_1} \right) + \boldsymbol{\nabla} \cdot \left(\frac{\tilde{\rho}_2 \boldsymbol{u}_2}{\rho_2} \right) \\ &= -\partial_t \left(\frac{\tilde{\rho}_1}{\rho_1} \right) - \partial_t \left(\frac{\tilde{\rho}_2}{\rho_2} \right) \\ &= -\partial_t \left(\frac{\tilde{\rho}_1}{\rho_1} + \frac{\tilde{\rho}_2}{\rho_2} \right) \\ &= \partial_t (1) = 0 \end{aligned} \tag{3.28}$$

However, it does not satisfy the general continuity condition $\partial_t \rho + \boldsymbol{\nabla} \cdot (\rho \boldsymbol{u}) = 0$ as before and instead, it satisfies the following continuity equation while conserving the mass of the individual species.

$$\partial_t \rho + \boldsymbol{\nabla} \cdot (\rho \boldsymbol{u}) + \frac{\partial \rho}{\partial \phi} \boldsymbol{\nabla} \cdot \boldsymbol{j} = 0 \tag{3.29}$$

It is worthy to note that one can recover the general continuity equation by taking fluids of equal densities, where $\frac{\partial \rho}{\partial \phi}$ becomes identically zero. One can also show that the above

PDE conserves the system's total mass by choosing appropriate boundary conditions, for example, the no-flux boundary conditions at the walls. We can integrate the above non-trivial continuity equation over the entire domain of interest.

$$\int_{\mathscr{V}} \partial_t \rho d\mathscr{V} + \int_{\partial\mathscr{V}} \rho \boldsymbol{u} \cdot \boldsymbol{n} d\mathscr{A} + \frac{\partial \rho}{\partial \phi} \int_{\partial\mathscr{V}} \boldsymbol{j}.\boldsymbol{n} d\mathscr{A} = 0 \tag{3.30}$$

The total mass of the system will be conserved *i. e.* $\frac{d}{dt}\int_{\mathscr{V}} \rho d\mathscr{V} = 0$, if there is no exchange of fluxes across the domain boundaries :

$$\begin{aligned} \boldsymbol{j} \cdot \boldsymbol{n} &= 0 \\ \boldsymbol{u} \cdot \boldsymbol{n} &= 0 \end{aligned} \tag{3.31}$$

With the above volume-averaging of the velocity field, the Cahn-Hilliard (CH) equation still remains the same as before.

$$\frac{\partial \phi}{\partial t} + \boldsymbol{u} \cdot \boldsymbol{\nabla} \phi = \boldsymbol{\nabla} \cdot \left[\gamma \boldsymbol{\nabla} \left\{ \Lambda \left(\frac{r^q \phi^3 - r\phi}{\varepsilon^2} - r^p \nabla^2 \phi \right) \right\} \right] \tag{3.32}$$

However, the conservative form of the momentum equation takes the form [20]:

$$\frac{\partial \rho \boldsymbol{u}}{\partial t} + \boldsymbol{\nabla} \cdot (\rho \boldsymbol{u}\boldsymbol{u}) + \boldsymbol{u} \frac{\partial \rho}{\partial \phi} \boldsymbol{\nabla} \cdot \boldsymbol{j}_\phi = -\boldsymbol{\nabla} p + \boldsymbol{\nabla} \cdot \left(\eta \left(\boldsymbol{\nabla} \boldsymbol{u} + (\boldsymbol{\nabla} \boldsymbol{u})^+ \right) \right) + \mu \boldsymbol{\nabla} \phi - \rho^{'} g \hat{\mathbf{1}}_y \tag{3.33}$$

$$\boldsymbol{\nabla} \cdot \boldsymbol{u} = 0 \tag{3.34}$$

The equation accounts for the advection due to the relative diffusional flux of species, and this eliminates an artificial interfacial force. Fortunately, the non-conservative form of the above equation can be written in simple form as follows:

$$\rho_0 \left(\frac{\partial \boldsymbol{u}}{\partial t} + \boldsymbol{u} \cdot \boldsymbol{\nabla} \boldsymbol{u} \right) = -\boldsymbol{\nabla} p + \boldsymbol{\nabla} \cdot \left(\eta \left(\boldsymbol{\nabla} \boldsymbol{u} + (\boldsymbol{\nabla} \boldsymbol{u})^+ \right) \right) + \mu \boldsymbol{\nabla} \phi - \rho^{'} g \hat{\mathbf{1}}_y \tag{3.35}$$

The conservative form of the energy equation takes the form:

$$\frac{\partial \rho_0 c \theta}{\partial t} + \boldsymbol{\nabla} \cdot (\rho_0 \boldsymbol{u} c \theta) + \theta \frac{\partial \rho_0 c}{\partial \phi} \boldsymbol{\nabla} \cdot \boldsymbol{j}_\phi + \mu \frac{D\phi}{Dt} = \boldsymbol{\nabla} \cdot (\kappa \boldsymbol{\nabla} \theta) \tag{3.36}$$

where we have neglected the viscous dissipation since the magnitude of the dissipation is much lower compared to the storage/advection of the energy in a naturally convected flow

[24]. Its non-conservative counterpart is

$$\rho_0 c\left(\frac{\partial \theta}{\partial t}+\boldsymbol{u}\cdot\boldsymbol{\nabla}\theta\right)+\mu\frac{D\phi}{Dt}=\boldsymbol{\nabla}\cdot(\kappa\boldsymbol{\nabla}\theta) \tag{3.37}$$

In summary, the governing equations considered for the current analysis are given below.

$$\frac{\partial \phi}{\partial t}+\boldsymbol{u}\cdot\boldsymbol{\nabla}\phi=\boldsymbol{\nabla}\cdot\left[\gamma\boldsymbol{\nabla}\left\{\Lambda\left(\frac{r^q\phi^3-r\phi}{\varepsilon^2}-r^p\nabla^2\phi\right)\right\}\right] \tag{3.38}$$

$$\boldsymbol{\nabla}\cdot\boldsymbol{u}=0 \tag{3.39}$$

$$\rho_0\left(\frac{\partial \boldsymbol{u}}{\partial t}+\boldsymbol{u}\cdot\boldsymbol{\nabla}\boldsymbol{u}\right)=-\boldsymbol{\nabla}p+\boldsymbol{\nabla}\cdot\left(\eta\left(\boldsymbol{\nabla}\boldsymbol{u}+(\boldsymbol{\nabla}\boldsymbol{u})^{+}\right)\right)+\mu\boldsymbol{\nabla}\phi-\rho^{'}g\hat{\mathbf{1}}_y \tag{3.40}$$

$$\rho_0 c\left(\frac{\partial \theta}{\partial t}+\boldsymbol{u}\cdot\boldsymbol{\nabla}\theta\right)+\mu\frac{D\phi}{Dt}=\boldsymbol{\nabla}\cdot(\kappa\boldsymbol{\nabla}\theta) \tag{3.41}$$

3.4.2 Linear stability analysis

With the phase-field formulation described above, we now proceed with the actual objective of understanding the onset of RBM convection in binary fluid systems. To this effect, we now carry out linear stability analysis, which will provide information on the critical parameter value for the onset of convection and the nature of convection, say oscillatory or non-oscillatory. Note that the oscillatory mode of onset is observed when two non-oscillatory modes (mechanical and thermal coupling modes) compete with each other. This overstability condition happens when the value of $\rho\beta\kappa_T$ differs significantly from unity [54]. We essentially intend to understand the evolution of infinitesimal perturbations that are imposed on a quiescent base state. As discussed earlier, the base state conditions are given as follows:

$$\Phi^b(y)=\pm r^{\frac{1-q}{2}}\tanh\left(\frac{y}{\sqrt{2}\varepsilon}r^{\frac{1-p}{2}}\right) \tag{3.42}$$

$$\boldsymbol{\nabla}p=-\rho^{'}g\mathbf{1}_y \tag{3.43}$$

$$\boldsymbol{\nabla}\cdot(\kappa\boldsymbol{\nabla}\theta)=0 \tag{3.44}$$

Correspondingly, all the relevant quantities are represented as

$$\begin{aligned}\phi&=\Phi^b(y)+\phi^{'}(x,y,t)\\ u_i&=u_i^{'}(x,y,t)\\ \theta&=\Theta^b(y)+\theta^{'}(x,y,t)\\ p&=p^b(y)+p^{'}(x,y,t)\end{aligned} \tag{3.45}$$

The perturbed quantities are assumed to be very small compared to the corresponding base quantities; hence, any product of perturbed quantities can be neglected. So, upon substitution of the above expressions in the governing equations and subtracting the corresponding base state relations, we obtain the linearized equations for the evolution of perturbations as

$$\frac{\partial \phi^{'}}{\partial t} + u_j^{'} \frac{\partial \Phi^b}{\partial x_j} = \nabla_m \left[\gamma \nabla_m \left\{ \Lambda \left(\frac{r^q 3 (\Phi^b)^2 \phi^{'} - r\phi^{'}}{\varepsilon^2} - r^p \nabla^2 \phi^{'} \right) \right\} \right] \tag{3.46}$$

$$\begin{aligned} \frac{\partial u_i^{'}}{\partial t} = & -\frac{\nabla_i p^{'}}{\rho(\Phi^b)} + \frac{\eta_2}{\rho(\Phi^b)} \nabla_j \left[\left(\frac{1}{2}(1 + \frac{\eta_1}{\eta_2}) + \frac{\Phi^b}{2}(\frac{\eta_1}{\eta_2} - 1) \right) (\nabla_j u_i^{'} + \nabla_i u_j^{'}) \right] + \frac{1}{\rho(\Phi^b)} \mu^{'} \nabla_i \phi^b \\ & + \frac{1}{\rho(\Phi^b)} \frac{\rho_1 \beta_1 - \rho_2 \beta_2}{2} \Theta^b \phi^{'} g \delta_{i2} + \frac{1}{\rho(\Phi^b)} \left[\frac{\rho_1 \beta_1 + \rho_2 \beta_2}{2} + \frac{\rho_1 \beta_1 - \rho_2 \beta_2}{2} \Phi^b \right] \theta^{'} g \delta_{i2} \end{aligned} \tag{3.47}$$

$$\nabla_i u_i^{'} = 0 \tag{3.48}$$

$$\begin{aligned} \rho c(\Phi^b) \left[\frac{\partial \theta^{'}}{\partial t} + u_j^{'} \frac{\partial \Theta^b}{\partial x_j} \right] = & \kappa^b \nabla_m{}^2 \theta^{'} + (\nabla_m \kappa^b)(\nabla_m \theta^{'}) \\ & + (\nabla_m k^{'})(\nabla_m \Theta^b) + \kappa_f(\phi^{'}) \nabla_m{}^2 \Theta^b \end{aligned} \tag{3.49}$$

We now non-dimensionalize the above equations using the following scales.

$$L_R = H_2 \qquad t_R = \frac{H_2{}^2}{\kappa_{T2}} \qquad u_R = \frac{\kappa_{T2}}{H_2} \qquad \theta_R = \theta_B - \theta_T \qquad p_R = \frac{\rho_2 \kappa_{T2} \nu_2}{H_2{}^2}$$

The resulting dimensionless equations can be written as follows.

$$\frac{\partial \phi^{'}}{\partial t} + u_j^{'} \frac{\partial \Phi^b}{\partial x_j} = M \nabla_m^2 \left[\left(r^q 3 (\Phi^b)^2 \phi^{'} - r\phi^{'} - \left(\frac{\varepsilon}{H_2} \right)^2 r^p \nabla_n^2 \phi^{'} \right) \right] \tag{3.50}$$

$$\begin{aligned}\frac{\partial u_i^{'}}{\partial t} &= -Pr_2\frac{\nabla_i p^{'}}{\rho_f(\Phi^b)} + Pr_2\frac{1}{\rho_f(\Phi^b)}\nabla_j\left[\left(\frac{1}{2}(1+\frac{\eta_1}{\eta_2})+\frac{\Phi^b}{2}(\frac{\eta_1}{\eta_2}-1)\right)(\nabla_j u_i^{'}+\nabla_i u_j^{'})\right] \\ &+ (\frac{H_2}{\varepsilon})^2\Gamma_\theta\frac{1}{\rho_f(\Phi^b)}\mu^{'}\nabla_i\phi^b + \frac{1}{\rho_f(\Phi^b)}Ra_2Pr_2\frac{1}{2}\left(\frac{\rho_1\beta_1}{\rho_2\beta_2}-1\right)\Theta^b\phi^{'}\delta_{i2} \\ &+ \frac{1}{\rho_f(\Phi^b)}Ra_2Pr_2\left[\frac{1}{2}\left(\frac{\rho_1\beta_1}{\rho_2\beta_2}+1\right)+\frac{1}{2}\left(\frac{\rho_1\beta_1}{\rho_2\beta_2}-1\right)\Phi^b\right]\theta^{'}\delta_{i2}\end{aligned} \tag{3.51}$$

$$\nabla_i u_i^{'} = 0 \tag{3.52}$$

$$\begin{aligned}(\rho c)_f(\Phi^b)\left[\frac{\partial\theta^{'}}{\partial t}+u_j{}^{'}\frac{\partial\Theta^b}{\partial x_j}\right] =& \kappa_f(\Phi^b)\nabla_m{}^2\theta^{'} + (\nabla_m\kappa_f(\Phi^b))(\nabla_m\theta^{'}) \\ &+ (\nabla_m\kappa_f(\phi^{'}))(\nabla_m\Theta^b) + \kappa_f(\phi^{'})\nabla_m{}^2\Theta^b\end{aligned} \tag{3.53}$$

Here, $M = \frac{\gamma\Lambda_0}{\varepsilon^2\kappa_{T_2}}$ is the non-dimensional mobility, which is the ratio of the diffusivity of the interface to the thermal diffusivity of the reference fluid. $\Gamma_\theta = \frac{\Lambda_0}{\rho_2\kappa_{T_2}^2}$ represents the modified inverse Capillary number, which gives the ratio of capillary forces. Here, the word 'modified' essentially refers to the fact that thermal diffusivity κ_T has been used instead of kinematic viscosity ν to calculate these dimensionless numbers. μ is dimensionless here. $(\rho c)_f(\Phi^b) = \frac{1}{2}(1+\frac{\rho_1 c_1}{\rho_2 c_2})+\frac{\Phi^b}{2}(\frac{\rho_1 c_1}{\rho_2 c_2}-1)$, and $\rho_f(\Phi^b) = \frac{1}{2}(1+\frac{\rho_1}{\rho_2})+\frac{\Phi^b}{2}(\frac{\rho_1}{\rho_2}-1)$

Proceeding further, we now expand all the perturbed quantities in terms of normal modes. Note that the modes are periodic in the horizontal direction for the present consideration. Correspondingly, we use

$$\begin{aligned}\phi &= \Phi^b(y) + \hat{\phi}(y)\exp(\lambda t + ikx) \\ u_i &= \hat{u}_i(y)\exp(\lambda t + ikx) \\ \theta &= \Theta^b(y) + \hat{\theta}(y)\exp(\lambda t + ikx) \\ p &= p^b(y) + \hat{p}(y)\exp(\lambda t + ikx)\end{aligned} \tag{3.54}$$

All the linearized perturbation equations get transformed as follows:

$$\lambda\hat{\phi}+\hat{v}\frac{\partial\Phi^b}{\partial y}=M\Bigg[r^q 3\Bigg(-(\Phi^b)^2k^2\hat{\phi}+2(\frac{d\Phi^b}{dy})^2\hat{\phi}+2\Phi^b\frac{d^2\Phi^b}{dy^2}\hat{\phi}+4\Phi^b\frac{d\Phi^b}{dy}\frac{d\hat{\phi}}{dy}+(\Phi^b)^2\frac{d^2\hat{\phi}}{dy^2}\Bigg) -r\Bigg(-k^2\hat{\phi}+\frac{d^2\hat{\phi}}{dy^2}\Bigg)-\left(\frac{\varepsilon}{H_2}\right)^2 r^p\left(\frac{d^4\hat{\phi}}{dy^4}-2k^2\frac{d^2\hat{\phi}}{dy^2}+k^4\hat{\phi}\right)\Bigg] \tag{3.55}$$

$$\begin{aligned}\lambda\hat{u}=&-\frac{1}{\rho_f(\Phi^b)}Pr_2(\imath k)\hat{p}+\frac{1}{\rho_f(\Phi^b)}Pr_2\left[\frac{1}{2}(1+\frac{\eta_1}{\eta_2})+\frac{\Phi^b}{2}(\frac{\eta_1}{\eta_2}-1)\right](-k^2+\frac{d^2}{dy^2})\hat{u}\\&+\frac{1}{\rho_f(\Phi^b)}Pr_2\frac{1}{2}(\frac{\eta_1}{\eta_2}-1)\frac{d\Phi^b}{dy}\frac{d\hat{u}}{dy}+\frac{1}{\rho_f(\Phi^b)}Pr_2\frac{1}{2}(\frac{\eta_1}{\eta_2}-1)\frac{d\Phi^b}{dy}(ik\hat{v})\end{aligned} \tag{3.56}$$

$$\begin{aligned}\lambda\hat{v}=&-\frac{1}{\rho_f(\Phi^b)}Pr_2\frac{d\hat{p}}{dy}+\frac{1}{\rho_f(\Phi^b)}Pr_2\left[\frac{1}{2}(1+\frac{\eta_1}{\eta_2})+\frac{1}{\rho_f(\Phi^b)}\frac{\Phi^b}{2}(\frac{\eta_1}{\eta_2}-1)\right](-k^2+\frac{d^2}{dy^2})\hat{v}\\&+\frac{1}{\rho_f(\Phi^b)}Pr_2(\frac{\eta_1}{\eta_2}-1)\frac{d\Phi^b}{dy}\frac{d\hat{v}}{dy}\\&-(\frac{H_2}{\varepsilon})^2\Gamma_\theta\frac{1}{\rho_f(\Phi^b)}\left(r^q 3(\Phi^b)^2\hat{\phi}-r\hat{\phi}-\left(\frac{\varepsilon}{H_2}\right)^2 r^p\nabla^2\hat{\phi}\right)\frac{d\Phi^b}{dy}\\&+\frac{1}{\rho_f(\Phi^b)}Ra_2Pr_2\frac{1}{2}\left(\frac{\rho_1\beta_1}{\rho_2\beta_2}-1\right)\Theta^b\hat{\phi}\\&+\frac{1}{\rho_f(\Phi^b)}Ra_2Pr_2\left[\frac{1}{2}\left(\frac{\rho_1\beta_1}{\rho_2\beta_2}+1\right)+\frac{1}{2}\left(\frac{\rho_1\beta_1}{\rho_2\beta_2}-1\right)\Phi^b\right]\hat{\theta}\end{aligned} \tag{3.57}$$

$$ik\hat{u}+\frac{d\hat{v}}{dy}=0 \tag{3.58}$$

$$\begin{aligned}(\rho c)_f(\Phi^b)\left[\lambda\hat{\theta}+\hat{v}\frac{\partial\Theta^b}{\partial y}\right]=&\left[\frac{1}{2}(1+\frac{\kappa_1}{\kappa_2})+\frac{\Phi^b}{2}(\frac{\kappa_1}{\kappa_2}-1)\right](-k^2+\frac{d^2}{dy^2})\hat{\theta}\\&+\frac{1}{2}(\frac{\kappa_1}{\kappa_2}-1)\frac{d\Phi^b}{dy}\frac{d\hat{\theta}}{dy}+\frac{1}{2}(\frac{\kappa_1}{\kappa_2}-1)\frac{d\hat{\phi}}{dy}\frac{d\Theta^b}{dy}\\&+\left[\frac{\hat{\phi}}{2}(\frac{\kappa_1}{\kappa_2}-1)\right]\frac{d^2\Theta^b}{dy^2}\end{aligned} \tag{3.59}$$

The associated boundary conditions at the top and bottom plates are as follows:

$$\begin{aligned} \frac{\partial \hat{\phi}}{\partial y} = \frac{\partial^3 \hat{\phi}}{\partial y^3} = 0 \quad @y = 0,1 \\ \hat{u_i} = 0 \quad @y = 0,1 \\ \hat{\theta} = 0 \quad @y = 0,1 \end{aligned} \tag{3.60}$$

Following the linearization and normal mode expansion, we have all the unknowns in terms of the vertical coordinate. Owing to the accuracy requirements for predicting critical values for the onset of convection, we spatially discretize the variables using the Chebyshev pseudo-spectral method. Here, any variable Ξ can be expressed via a Lagrangian interpolation of values at the collocation points as

$$\Xi_N(y) = \sum_{i=0}^{N} h_i(y)\Xi(y_i), \tag{3.61}$$

where N is the number of collocation points along the vertical direction. The cardinal function, $h_i(y)$, defined over the collocation points, $y_i = \cos\frac{\pi N}{i}$, is expressed as

$$h_i(y) = \frac{(-1)^{i+1}(1-y^2){T_N}'(y)}{\overline{c_i}N^2(y-y_i)} \tag{3.62}$$

where $\overline{c_i} = 2$ for the endpoints and 1 for all in-between points. ${T_N}'(y)$ is the N^{th} derivative of the Chebyshev polynomial of the first kind. To avoid the generation of spurious pressure modes, the pressure variable alone is expanded as

$$p_{N-2}(y) = \sum_{i=1}^{N-1} \hat{h}_i(y)p(y_i) \tag{3.63}$$

wherein, the cardinal function, $\hat{h}_i(y)$, is defined as

$$\hat{h}_i(y) = \frac{(1-{y_i}^2)}{(1-y)}h_i(y) \tag{3.64}$$

Note that the choice of grid points in the above formulation is restricted to the standard Gauss-Lobatto-Chebyshev (G-L-C) points owing to the stringent accuracy requirements. Unfortunately, these G-L-C points are finer at domain extremities and are coarser in the middle. Such a configuration poses an issue in the present scenario, where sufficient grid points are required around the diffuse interface to calculate the gradients of all variables accurately.

Thus one might have to use an exorbitant number of points so that the diffuse interface is sufficiently resolved. In this work, we use an alternate and effective means of resolving the diffuse interface by mapping the clustered points around the diffuse interface in the physical domain to the classical G-L-C points in the computational domain. Correspondingly, we use a transformation suggested by Tee and Trefethen [67] instead of the standard G-L-C grid points:

$$\tilde{y} = g(y) = \delta + \in \sinh\left[\left(\sinh^{-1}\left(\frac{1-\delta}{\in}\right) + \sinh^{-1}\left(\frac{1+\delta}{\in}\right)\right)\frac{y-1}{2} + \sinh^{-1}\left(\frac{1-\delta}{\in}\right)\right] \tag{3.65}$$

Here, $\in$ is the factor that decides the arrangement of the nodes in the transformed grid system, and the value of δ determines the position of the interface in the domain. Lower the value of $\in$, denser the interfacial region in the mapped domain (refer to Fig.2 from [23]). One has to be careful while choosing the $\in$ value as too dense an interfacial region would starve other regions of points and eventually blow up for higher order derivatives.

Since the spatial derivative values are calculated in the original Chebyshev grid system, we will use the following transformation relations to get the derivatives of any variable Ξ in the physical domain.

$$\begin{aligned}
\frac{d\Xi}{d\tilde{y}} &= \frac{1}{g'}\frac{d\Xi}{dy} \\
\frac{d^2\Xi}{d\tilde{y}^2} &= \frac{1}{(g')^2}\frac{d^2\Xi}{dy^2} - \frac{g''}{(g')^3}\frac{d\Xi}{dy} \\
\frac{d^3\Xi}{d\tilde{y}^3} &= \frac{1}{(g')^3}\frac{d^3\Xi}{dy^3} - \frac{3g''}{(g')^4}\frac{d^2\Xi}{dy^2} - \frac{g'g''' - 3(g'')^2}{(g')^5}\frac{d\Xi}{dy} \\
\frac{d^4\Xi}{d\tilde{y}^4} &= \frac{1}{(g')^4}\frac{d^4\Xi}{dy^4} - \frac{6g''}{(g')^5}\frac{d^3\Xi}{dy^3} - \frac{4g'g''' - 15(g'')^2}{(g')^6}\frac{d^2\Xi}{dy^2} \\
&\quad - \frac{(g')^2 g'''' - 10g'g''g''' + 15(g'')^3}{(g')^7}\frac{d\Xi}{dy}
\end{aligned} \tag{3.66}$$

With the above polynomial expansions and grid transformations applied for different variables, the set of normal-mode equations that govern equations that govern the evolution of perturbations can be represented as a generalized eigenvalue problem of the form $A\underline{X} = \lambda B\underline{X}$. This eigenvalue problem has been presently solved by using the standard QR algorithm. Note that solving the generalized eigenvalue problem in the above form may typically give rise to spurious modes due to the zero-valued rows in matrix B occurring on account of the continuity equation and the boundary conditions. These spurious modes pose a serious threat to finding the largest eigenvalue since these large spurious modes may be confused

with the actual eigenvalues. To avoid such a scenario, we employ the reciprocal approach. Instead of finding the largest eigenvalue for $A\underline{X} = \lambda B\underline{X}$, we aim for the smallest eigenvalue for $\lambda A\underline{X} = B\underline{X}$. We check for the presence of zero-valued eigenvectors while calculating these eigenvalues, and if found, we discard those from the eigenvalue calculation process.

3.5 Single-layer counterpart

The underlying premise of the phase-field model is that it treats the entire domain as a single continuum, and the phase variable acts as a marker for different fluids present in the system and the intervening interface between the fluids. Therefore, with appropriate property considerations, it should be possible to verify this premise and make the present formulation mimic the single-layer Rayleigh-Bénard convection. Correspondingly, we carry out our first consistency test wherein we assume the same properties for both the fluids and a uniform phase-field distribution in the domain. Here, the phase evolution equation gets decoupled from other equations, and latter get transformed to

$$\frac{\partial u_i^{'}}{\partial t} = -\frac{\nabla_i p^{'}}{\rho_0} + \nu \nabla_j^2 u_i^{'} + \beta \theta^{'} g \delta_{i2} \tag{3.67}$$

$$\nabla_i u_i^{'} = 0 \tag{3.68}$$

$$\frac{\partial \theta^{'}}{\partial t} + u_j^{'} \frac{\partial \Theta^b}{\partial x_j} = \kappa_T \nabla_j^2 \theta^{'} \tag{3.69}$$

We evaluate the critical Rayleigh number for different modes by employing the normal mode analysis and computing the eigen-spectra. Fig. 3.4 shows the variation of the marginal Rayleigh number with respect to the wave number of the imposed disturbances for the most dangerous mode (1st even mode) and the next dangerous mode (1st odd mode), scaled by a factor of $\frac{1}{10}$. Evidently, the present analysis is able to estimate the critical Ra and the critical wavelength of the system very accurately.

3.6 Choice of fluid properties

Any analysis of complex problems like a two-layer Rayleigh-Bénard problem is fraught with the challenge of identifying the proper parametric space for analysis. Along with the different property ratios of the fluids, the present phase-field formulation utilizes four more

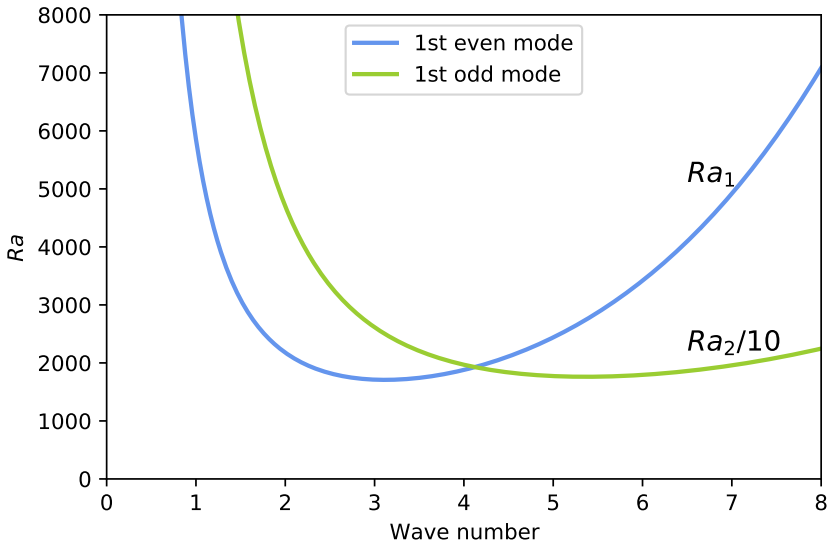

Fig. 3.4 Neutral curves for the first two modes
(Single layer RB problem)

non-dimensional parameters to characterize the two-layer RB convection. This complicates the scenario further, and as a remedy, we resort to the concept of balanced contrast proposed by Colinet and Legros [16]. Accordingly, we choose the properties such that the combination of properties, $(\rho\beta\kappa_T)_r$, is maintained at a value of 0.125. At the same time, following Diwakar *et al.* [22], we choose the other properties such that they yield unique values of a^*. Note that a^* is the critical height at which the Rayleigh numbers of the two layers are equal and is given as

$$a^* = \left(\frac{\beta_r \rho_r}{\kappa_r \kappa_{T\,r} \eta_r}\right)^{\frac{1}{4}}$$

Correspondingly, the following property ratios have been chosen to perform the grid independence test, consistency check and to obtain further results:

$$\rho_r = \frac{\rho_1}{\rho_2} = 2 \quad \eta_r = \frac{\eta_1}{\eta_2} = 1 \quad \beta_r = \frac{\beta_1}{\beta_2} = 0.125 \quad \kappa_r = \frac{\kappa_1}{\kappa_2} = 0.5 \quad c_r = \frac{c_1}{c_2} = 0.5$$

Different values of a^* have been obtained by varying the viscosity ratio, as shown in the table below.

Note that the lighter fluid is placed above the denser one to avoid Rayleigh-Taylor instability. Since we know the property ratios will approach unity once the miscibility of the fluids increases, we have kept the expansivity of the top layer to a relatively higher value to

a^*	1.0	0.667	1.5
$\frac{\eta_1}{\eta_2}$	1.0	5.0625	0.1975

Table 3.1 Viscosity ratios for different a^*

avoid the overturning of the fluids. The other non-dimensional parameters are

$$M = 1500 \qquad \Gamma_\theta = 1000 \qquad Pr_2 = 1.0$$

3.7 Consistency check: Sharp interface and the immiscible limit

3.7.1 Grid independence test

To begin with, we perform a grid independence test to ensure that the results are insensitive to the number of collocation points used to spatially discretize the variables in the y-direction. Here, the test has been performed for different values of $N(= 72, 96, 120, 144)$, where N is the number of collocation points in the domain. The a^* value of the system is 1.0. Fig. 3.5 shows the identical results obtained for all grid sizes greater than 72. Hence, all the current calculations have been performed here with $N = 72$ to save on the computational effort.

3.7.2 Check for consistency

Despite the numerous modifications to the governing equations and the boundary conditions, the phase-field method (PFM) should ideally recover the sharp interface results in the limit of vanishing interfacial thickness. Hence, we now check the consistency of the current model by choosing $\frac{\varepsilon}{H_2} = 10^{-4}$ to mimic the sharp interface limit of the immiscible fluids. The details of the current implementation of the sharp interface approach via a domain decomposition model (DDM) is presented in Appendix - A. Figures 3.6 and 3.7 show the consistency results for different values of viscosity and conductivity ratios while the other properties are maintained as follows: $\frac{\rho_1}{\rho_2} = 2, \frac{\beta_1}{\beta_2} = 0.125, \frac{\kappa_1}{\kappa_2} = 0.5, \frac{c_1}{c_2} = 0.5$.

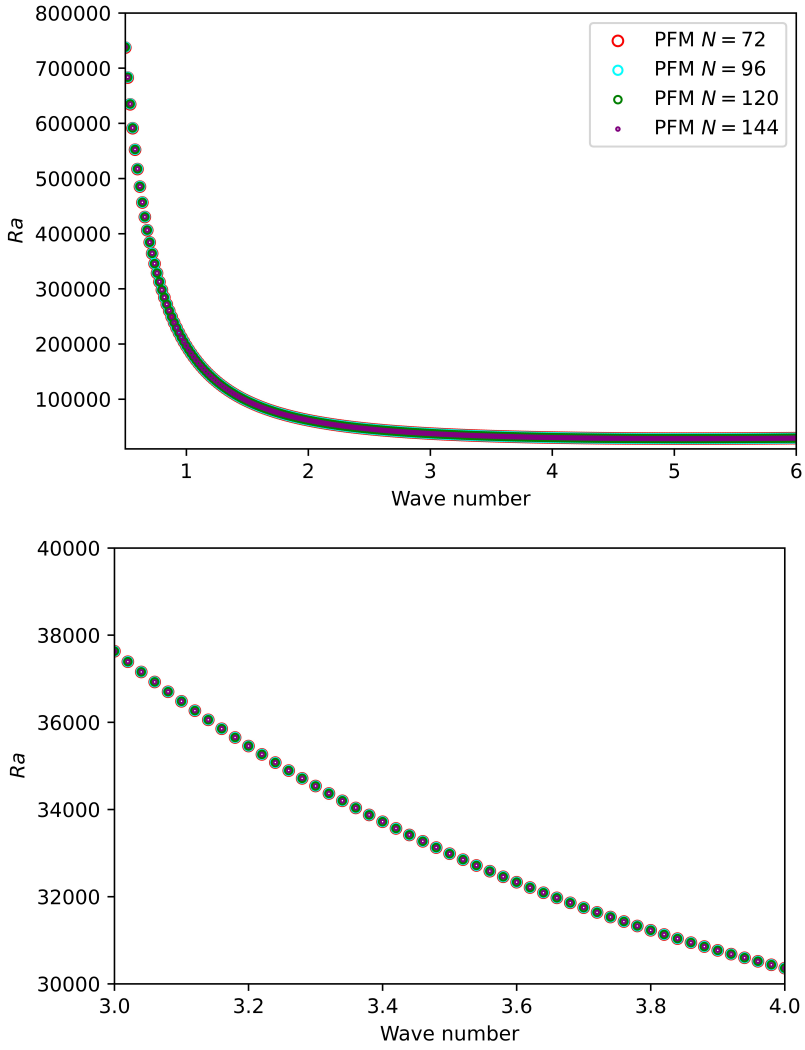

Fig. 3.5 Top: Grid Independence Result; Bottom: Magnified View

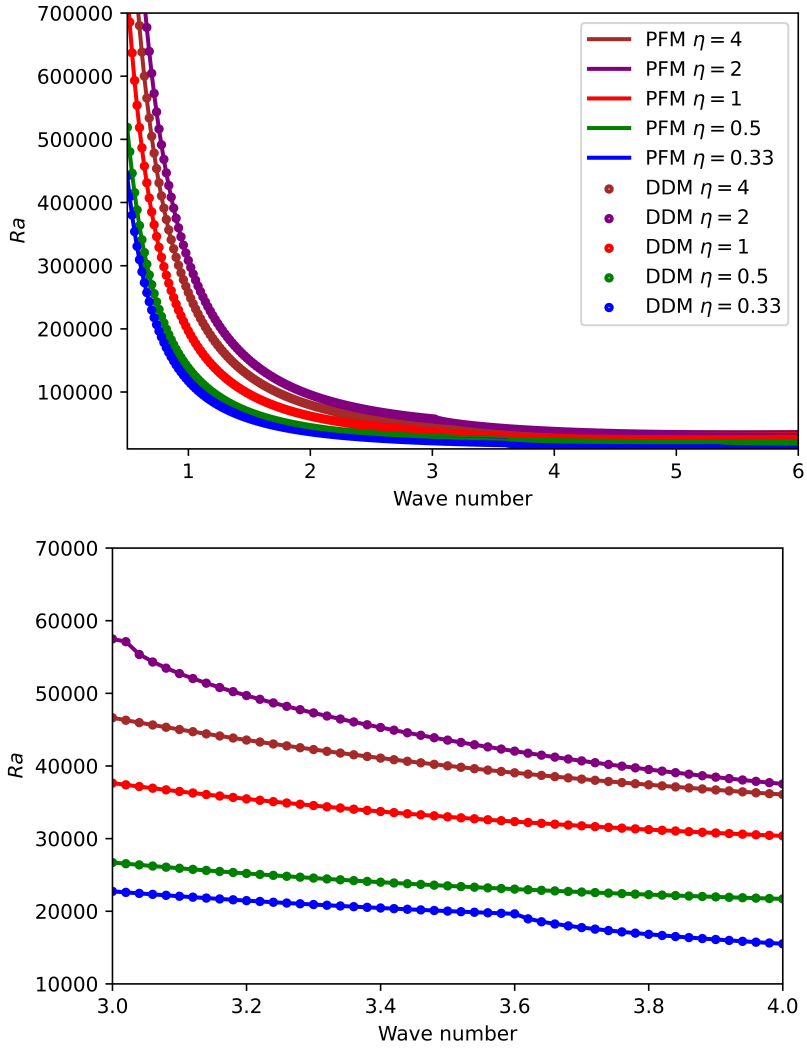

Fig. 3.6 Top: Comparison between PFM and DDM (Variable Viscosity); Bottom: Magnified view

In Figs. 3.6 and 3.7, the calculations have been carried out at an interfacial height, $y_I = 0.5$, and the values of the marginal Rayleigh number have been plotted against the wave number of the disturbance.

Figure 3.8 shows the critical values of the Rayleigh number plotted against the position of the interface. The properties are the same as those chosen for the grid independence test. It is evident from the figures that an exact match is obtained between the results of the domain decomposition method and the current phase field model for a limiting value of interfacial thickness.

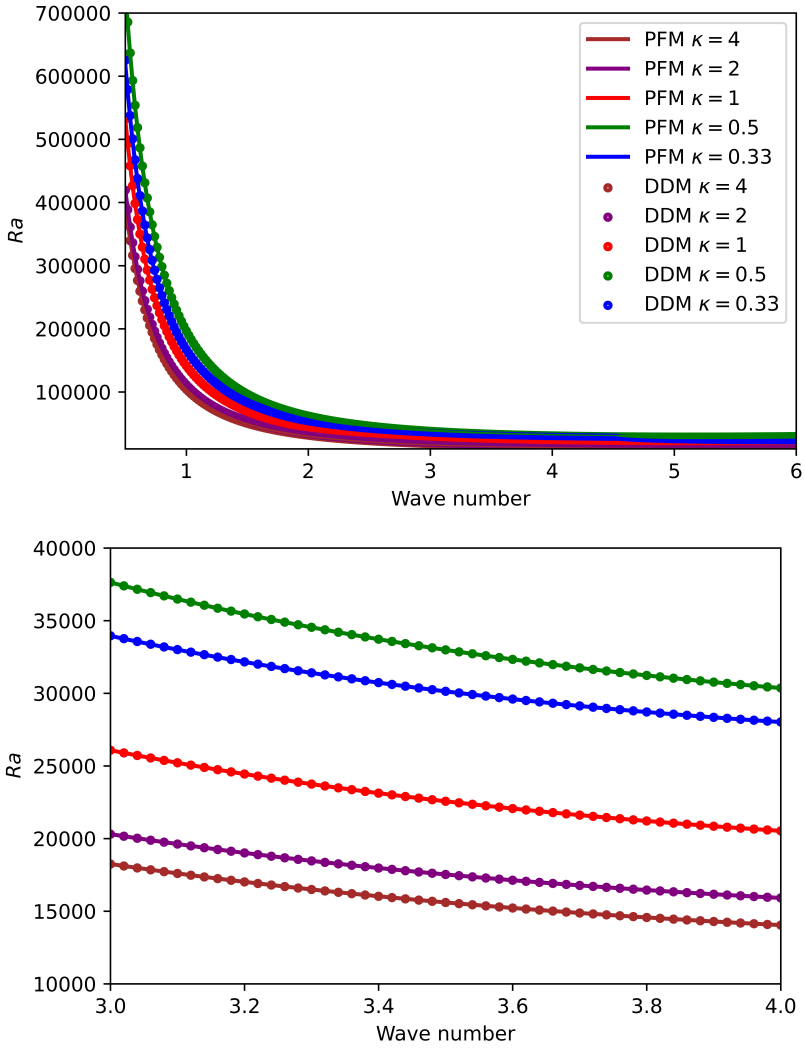

Fig. 3.7 Top: Comparison between PFM and DDM (Variable Conductivity); Bottom: Magnified view

3.8 Results and discussions

In this results section, our primary goal is to understand how the onset characteristics of Rayleigh-Bénard convection, starting with a completely immiscible state of a binary fluid system, varies as the system approaches the critical point. In other words, the interest is to understand the pattern of deviation from the pure immiscible behavior as the fluid system approaches the UCST. Correspondingly, we start with the immiscible consideration of fluids (far below UCST) and then introduce the factor of miscibility 'r' that changes with the system's temperature. The range of r considered here varies between 1.0 and 0.005; $r = 1.0$

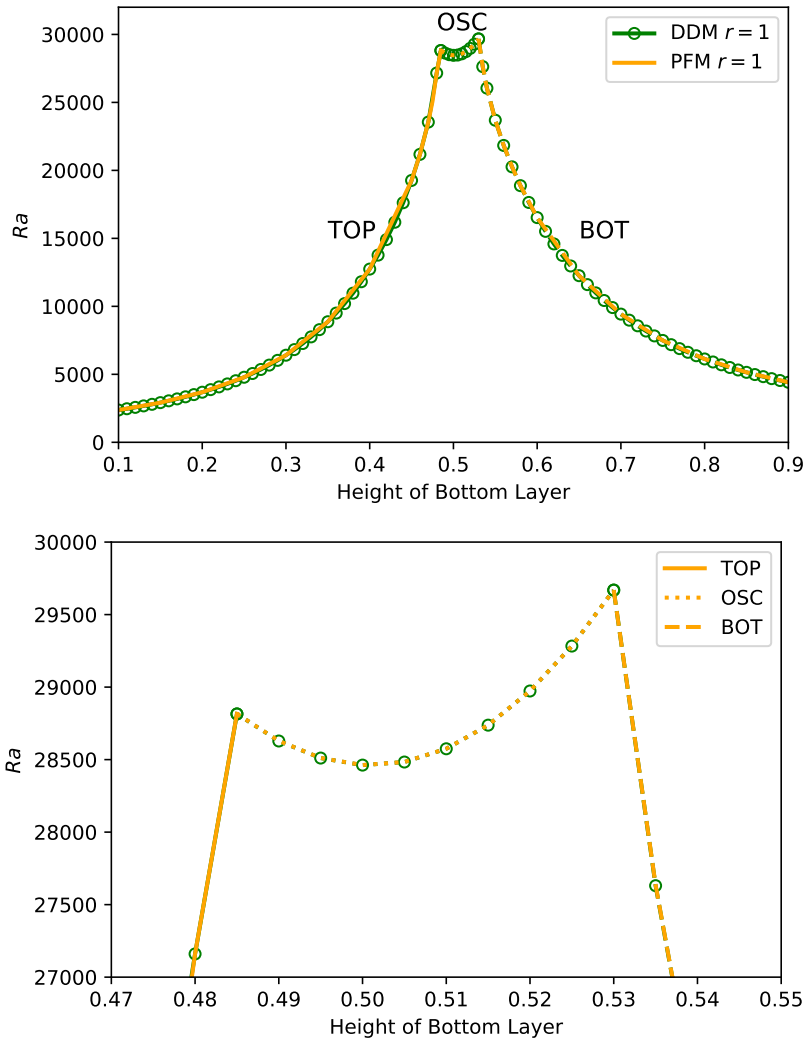

Fig. 3.8 Top: A comparison between the neutral curves obtained from domain decomposition method (DDM) and phase-field method (PFM) for immiscible fluids; Bottom: Magnified view

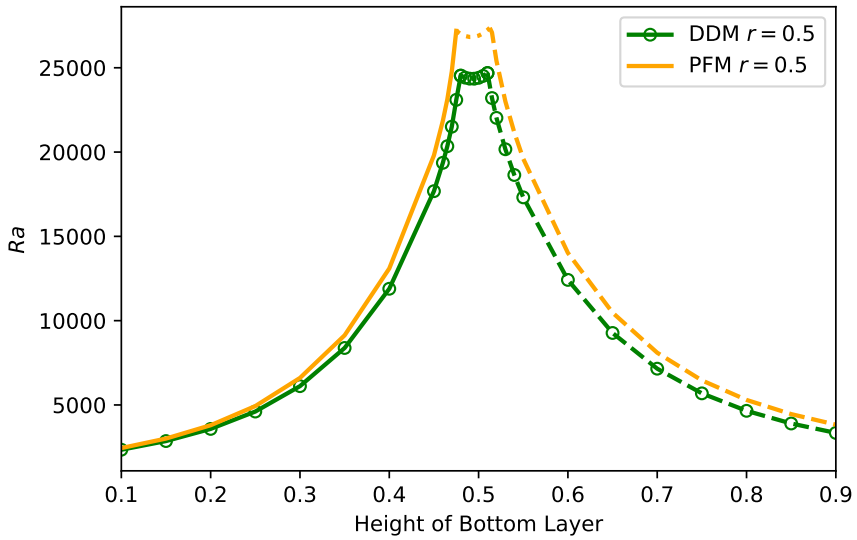

Fig. 3.9 A comparison between the marginal stability curves obtained from domain decomposition method (DDM) and phase-field method (PFM) for sparingly miscible fluids.

corresponds to the pure immiscible states of the fluids, whereas $r = 0.005$ refers to the operating condition closer to UCST.

As mentioned above, we now begin by characterizing the behavior of R-B convection in pure immiscible fluids. This was already presented in the Figure 3.8 for a sample system with $(\rho\beta\kappa_T)_r = 0.125$ and $a^* = 1.0$. This figure represents the least stable modes at different interfacial heights. Here the distinct modes are marked as 'TOP', 'BOT', and 'OSC', respectively. The part marked as 'TOP' corresponds to the 'upper dragging mode' wherein there is active buoyancy-driven convection in the top layer owing to its larger thickness. The bottom layer is passively driven by the continuity of velocity and shear stress at the interface. The 'BOT' curve represents the case vice-versa wherein the bottom layer is the driver, and the top layer is driven.

At intermediate heights, $0.485 \leq y_I \leq 0.53$, the two modes intersect and result in the manifestation of oscillatory (OSC) mode, wherein the system transiently oscillates between a mechanically coupled state and a thermally coupled state. Here, both the layers have an equal propensity for primary excitation, and the system responds by oscillating between two possible modes of coupling between the layers. In fact, on either side of this oscillatory range, the system exhibits stationary mechanical and thermal coupling modes depending on the properties chosen. The occurrence of oscillatory convection in a system is not always a guaranteed feature. A favorable combination of property ratios such as $(\rho\beta\kappa_T)_r$ being far from unity and a^* being closer to unity is essential for the manifestation of oscillatory excitation.

Figure 3.8 showed the ability of the present phase-field model to exactly reproduce the behavior of the sharp-interface system modelled via the domain decomposition method. Interestingly, this exact match makes one question the necessity of the current phase-field formulation. In fact, one would be tempted to consider the possibility of using DDM in the binary fluid context wherein the fluid properties are obtained from the equilibrium composition (Eq. (3.10)) of each layer at different temperatures. After all, the diffuse-interface thickness is much smaller than the layer heights for the range of 'r' considered in the present analysis. The answers to such quandaries are evident from Fig. 3.9 where the results obtained from the phase-field model are compared with that of the DDM with properties modified according to the equilibrium composition. The value of r used in this comparison is 0.5 making the system not very close to the consolute temperature. Even in this scenario, there is a noticeable difference between the neutral curves of PFM and DDM. The latter approach underpredicts the critical behavior essentially due to the neglect of the small diffuse interface. By properly accounting for the dissipative effects in this small region, the PFM provides a more realistic picture of the onset behavior of the binary system.

Proceeding further to understanding the influence of miscibility, Fig. 3.10 shows the variation of the marginal Rayleigh number with the position of interface, for different r values. It is evident that with the increased miscibility of fluids in the system, the peaks of the marginal stability curves move towards the left and the windows of oscillation become narrow (From Fig 3.10). This decrease in the oscillatory window can be attributed to the change in equilibrium composition of the two layers that results in a decrease in the effective $(\rho\beta\kappa_T)_r$ values, with a diminishing value of r. Also evident from Fig. 3.10 is that the change in equilibrium composition has different influences on the 'TOP' and 'BOT' modes. Recall that for the present fluid system with $(\rho\beta\kappa_T)_r = 0.125$ and $a^* = 1.0$, the values of other properties in the immiscible limit are $\frac{\nu_1}{\nu_2} = 0.5$, $\frac{\beta_1}{\beta_2} = 0.125$, $\frac{\kappa_{T_1}}{\kappa_{T_2}} = 0.5$. Thus, an increase in temperature of the system alters these ratios such that the thermal expansivity coefficient of the bottom layer increases, and so do the kinematic viscosity and thermal diffusivity. However, the increase in the former coefficient is significant compared to the later dissipative effects such that it becomes easy to destabilize the bottom layer. Hence, there is an effective reduction in the critical Ra value for the 'BOT' mode. Obviously, the scenario for the top layer is the opposite, and we observe a marginal stabilization of the 'TOP' mode.

Moving forward with other fluid combinations, we now consider a system with $(\rho\beta\kappa_T)_r = 0.125$ and $a^* = 0.667$. From Fig. 3.11, we again see a similar behavior as observed in the previous case. The peaks of the marginal curves swift leftward with the increase in temperature. Note that for the present system, in the immiscible limit, the kinematic viscosity ratio ($\frac{\nu_1}{\nu_2} = 2.53$) and any change in composition brought in by mixing makes the bottom layer

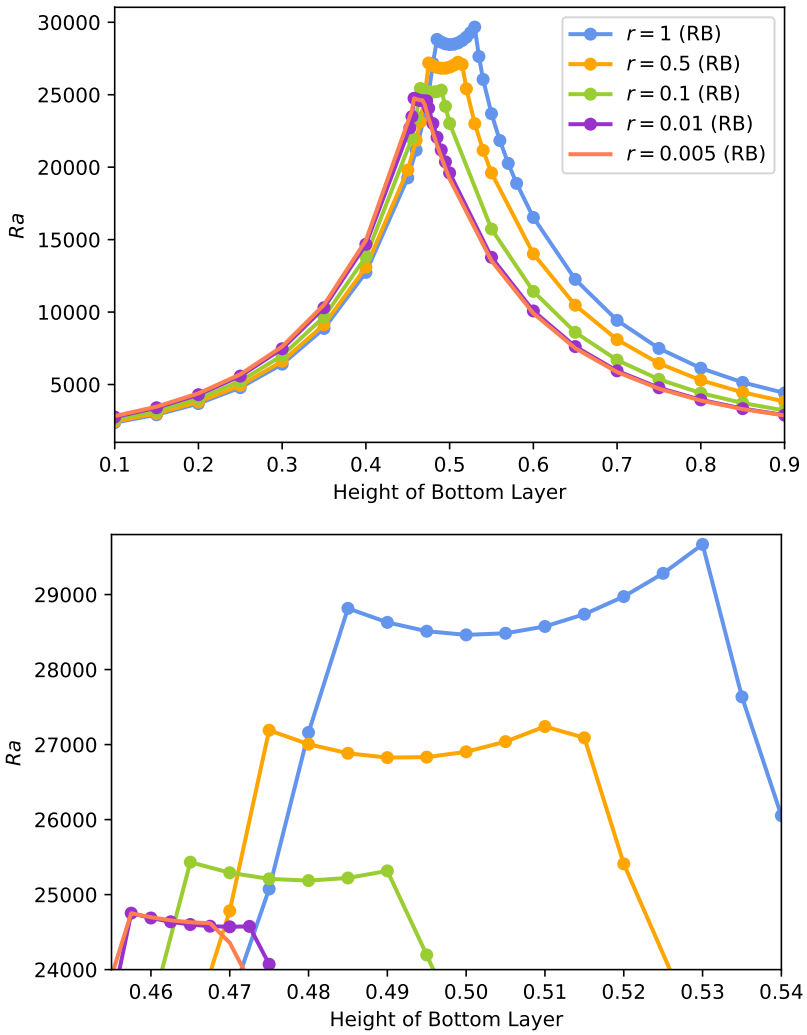

Fig. 3.10 Top: Neutral curves for different values of r; Bottom: Magnified over the regime of oscillatory onset

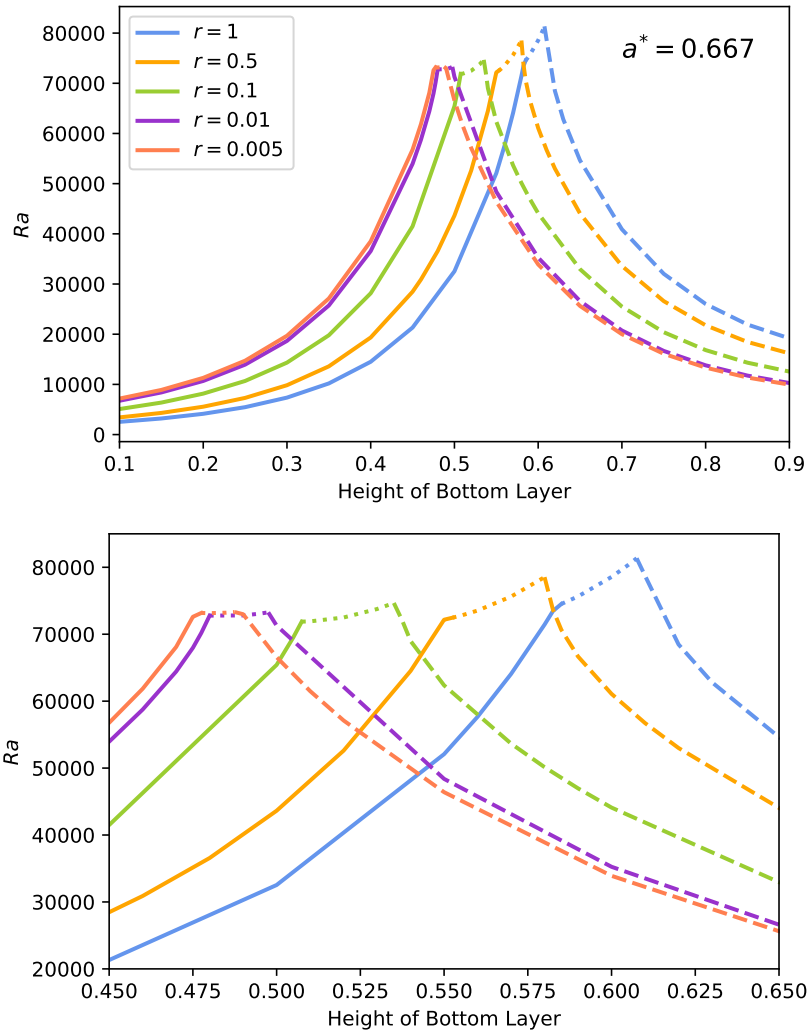

Fig. 3.11 Neutral curves for different values of r for $(\rho\beta\kappa_T)_r = 0.125, a^* = 0.667$

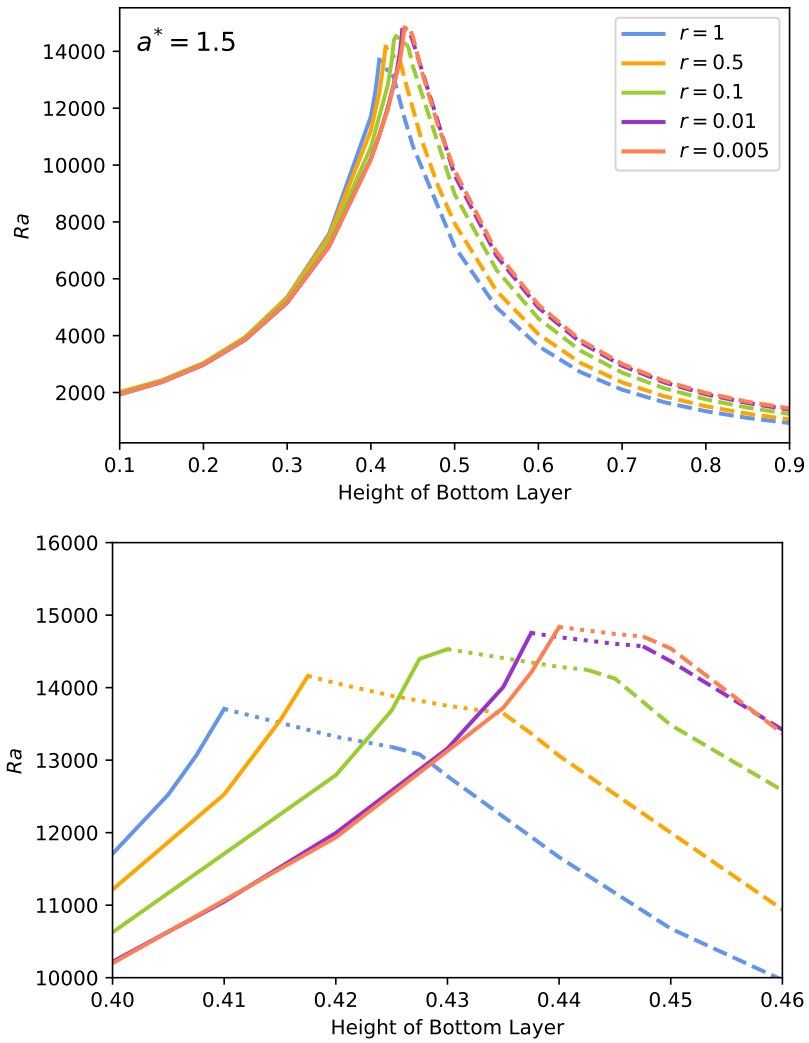

Fig. 3.12 Neutral curves for different values of r for $(\rho\beta\kappa_T)_r = 0.125, a^* = 1.5$

less dissipative. Hence, there is a significant reduction in critical *Ra* of 'BOT' mode as it becomes easy to establish convection in the bottom layer. This also makes the increase in the critical *Ra* for the 'TOP' mode more prominent compared to the $a^* = 1.0$ system.

Interestingly, the peak values of critical *Ra* do not decrease here as much as in the previous case, mainly owing to the choice of fluid properties. Nonetheless, we observe a similar reduction in the window of the oscillatory convection, and the peak value settles around the interfacial height of $0.46 - 0.47$.

Lastly, we analyse the behavior of the two-layer system with property ratio combinations, $(\rho\beta\kappa_T)_r = 0.125$ and $a^* = 1.5$. Note that the kinematic viscosity ratio of the system, $\frac{\nu_1}{\nu_2}$, is approximately 0.09875. Figure 3.12 shows the marginal stability curves for different values of r. Interestingly, the curves undergo a rightward shift though we observe a similar decrease in the window for the occurrence of oscillatory excitation in the system. The latter behavior again relates to the increase in the effective $(\rho\beta\kappa_T)_r$ value that makes the occurrence of oscillatory excitation less probable. The rightward shift, however, occurs due to the large disparity in the kinematic viscosities of the two layers. The change in equilibrium composition due to the temperature increases the viscosity of the bottom layer significantly such that it overwhelms the influence brought in by the increase in thermal expansion coefficient. Consequently, the 'BOT' mode becomes more stable, requiring a larger temperature gradient to provoke instability in the system. The behavior observed for the 'TOP' mode is the case vice-versa.

3.9 Closure

The analysis of the onset of RB convection in binary fluids closer to UCST via a diffuse-interface approach reveals interesting features. Firstly, it is evident that the phase-field approach is potent enough to exactly reveal the sharp-interface features in the truly immiscible limit. Secondly, the analysis reveals that the effect of the actual diffused nature of the interface is too significant and cannot be ignored in the vicinity of the critical point. Thirdly, the propensity of the system to exhibit oscillatory convection decreases as it approaches UCST. The equilibrium composition at these states would have a lesser disparity in the property ratios. Particularly, the combination $(\rho\beta\kappa_T)_r$ approaches unity, and as shown by Renardy [54] such systems would become devoid of any oscillatory convection. Of course, each system would come with its own drift pattern in the stability curves, essentially determined by the thermo-physical/transport properties of the fluids.

Chapter 4

Onset of Rayleigh-Bénard-Marangoni convection in a two-layer binary fluid system

4.1 Introduction

In the previous chapter, we explored the marginal attributes of RB convection using the phase-field method while neglecting the variation of the interfacial tension coefficient. In the current chapter, we will extend the analysis to understand how adding the surface tension gradient influences the onset characteristics of convection in binary fluid systems. Here, the focus will be only on the variation of the surface tension brought in by the temperature. While the numerical methodology deployed here remains the same, the underlying free energy formulation is modified to account for the variation of surface tension parameter with temperature. We now begin this chapter by formulating the governing equations. Note that the variation of surface tension parameter is considered to be linear with temperature.

4.2 Phase-field modeling and Governing equations

We start with the same free energy functional expression given in the previous chapter Eq (3.4) *i. e.*

$$F(\phi,\theta,\nabla\phi)=\int_{\Omega}\left[f_{bulk}(\phi,\theta)+\mathscr{H}(r)\frac{\Lambda}{2}r^{p}|\nabla\phi|^{2}\right]d\underline{\mathrm{x}} \tag{4.1}$$

where $f_{bulk}(\phi,\theta)$ represents the bulk energy part and is expressed in the following form

$$f_{bulk}(\phi,\theta) = \rho c(\phi)\theta - \rho c(\phi)\theta\log\theta + \mathscr{H}(r)\frac{\Lambda}{4\varepsilon^2}r^q\phi^4 - \frac{\Lambda}{2\varepsilon^2}r\phi^2 \tag{4.2}$$

Unlike the previous case, Λ is not a constant anymore. We assume it to linearly decrease with the temperature. Hence, one can write $\Lambda = \Lambda_0 - \Lambda_\theta\theta$. Once again, the generalized chemical potential μ [3], which is responsible for driving any change in the chemical composition of the system, is given by

$$\mu = \frac{\delta F}{\delta\phi} = \Lambda\left[\frac{\mathscr{H}(r)r^q\phi^3 - r\phi}{\varepsilon^2} - \mathscr{H}(r)r^p\nabla^2\phi\right] \tag{4.3}$$

We now restart formulating the problem from the basic governing equations given as

$$\frac{\partial\phi}{\partial t} + \boldsymbol{u}\cdot\boldsymbol{\nabla}\phi = \boldsymbol{\nabla}\cdot\left[\gamma\boldsymbol{\nabla}\left\{\Lambda\left(\frac{r^q\phi^3 - r\phi}{\varepsilon^2} - r^p\nabla^2\phi\right)\right\}\right] \tag{4.4}$$

$$\frac{\partial\rho\boldsymbol{u}}{\partial t} + \boldsymbol{\nabla}\cdot(\rho\boldsymbol{u}\boldsymbol{u}) = -\boldsymbol{\nabla}p + \boldsymbol{\nabla}\cdot\left(\eta\left(\boldsymbol{\nabla}\boldsymbol{u} + (\boldsymbol{\nabla}\boldsymbol{u})^+ - \frac{2}{3}\boldsymbol{\nabla}\cdot\boldsymbol{u}\boldsymbol{I}\right)\right) + \boldsymbol{\nabla}\cdot\boldsymbol{\tau}^{nv} - \rho^{'}g\mathbf{1}_y \tag{4.5}$$

$$\frac{D\rho}{Dt} + \rho\boldsymbol{\nabla}\cdot\boldsymbol{u} = 0 \tag{4.6}$$

$$\frac{\partial\rho(c\theta)}{\partial t} + \boldsymbol{\nabla}\cdot(\rho\boldsymbol{u}c\theta) + \Lambda_0\left[\frac{r^q\phi^3 - r\phi}{\varepsilon^2} - r^p\nabla^2\phi\right]\frac{D\phi}{Dt} + \mathscr{L}\boldsymbol{\nabla}\cdot\boldsymbol{u} = \boldsymbol{\nabla}\cdot(\kappa\boldsymbol{\nabla}\theta) \tag{4.7}$$

where

$$\boldsymbol{\tau}^{nv} = \mathscr{L}\boldsymbol{I} - \boldsymbol{\nabla}\phi\frac{\partial\mathscr{L}}{\partial(\boldsymbol{\nabla}\phi)} \tag{4.8}$$

and $\mathscr{L} = f_{mix}(\phi,\theta) + \mathscr{H}(r)\frac{\Lambda}{2}r^p|\partial\phi(x)|^2$ is the Lagrangian energy density.

Since the phase-parameter ϕ acts as a marker for the phases and the interfaces, the properties of the fluids can be expressed as a linear function of ϕ as:

$$\begin{aligned}
\frac{\eta}{\eta_2} &= \frac{1}{2}(1+\frac{\eta_1}{\eta_2}) + \frac{\phi}{2}(\frac{\eta_1}{\eta_2} - 1)\\
\frac{\kappa}{\kappa_2} &= \frac{1}{2}(1+\frac{\kappa_1}{\kappa_2}) + \frac{\phi}{2}(\frac{\kappa_1}{\kappa_2} - 1)\\
\frac{\rho c}{\rho_2 c_2} &= \frac{1}{2}(1+\frac{\rho_1 c_1}{\rho_2 c_2}) + \frac{\phi}{2}(\frac{\rho_1 c_1}{\rho_2 c_2} - 1)\\
\frac{\kappa_T}{\kappa_{T_2}} &= \frac{1}{2}(1+\frac{\kappa_{T_1}}{\kappa_{T_2}}) + \frac{\phi}{2}(\frac{\kappa_{T_1}}{\kappa_{T_2}} - 1)
\end{aligned} \tag{4.9}$$

The phase evolution equation obeys the no flux boundary condition owing to the assumption of impenetrable walls.

$$\begin{aligned} \mathbf{1}_y \cdot \boldsymbol{\nabla}\phi &= 0 \ @y = 0, H \\ \mathbf{1}_y \cdot \boldsymbol{\nabla}\mu &= 0 \ @y = 0, H \end{aligned} \tag{4.10}$$

Since $\mu = \Lambda\left[\frac{r^q\phi^3 - r\phi}{\varepsilon^2} - r^p\nabla^2\phi\right]$, simplifying the above equations leads to the condition

$$\frac{\partial\phi}{\partial y} = \frac{\partial^3\phi}{\partial y^3} = 0 \ @y = 0, H \tag{4.11}$$

The no-slip and impenetrable walls at the top and bottom lead to the condition,

$$\boldsymbol{u} = 0 \ @y = 0, H \tag{4.12}$$

Both the walls in the current problem are maintained at constant temperatures; hence, the energy equation will obey the following boundary conditions.

$$\begin{aligned} \theta &= \theta_B \ @y = 0 \\ \theta &= \theta_T \ @y = H \end{aligned} \tag{4.13}$$

4.3 Partial Non-Boussinesq/Boussinesq Approximation

4.3.1 Incompressible Approach

Once again, we adopt the same incompressible approach as mentioned in the previous chapter. The velocity field is defined as a volume-average field *i. e.*

$$\boldsymbol{u} = \frac{\tilde{\rho}_1}{\rho_1}\boldsymbol{u}_1 + \frac{\tilde{\rho}_2}{\rho_2}\boldsymbol{u}_2 \tag{4.14}$$

which gives a solenoidal velocity field throughout the domain.

The Cahn-Hilliard (CH) equation remains the same as before:

$$\frac{\partial\phi}{\partial t} + \boldsymbol{u}\cdot\boldsymbol{\nabla}\phi = \boldsymbol{\nabla}\cdot\left[\gamma\boldsymbol{\nabla}\left\{\Lambda\left(\frac{r^q\phi^3 - r\phi}{\varepsilon^2} - r^p\nabla^2\phi\right)\right\}\right] \tag{4.15}$$

The conservative form of the momentum equation takes the form,

$$\frac{\partial \rho \boldsymbol{u}}{\partial t} + \boldsymbol{\nabla}\cdot(\rho \boldsymbol{u}\boldsymbol{u}) + \boldsymbol{u}\frac{\partial \rho}{\partial \phi}\boldsymbol{\nabla}\cdot\boldsymbol{j}_\phi = -\boldsymbol{\nabla}p + \boldsymbol{\nabla}\cdot\left(\eta\left(\boldsymbol{\nabla}\boldsymbol{u} + (\boldsymbol{\nabla}\boldsymbol{u})^+\right)\right) + \mu\boldsymbol{\nabla}\phi - \rho^{'} g\hat{\mathbf{1}}_y + \left(\frac{1}{4\varepsilon^2}r^q\phi^4 - \frac{1}{2\varepsilon^2}r\phi^2 + \frac{1}{2}r^p|\partial\phi(x)|^2\right)\frac{\partial\Lambda}{\partial\theta}\boldsymbol{\nabla}\theta - r^p\boldsymbol{\nabla}\phi\frac{\partial\Lambda}{\partial\theta}\boldsymbol{\nabla}\theta\cdot\boldsymbol{\nabla}\phi \tag{4.16}$$

$$\boldsymbol{\nabla}\cdot\boldsymbol{u} = 0 \tag{4.17}$$

The derivation of the above form of interfacial stress is provided in detail in Appendix C. The above form of momentum balance accounts for the advection due to the relative diffusional flux of species. The non-conservative form of the above equation can be written in the following form:

$$\rho_0\left(\frac{\partial \boldsymbol{u}}{\partial t} + \boldsymbol{u}\cdot\boldsymbol{\nabla}\boldsymbol{u}\right) = -\boldsymbol{\nabla}p + \boldsymbol{\nabla}\cdot\left(\eta\left(\boldsymbol{\nabla}\boldsymbol{u} + (\boldsymbol{\nabla}\boldsymbol{u})^+\right)\right) + \mu\boldsymbol{\nabla}\phi - \rho^{'} g\hat{\mathbf{1}}_y + \left(\frac{1}{4\varepsilon^2}r^q\phi^4 - \frac{1}{2\varepsilon^2}r\phi^2 + \frac{1}{2}r^p|\partial\phi(x)|^2\right)\frac{\partial\Lambda}{\partial\theta}\boldsymbol{\nabla}\theta - r^p\boldsymbol{\nabla}\phi\frac{\partial\Lambda}{\partial\theta}\boldsymbol{\nabla}\theta\cdot\boldsymbol{\nabla}\phi \tag{4.18}$$

Finally, the conservative form of the energy equation takes the form (refer to Appendix-D for the derivation):

$$\frac{\partial \rho_0 c\theta}{\partial t} + \boldsymbol{\nabla}\cdot(\rho_0 \boldsymbol{u} c\theta) + \theta\frac{\partial \rho_0 c}{\partial \phi}\boldsymbol{\nabla}\cdot\boldsymbol{j}_\phi + \Lambda_0\left[\frac{r^q\phi^3 - r\phi}{\varepsilon^2} - r^p\nabla^2\phi\right]\frac{D\phi}{Dt} = \boldsymbol{\nabla}\cdot(\kappa\boldsymbol{\nabla}\theta) \tag{4.19}$$

Here, like before, we have neglected the viscous dissipation since the magnitude of the dissipation is much lower compared to the storage/advection of the energy in a naturally convected flow [24]. The non-conservative counterpart is given as

$$\rho_0 c\left(\frac{\partial \theta}{\partial t} + \boldsymbol{u}\cdot\boldsymbol{\nabla}\theta\right) + \Lambda_0\left[\frac{r^q\phi^3 - r\phi}{\varepsilon^2} - r^p\nabla^2\phi\right]\frac{D\phi}{Dt} = \boldsymbol{\nabla}\cdot(\kappa\boldsymbol{\nabla}\theta) \tag{4.20}$$

4.3.2 Linear Stability Analysis

As discussed earlier, the linear stability analysis is sufficient to give the nature of the onset of convection in the RBM setting. The oscillatory mode of onset is observed when two non-oscillatory modes (two bulk modes or one bulk and one interfacial mode) compete with each other. For the two-layer Rayleigh-Bénard problem, oscillatory instability happens when

the value of $(\rho\beta\kappa_T)_r$ differs from unity [54]. The present chapter focuses on understanding how the Marangoni effect modifies this criterion in the context of binary fluids. Following the conventional procedures, we decompose any quantity into the base and perturbed quantities as

$$\begin{aligned}\phi &= \Phi^b(y) + \phi^{'}(x,y,t)\\ u_i &= u_i^{'}(x,y,t)\\ \theta &= \Theta^b(y) + \theta^{'}(x,y,t)\\ p &= p^b(y) + p^{'}(x,y,t)\end{aligned} \tag{4.21}$$

The perturbed quantities are assumed to be very small compared to the corresponding base quantities. Hence, any product of perturbed quantities can be neglected. So, the linearized equations are written as

$$\frac{\partial \phi^{'}}{\partial t} + u_j^{'}\frac{\partial \Phi^b}{\partial x_j} == \nabla_k\left[\gamma\nabla_k\left\{\Lambda\left(\frac{r^q 3(\Phi^b)^2\phi^{'} - r\phi^{'}}{\varepsilon^2} - r^p\nabla^2\phi^{'}\right)\right\}\right] \tag{4.22}$$

$$\begin{aligned}\frac{\partial u_i^{'}}{\partial t} &= -\frac{\nabla_i p^{'}}{\rho(\Phi^b)} + \frac{\eta_2}{\rho(\Phi^b)}\nabla_j\left[\left(\frac{1}{2}(1+\frac{\eta_1}{\eta_2}) + \frac{\Phi^b}{2}(\frac{\eta_1}{\eta_2}-1)\right)(\nabla_j u_i^{'} + \nabla_i u_j^{'})\right] + \frac{1}{\rho(\Phi^b)}\mu^{'}\nabla_i\phi^b\\ &+ \frac{1}{\rho(\Phi^b)}\frac{\rho_1\beta_1 - \rho_2\beta_2}{2}\Theta^b\phi^{'}g\delta_{i2} + \frac{1}{\rho(\Phi^b)}\left[\frac{\rho_1\beta_1+\rho_2\beta_2}{2} + \frac{\rho_1\beta_1-\rho_2\beta_2}{2}\Phi^b\right]\theta^{'}g\delta_{i2}\\ &+ \frac{1}{\rho(\Phi^b)}\left(\frac{1}{4\varepsilon^2}r^q(\Phi^b)^4 - \frac{1}{2\varepsilon^2}r(\Phi^b)^2 + \frac{1}{2}r^p|\nabla_k(\Phi^b)|^2\right)\frac{\partial\Lambda}{\partial\theta}\nabla_i\theta^{'}\\ &+ \frac{1}{\rho(\Phi^b)}\left(\frac{1}{4\varepsilon^2}r^q 4(\Phi^b)^3\phi^{'} - \frac{1}{2\varepsilon^2}r2(\Phi^b)\phi^{'} + \frac{1}{2}r^p 2\nabla_k\Phi^b\nabla_k\phi^{'}\right)\frac{\partial\Lambda}{\partial\theta}\nabla_i\Theta^b\\ &- \frac{1}{\rho(\Phi^b)}r^p\nabla_j\Phi^b\frac{\partial\Lambda}{\partial\theta}\nabla_i\Theta^b\nabla_i\phi^{'} - \frac{1}{\rho(\Phi^b)}r^p\nabla_j\Phi^b\frac{\partial\Lambda}{\partial\theta}\nabla_i\theta^{'}\nabla_i\Phi^b - \frac{1}{\rho(\Phi^b)}r^p\nabla_j\phi^{'}\frac{\partial\Lambda}{\partial\theta}\nabla_i\Theta^b\nabla_i\Phi^b\end{aligned} \tag{4.23}$$

$$\nabla_i u_i^{'} = 0 \tag{4.24}$$

$$\begin{aligned}\rho c(\Phi^b)\left[\frac{\partial\theta^{'}}{\partial t} + u_j^{'}\frac{\partial\Theta^b}{\partial x_j}\right] &= \kappa^b\nabla_m{}^2\theta^{'} + (\nabla_m\kappa^b)(\nabla_m\theta^{'})\\ &+ (\nabla_m k^{'})(\nabla_m\Theta^b) + \kappa(\phi^{'})\nabla_m{}^2\Theta^b\end{aligned} \tag{4.25}$$

We now perform non-dimensionalization of the above equations using the following scales.

$$L_R = H_2 \qquad t_R = \frac{{H_2}^2}{\kappa_{T2}} \qquad u_R = \frac{\kappa_{T2}}{H_2} \qquad \theta_R = \theta_B - \theta_T \qquad p_R = \frac{\rho_2 \kappa_{T2} \nu_2}{{H_2}^2}$$

The resulting dimensionless equations can be written as follows.

$$\frac{\partial \phi^{'}}{\partial t} + u_j^{'} \nabla_j \Phi^b = M \nabla^2 \left[\left(1 - \frac{\Upsilon Ra}{Ca} \Theta^b\right) \left(r^q 3 (\Phi^b)^2 \phi^{'} - r \phi^{'} - \left(\frac{\varepsilon}{H_2}\right)^2 r^p \nabla^2 \phi^{'} \right) \right] \tag{4.26}$$

$$\begin{aligned}
\frac{\partial u_i^{'}}{\partial t} =& -Pr_2 \frac{\nabla_i p^{'}}{\rho_f(\Phi^b)} + Pr_2 \frac{1}{\rho_f(\Phi^b)} \nabla_j \left[\left(\frac{1}{2}(1 + \frac{\eta_1}{\eta_2}) + \frac{\Phi^b}{2}(\frac{\eta_1}{\eta_2} - 1) \right) (\nabla_j u_i^{'} + \nabla_i u_j^{'}) \right] \\
&+ (\frac{H_2}{\varepsilon})^2 \Gamma_\theta \frac{1}{\rho_f(\Phi^b)} \mu^{'} \nabla_i \Phi^b + \frac{1}{\rho_f(\Phi^b)} Ra_2 Pr_2 \frac{1}{2} \left(\frac{\rho_1 \beta_1}{\rho_2 \beta_2} - 1 \right) \Theta^b \phi^{'} \delta_{i2} \\
&+ \frac{1}{\rho_f(\Phi^b)} Ra_2 Pr_2 \left[\frac{1}{2} \left(\frac{\rho_1 \beta_1}{\rho_2 \beta_2} + 1 \right) + \frac{1}{2} \left(\frac{\rho_1 \beta_1}{\rho_2 \beta_2} - 1 \right) \Phi^b \right] \theta^{'} \delta_{i2} \\
&+ \frac{1}{\rho_f(\Phi^b)} \frac{3}{2\sqrt{2}} \Upsilon Ra_2 Pr_2 \frac{H_2}{\varepsilon} \left(\frac{1}{4\varepsilon^2} r^q (\Phi^b)^4 - \frac{1}{2\varepsilon^2} r (\Phi^b)^2 + \left(\frac{\varepsilon}{H_2}\right)^2 \frac{1}{2} r^p |\nabla_k (\Phi^b)|^2 \right) \nabla_i \theta^{'} \\
&+ \frac{1}{\rho_f(\Phi^b)} \frac{3}{2\sqrt{2}} \Upsilon Ra_2 Pr_2 \frac{H_2}{\varepsilon} \left(\frac{1}{4\varepsilon^2} r^q 4 (\Phi^b)^3 \phi^{'} - \frac{1}{2\varepsilon^2} r 2 (\Phi^b) \phi^{'} + \left(\frac{\varepsilon}{H_2}\right)^2 \frac{1}{2} r^p 2 \nabla_k \Phi^b \nabla_k \phi^{'} \right) \nabla_i \Theta^b \\
&- \frac{1}{\rho_f(\Phi^b)} \frac{3}{2\sqrt{2}} \Upsilon Ra_2 Pr_2 \frac{\varepsilon}{H_2} r^p \nabla_i \Phi^b \nabla_j \Theta^b \nabla_j \phi^{'} - \frac{1}{\rho_f(\Phi^b)} \frac{3}{2\sqrt{2}} \Upsilon Ra_2 Pr_2 \frac{\varepsilon}{H_2} r^p \nabla_i \Phi^b \nabla_j \theta^{'} \nabla_j \Phi^b \\
&- \frac{1}{\rho_f(\Phi^b)} \frac{3}{2\sqrt{2}} \Upsilon Ra_2 Pr_2 \frac{\varepsilon}{H_2} r^p \nabla_i \phi^{'} \nabla_j \Theta^b \nabla_j \Phi^b
\end{aligned} \tag{4.27}$$

$$\nabla_j u_j^{'} = 0 \tag{4.28}$$

$$\begin{aligned}
(\rho c)_f (\Phi^b) \left[\frac{\partial \theta^{'}}{\partial t} + {u_j}^{'} \frac{\partial \Theta^b}{\partial x_j} \right] =& \kappa_f (\Phi^b) {\nabla_m}^2 \theta^{'} + (\nabla_m \kappa_f (\Phi^b))(\nabla_m \theta^{'}) \\
&+ (\nabla_m \kappa_f (\phi^{'}))(\nabla_m \Theta^b) + \kappa_f (\phi^{'}) {\nabla_m}^2 \Theta^b
\end{aligned} \tag{4.29}$$

Non-dimensional numbers $M\left(=\frac{\gamma \Lambda_0}{\varepsilon^2 \kappa_{T_2}}\right)$, $\Gamma_\theta\left(=\frac{\Lambda_0}{\rho_2 \kappa_{T_2}^2}\right)$ are the same as described in chapter 3. We presently have two more dimensionless numbers, 1) the capillary number: $Ca = \frac{\sigma H_2}{\eta \kappa_{T_2}}$, and 2) the Marangoni number: $Ma = \frac{\sigma_\theta \Delta\theta H_2}{\eta_2 \kappa_{T_2}}$, that gives the relative importance

of the transport due to surface tension gradient to the diffusive effects of the gradient. Since the Marangoni number (Ma) and the Rayleigh number (Ra) are not independent, we defined another non-dimensional number Υ, given as

$$\frac{Ma}{Ra} = \frac{\sigma_\theta}{g\rho_2\beta_2 H_2^2} = \Upsilon \tag{4.30}$$

The strength of the surface tension gradient is given by Υ.

We assume the normal mode form of the perturbed quantities. In normal mode analysis, we take the perturbation in the form of sinusoidal waves

$$\begin{aligned}
\phi &= \Phi^b(y) + \hat{\phi}(y)\exp(\lambda t + ikx) \\
\boldsymbol{u} &= \hat{\boldsymbol{u}}(y)\exp(\lambda t + ikx) \\
\theta &= \Theta^b(y) + \hat{\theta}(y)\exp(\lambda t + ikx) \\
p &= p^b(y) + \hat{p}(y)\exp(\lambda t + ikx)
\end{aligned} \tag{4.31}$$

The linearized perturbation equations are as follows:

$$\begin{aligned}
\lambda\hat{\phi} + \hat{v}\frac{\partial\Phi^b}{\partial y} &= M\left[3r^q\left(-(\Phi^b)^2k^2\hat{\phi} + 2(\frac{d\Phi^b}{dy})^2\hat{\phi} + 2\Phi^b\frac{d^2\Phi^b}{dy^2}\hat{\phi} + 4\Phi^b\frac{d\Phi^b}{dy}\frac{d\hat{\phi}}{dy} + (\Phi^b)^2\frac{d^2\hat{\phi}}{dy^2}\right)\right. \\
&\qquad \left. - r\left(-k^2\hat{\phi} + \frac{d^2\hat{\phi}}{dy^2}\right) - \left(\frac{\varepsilon}{H_2}\right)^2 r^p\left(\frac{d^4\hat{\phi}}{dy^4} - 2k^2\frac{d^2\hat{\phi}}{dy^2} + k^4\hat{\phi}\right)\right] \\
&\quad -M\left(\frac{\Upsilon Ra}{Ca}\right)\Theta^b\left[3r^q\left(-(\Phi^b)^2k^2\hat{\phi} + 2(\frac{d\Phi^b}{dy})^2\hat{\phi} + 2\Phi^b\frac{d^2\Phi^b}{dy^2}\hat{\phi} + 4\Phi^b\frac{d\Phi^b}{dy}\frac{d\hat{\phi}}{dy} + (\Phi^b)^2\frac{d^2\hat{\phi}}{dy^2}\right)\right. \\
&\qquad \left. - r\left(-k^2\hat{\phi} + \frac{d^2\hat{\phi}}{dy^2}\right) - \left(\frac{\varepsilon}{H_2}\right)^2 r^p\left(\frac{d^4\hat{\phi}}{dy^4} - 2k^2\frac{d^2\hat{\phi}}{dy^2} + k^4\hat{\phi}\right)\right] \\
&\quad -2M\left(\frac{\Upsilon Ra}{Ca}\right)\frac{d\Theta^b}{dy}\left[3r^q(\Phi^b)^2\frac{d\hat{\phi}}{dy} + 6r^q(\Phi^b)\frac{d\Phi^b}{dy}\hat{\phi} - r\frac{d\hat{\phi}}{dy} - r^p\left(\frac{d^2}{dy^2} - k^2\right)\frac{d\hat{\phi}}{dy}\right] \\
&\quad -M\left(\frac{\Upsilon Ra}{Ca}\right)\frac{d^2\Theta^b}{dy^2}\left(r^q 3(\Phi^b)^2\hat{\phi} - r\hat{\phi} - \left(\frac{\varepsilon}{H_2}\right)^2 r^p\nabla^2\hat{\phi}\right)
\end{aligned} \tag{4.32}$$

The derivation of the above form is dealt with in detail in Appendix B.

$$
\begin{aligned}
\lambda\hat{u} = &-\frac{1}{\rho_f(\Phi^b)}Pr_2(\imath k)\hat{p} + \frac{1}{\rho_f(\Phi^b)}Pr_2\left[\frac{1}{2}(1+\frac{\eta_1}{\eta_2}) + \frac{\Phi^b}{2}(\frac{\eta_1}{\eta_2}-1)\right](-k^2+\frac{d^2}{dy^2})\hat{u} \\
&+ \frac{1}{\rho_f(\Phi^b)}Pr_2\frac{1}{2}(\frac{\eta_1}{\eta_2}-1)\frac{d\Phi^b}{dy}\frac{d\hat{u}}{dy} + \frac{1}{\rho_f(\Phi^b)}Pr_2\frac{1}{2}(\frac{\eta_1}{\eta_2}-1)\frac{d\Phi^b}{dy}(ik\hat{v}) \\
&+ \frac{1}{\rho_f(\Phi^b)}\frac{3}{2\sqrt{2}}\Upsilon Pr_2 Ra_2\frac{H_2}{\varepsilon}\left(\frac{1}{4}r^q(\Phi^b)^4 - \frac{1}{2}r(\Phi^b)^2 + \frac{1}{2}\frac{\varepsilon^2}{H_2^2}r^p\left(\frac{\partial\Phi^b}{\partial y}\right)^2\right)(ik\hat{\theta}) \\
&- \frac{1}{\rho_f(\Phi^b)}\frac{3}{2\sqrt{2}}\Upsilon Pr_2\frac{\varepsilon}{H_2}Ra_2 r^p\left(\frac{\partial\Phi^b}{\partial y}\frac{\partial\Theta^b}{\partial y}\right)(ik\hat{\phi})
\end{aligned}
\tag{4.33}
$$

$$
\begin{aligned}
\lambda\hat{v} = &-\frac{1}{\rho_f(\Phi^b)}Pr_2\frac{d\hat{p}}{dy} + \frac{1}{\rho_f(\Phi^b)}Pr_2\left[\frac{1}{2}(1+\frac{\eta_1}{\eta_2}) + \frac{\Phi^b}{2}(\frac{\eta_1}{\eta_2}-1)\right](-k^2+\frac{d^2}{dy^2})\hat{v} \\
&+ \frac{1}{\rho_f(\Phi^b)}Pr_2(\frac{\eta_1}{\eta_2}-1)\frac{d\Phi^b}{dy}\frac{d\hat{v}}{dy} \\
&- (\frac{H_2}{\varepsilon})^2\Gamma_\theta\frac{1}{\rho_f(\Phi^b)}\left(r^q 3(\Phi^b)^2\hat{\phi} - r\hat{\phi} - \left(\frac{\varepsilon}{H_2}\right)^2 r^p\nabla_n^2\hat{\phi}\right)\frac{d\Phi^b}{dy} \\
&+ \frac{1}{\rho_f(\Phi^b)}Ra_2Pr_2\frac{1}{2}\left(\frac{\rho_1\beta_1}{\rho_2\beta_2}-1\right)\Theta^b\hat{\phi} \\
&+ \frac{1}{\rho_f(\Phi^b)}Ra_2Pr_2\left[\frac{1}{2}\left(\frac{\rho_1\beta_1}{\rho_2\beta_2}+1\right) + \frac{1}{2}\left(\frac{\rho_1\beta_1}{\rho_2\beta_2}-1\right)\Phi^b\right]\hat{\theta} \\
&+ \frac{1}{\rho_f(\Phi^b)}\frac{3}{2\sqrt{2}}\Upsilon Pr_2 Ra_2\frac{H_2}{\varepsilon}\left(\frac{1}{4}r^q(\Phi^b)^4 - \frac{1}{2}r(\Phi^b)^2 + \frac{1}{2}\frac{\varepsilon^2}{H_2^2}r^p\left(\frac{\partial\Phi^b}{\partial y}\right)^2\right)\nabla_y\hat{\theta} \\
&+ \frac{1}{\rho_f(\Phi^b)}\frac{3}{2\sqrt{2}}\Upsilon Pr_2 Ra_2\frac{H_2}{\varepsilon}\left(\frac{1}{4}r^q 4(\Phi^b)^3\hat{\phi} - \frac{1}{2}r2(\Phi^b)\hat{\phi} + \frac{1}{2}\frac{\varepsilon^2}{H_2^2}r^p 2\frac{\partial\Phi^b}{\partial y}\frac{\partial\hat{\phi}}{\partial y}\right)\nabla_y\Theta^b \\
&- \frac{1}{\rho_f(\Phi^b)}\frac{3}{2\sqrt{2}}\Upsilon Pr_2\frac{\varepsilon}{H_2}Ra_2 r^p\left(\frac{\partial\Phi^b}{\partial y}\frac{\partial\Theta^b}{\partial y}\right)\nabla_y(\hat{\phi}) \\
&- \frac{1}{\rho_f(\Phi^b)}\frac{3}{2\sqrt{2}}\Upsilon Pr_2\frac{\varepsilon}{H_2}Ra_2 r^p\left(\frac{\partial\Phi^b}{\partial y}\frac{\partial\hat{\theta}}{\partial y} + \frac{\partial\hat{\phi}}{\partial y}\frac{\partial\Theta^b}{\partial y}\right)\nabla_y(\Phi^b)
\end{aligned}
\tag{4.34}
$$

$$
ik\hat{u} + \frac{d\hat{v}}{dy} = 0 \tag{4.35}
$$

$$
\begin{aligned}
(\rho c)_f(\Phi^b)\left[\lambda\hat{\theta}+\hat{v}\frac{\partial\Theta^b}{\partial y}\right] &= \left[\frac{1}{2}(1+\frac{\kappa_1}{\kappa_2})+\frac{\Phi^b}{2}(\frac{\kappa_1}{\kappa_2}-1)\right](-k^2+\frac{d^2}{dy^2})\hat{\theta} \\
&+\frac{1}{2}(\frac{\kappa_1}{\kappa_2}-1)\frac{d\Phi^b}{dy}\frac{d\hat{\theta}}{dy}+\frac{1}{2}(\frac{\kappa_1}{\kappa_2}-1)\frac{d\hat{\phi}}{dy}\frac{d\Theta^b}{dy} \\
&+\left[\frac{\hat{\phi}}{2}(\frac{\kappa_1}{\kappa_2}-1)\right]\frac{d^2\Theta^b}{dy^2}
\end{aligned}
\tag{4.36}
$$

The boundary conditions are written as follows:

$$
\begin{aligned}
\frac{\partial\hat{\phi}}{\partial y}=\frac{\partial^3\hat{\phi}}{\partial y^3}=0 \quad @y=0,1 \\
\hat{u}_i=0 \quad @y=0,1 \\
\hat{\theta}=0 \quad @y=0,1
\end{aligned}
\tag{4.37}
$$

The above set of equations is reduced to the generalized eigenvalue problem of type $A\boldsymbol{X}=\lambda B\boldsymbol{X}$. Once again, we solve the inverse problem so that spurious modes can be easily filtered. We essentially look for the *Ra* value at which the real part of the largest eigenvalue in the system is zero.

4.4 Consistency Check: Sharp interface and the immiscible limits

Like in the previous chapter, we will now check for the ability of the current formulation to mimic the sharp-interface behavior in the immiscible limits. In other words, we will compare the results obtained using the diffuse-interface approach with those obtained using the domain decomposition method shown in Appendix A. Here, we will maintain $\frac{\varepsilon}{H_2}$ at 10^{-4} to mimic the sharp interface behavior. Since we know the fluids are far from the critical temperature, we keep r to 1. Fig. 4.1 shows the exact match between the results obtained from these different approaches and implies the consistency of the current phase-field model. The fluid properties correspond to $a^*=1.0$ system of chapter 3 along with $\Upsilon=0.01$.

It is interesting to note the absence of the oscillatory onset window in the present case. We will discuss it in detail in the following section.

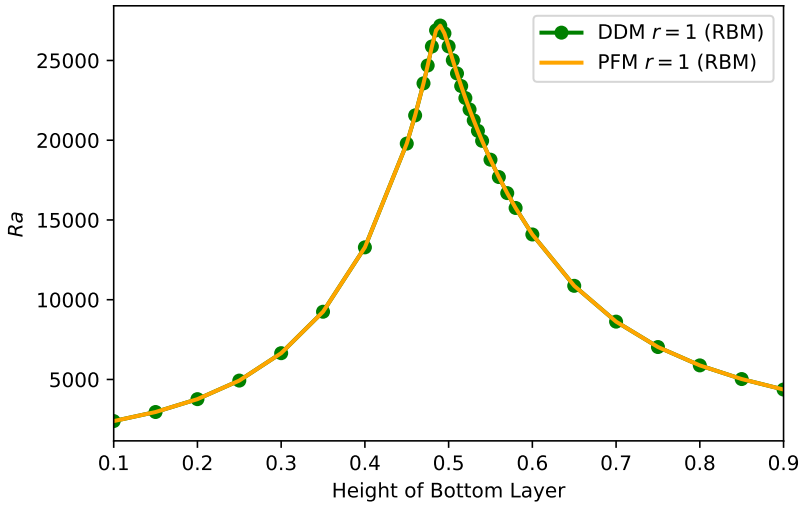

Fig. 4.1 A comparison between the curves of marginal stability for the RBM convection obtained from the domain decomposition method (DDM) and the phase-field method (PFM).

4.5 Results and Discussions

4.5.1 RBM convection in the immiscible limit

Before proceeding to understand the influence of solubility on the onset of RBM convection in a binary fluid system deviating from the immiscible limit assumption, we would spend some effort in understanding the behavior in the pure immiscible limit. It is well known from the works of Degen *et al.* [19] and Nepomnysky and Simanovoskii [42] that the presence of the Marangoni effect plays a significant role in the onset of oscillatory convection in a two-layer system. A classical example described by the above works is the system of Silicon-Oil and water combination, which would not exhibit oscillatory convection if not for the thermo-capillary effects present in the system. In such systems, when the interface is closer to the bottom plate, the critical Rayleigh number is higher in the RBM convection case than in the RB convection. Here, the gradient in surface tension has a stabilizing effect, and it inhibits the growth of the imposed perturbations. Thus, one would need a higher value of the temperature gradient to instigate fluid motion from a purely conductive system. The exact opposite behavior is observed when the interface is closer to the top plate. The Marangoni effect has a destabilizing effect and thus, promotes the convection at a lower *Ra* value compared to RB convection.

Unfortunately, beyond this, nothing much is comprehensively known in the literature about the special influence of the Marangoni effect. In the present work, we now systematically study its influence by considering again $(\rho\beta\kappa_T)_r = 0.125$ and $a^* = 1.0$ combination

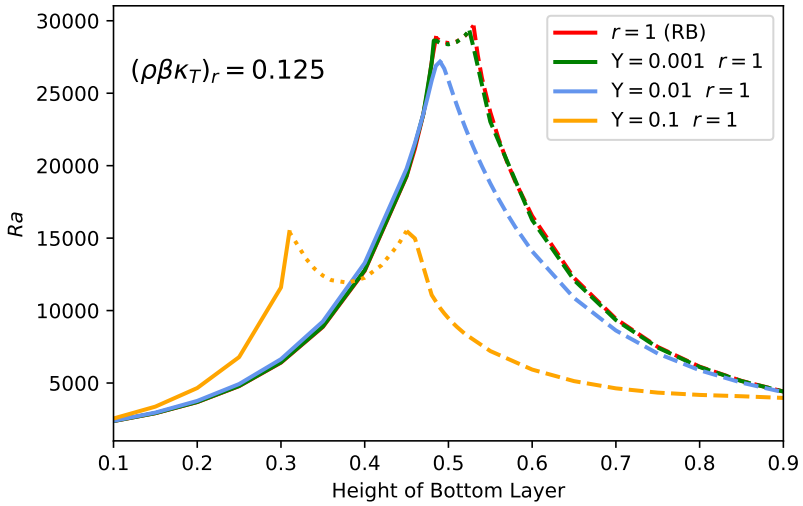

Fig. 4.2 A comparison between neutral curves between RB and RBM convections. For RBM convection, we have used different values of Υ to show how the strength of the surface tension gradient affects the onset characteristics.

from the previous chapter and gradually increase the magnitude of the thermo-capillary effect by increasing the Υ value in the analysis. Figure 4.2 shows the neutral curves obtained from the analysis, and it is very interesting to note that the thermo-capillarity does not always result in the increase of parametric window for oscillatory onset. Evidently, with an increase in Υ from zero, the window of oscillatory convection shrinks and vanishes at around $\Upsilon = 0.01$. Interestingly, a further increase in the Υ value results in the reappearance of the oscillatory onset. The reasons for this behavior can be obtained by extending the analysis of Renardy [54] to include the Marangoni effect. The details of the steps involved are shown in Appendix

E. For brevity, only the final equation is written below.

$$\begin{aligned}\lambda\left[\int_0^I \kappa_r|\theta_1|^2dy+\int_I^1 \kappa_{T_r}|\theta_2|^2dy\right] =& -\int_0^I \kappa_r(k^2|\theta_1|^2+|\nabla\theta_1|^2)dy-\int_I^1 (k^2|\theta_2|^2+|\nabla\theta_2|^2)dy\\ &-\frac{\lambda}{Pr_2}\frac{\Lambda_2}{k^2Ra_2}\left[\int_0^I (k^2|v_1|^2+|\nabla v_1|^2)dy+\int_I^1 \beta_r\kappa_{T_r}(k^2|v_2|^2+|\nabla v_2|^2)dy\right]\\ &+\frac{\Lambda_2}{k^2Ra_2}\left[\int_0^I |\nabla^2 v_1|^2dy+\int_I^1 \frac{(\rho\beta\kappa_T)_r}{\eta_r}|\nabla^2 v_2|^2dy\right]\\ &+\frac{\Lambda_2}{k^2Ra_2}\Big((\rho\beta\kappa_T)_r-1\Big)\frac{\partial\bar{v}_1}{\partial y}\frac{\partial^2 v_1}{\partial y^2}\bigg|_{y=I}\\ &+\Lambda_2(\rho\beta\kappa_T)_r\Upsilon\theta_1\frac{\partial\bar{v}_1}{\partial y}\bigg|_{y=I}\end{aligned} \tag{4.38}$$

It is evident that the interfacial term that leads to the non-self-adjointness of the system has an additional term involving the Marangoni effect that competes with the other interfacial term containing $\big((\rho\beta\kappa_T)_r-1\big)$ value. Thus, even in cases where $(\rho\beta\kappa_T)_r$ (=0.125) value is favorable to yield oscillatory convection, the magnitude of thermo-capillarity can nullify its influence and make the system have only stationary onset, as shown in Fig 4.1. As evident from Fig 4.2, this nullification happens around $\Upsilon = 0.01$ for present system under consideration.

4.5.2 RBM convection in binary fluid system

In this subsection, we will discuss the onset characteristics of RBM convection in a binary fluid system approaching UCST, *i.e.* once we start decreasing the value of r, the fluids become soluble in each other. Correspondingly, the value of surface tension decreases, and it approaches a trivial value once the system's temperature approaches UCST. Thus, the gradient of the surface tension term also decreases and attains a very small value for diminishing r. Therefore, one would expect the minimal effect from surface tension gradients on the convection characteristics for smaller values of r.

It is worthy to recall that in RB convection in the immiscible limit, the window of oscillatory instability invariably shrunk with the decrease in 'r' value. Fig 4.3 and 4.4 show the behavior of the neutral curves with reducing r for different Υ values. Note that the first system (Fig. 4.3) with $\Upsilon = 0.01$ has no oscillatory transition in pure immiscible state *i. e.* $r = 1$. With the increase in temperature, *i. e.* decrease in r, there is a sizable window where

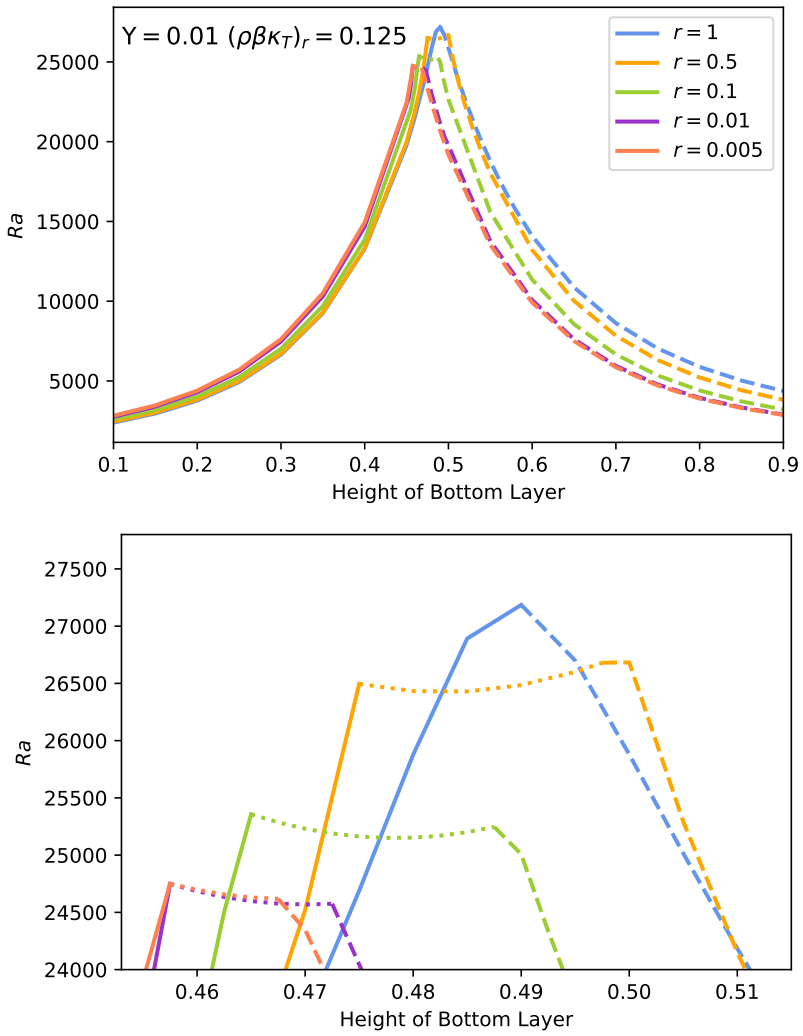

Fig. 4.3 Marginal stability curves for different values of r for $\Upsilon = 0.01$, $(\rho\beta\kappa_T)_r = 0.125$. A decrease in the value of r represents more soluble mixtures.

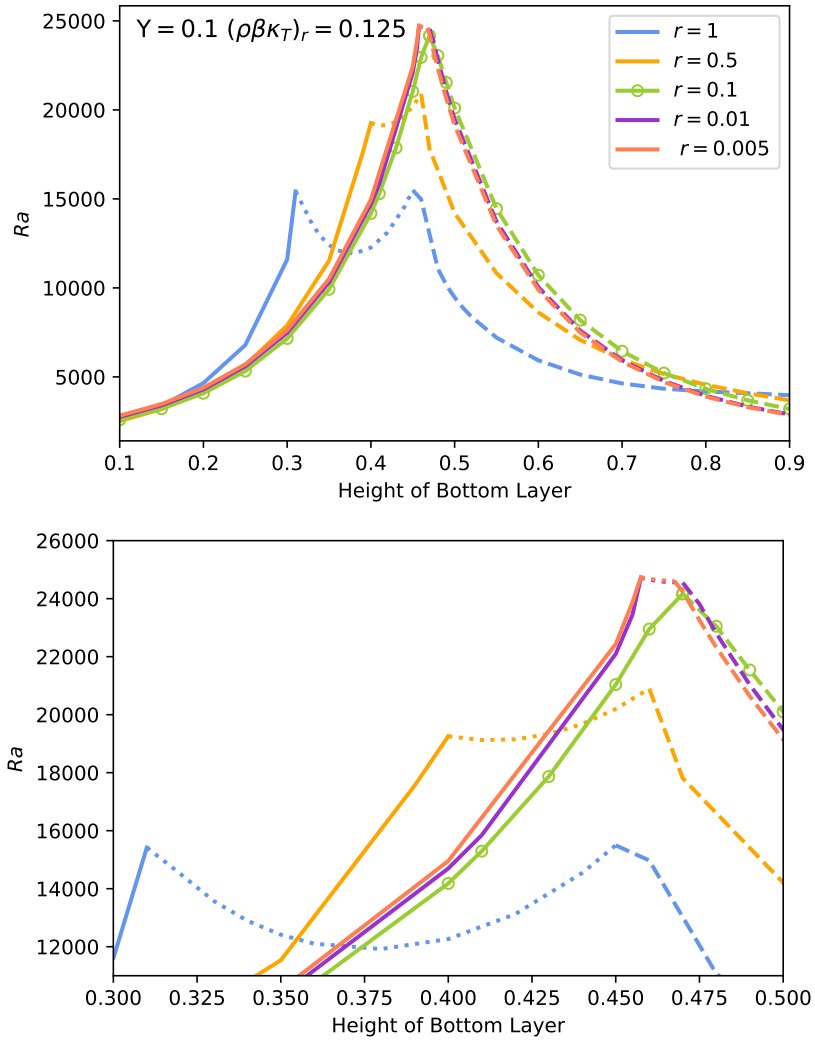

Fig. 4.4 Marginal stability curves for different values of r for $\Upsilon = 0.1$, $(\rho\beta\kappa_T)_r = 0.125$. A decrease in the value of r represents more soluble mixtures.

there is oscillatory onset. However, with the further decrease in 'r' the Marangoni effect becomes feeble, and the system exhibits similar behavior as observed for RB convection in the pure immiscible state.

The second system (Fig. 4.4) with $\Upsilon = 0.1$ possesses a relatively large window for oscillatory onset in the immiscible limit. Interestingly, this system exhibits a different behavior as compared to the previous one. Here, the oscillatory window initially shrinks with the decrease in r, and at a value of $r = 0.1$, it completely vanishes. With further reduction in 'r', we see the oscillatory window reappears and has features similar to the first system.

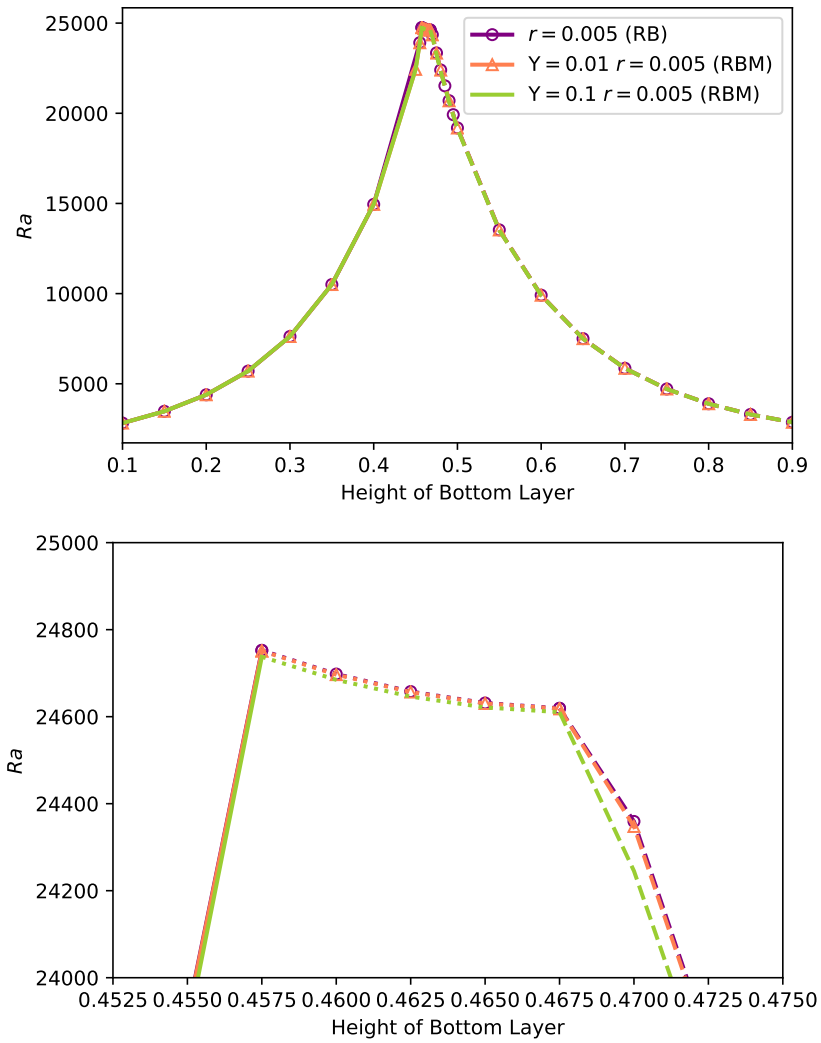

Fig. 4.5 A comparison between the marginal stability curves between the RB and RBM convections closer to the critical temperature.

This can be generalized that when we go closer to the UCST, the Marangoni effect will be negligible, and one observes similar kind of behavior from both RB and RBM convections. It is very evident from Fig. 4.5 that the onset behavior of both the systems are quite similar.

4.5.3 Oscillatory and non-oscillatory onset in RBM convection

We can observe from the above discussions that the addition of the thermo-capillary effect can affect the onset characteristics in both ways. It can either inhibit or expand the oscillatory regime. In order to put things under proper perspective, we now take a combination of data as shown in Fig 4.6. Here, the system with '$\Upsilon = 0.01$' has no oscillatory onset in the immiscible

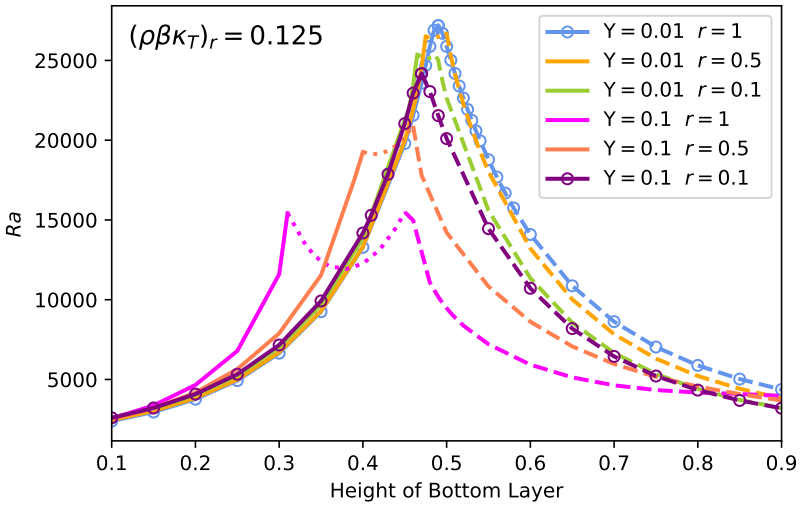

Fig. 4.6 Marginal stability curves for different values of Υ and r for $(\rho\beta\kappa_T)_r = 0.125$. We have put markers (o) in the lines where oscillatory onset is absent.

limit, whereas it manifests a sizable window with the reduction of 'r'. On the other hand, the system with '$\Upsilon = 0.1$' exhibits oscillatory onset in the immiscible limit and becomes completely non-oscillatory at $r = 0.1$. With further reduction of 'r', it regains the zones of oscillatory excitation.

It is worth remembering from the previous section that the nullification of the oscillatory regime in the completely immiscible limit occurs at $\Upsilon = 0.01$. Though it is premature to state that the $r\Upsilon$ plays the same role as Υ in the pure immiscible state ($r = 1.0$) without developing an expression similar to Eq (4.38) for the diffuse interface consideration. However, we have been able to verify this claim for other system with $(\rho\beta\kappa_T)_r = 0.25$ and 0.5 as shown in Fig 4.7. One can observe that the onset nature of the system becomes completely time-independent when $r\Upsilon \approx 10^{-2}$.

4.6 Closure

The current analysis of a two-layer RBM convection with a diffuse interface model provides some interesting information. In the pure immiscible limit, the Marangoni effect plays the dual role of suppressing the oscillatory convection in some range and enhancing it elsewhere. This is essentially due to the contribution played by two boundary terms, one involving $\left((\rho\beta\kappa_T)_r - 1\right)$ and the other involving the non-dimensional surface tension gradient (Υ). In some range of parameters, these terms cancel each other resulting in a self-adjoint system. In contrast, they do not nullify each other in other ranges to make the system non-self-adjoint

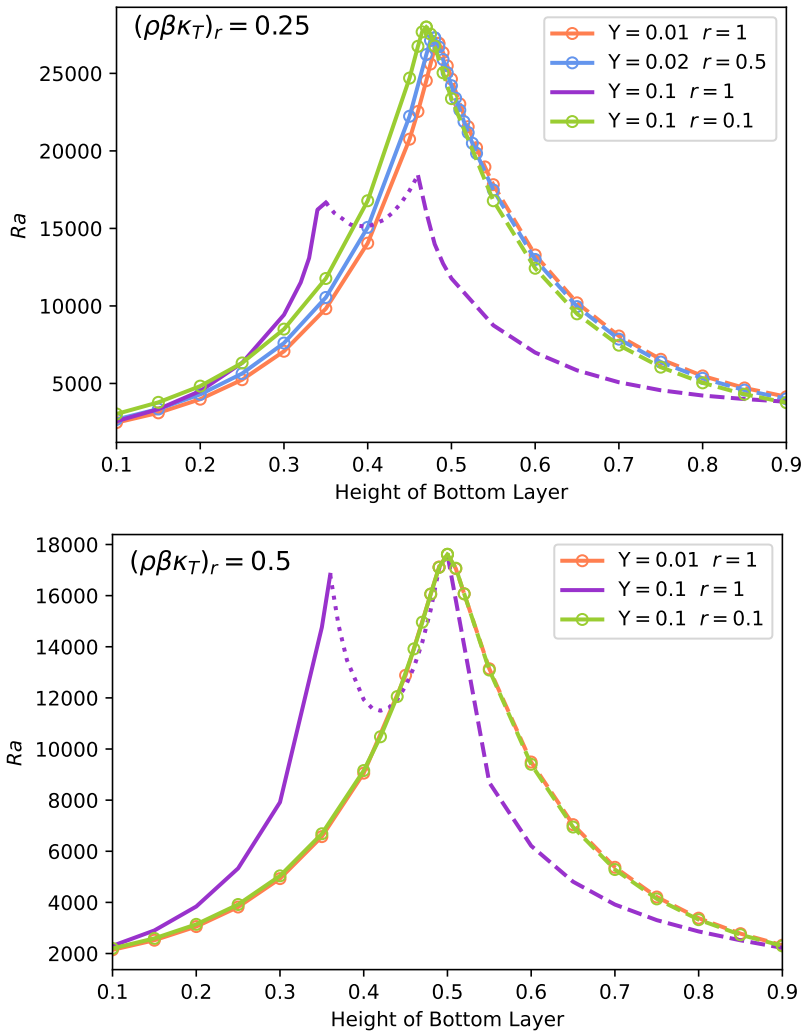

Fig. 4.7 Marginal stability curves for different values of Υ and r for $(\rho\beta\kappa_T)_r = 0.25, 0.5$. We have put markers (o) in the lines where oscillatory onset is absent.

and thus, exhibit oscillatory excitation. The role of solubility is quite intriguing as it acts in unison with the interfacial tension term to make the system either self-adjoint or non-self-adjoint. Thus, it comes with its own dual role, a behavior not particularly evident for the RB instability in the immiscible limit.

Chapter 5

Summary and Conclusions

In the current work, we have utilised a diffuse-interface approach to understand an interesting two-phase instability problem. Notably, our efforts have been focused on predicting the onset behavior of the Rayleigh-Bénard-Marangoni convection in a binary fluid system. A summary of the significant outcomes from the present thesis is provided below.

- A diffuse-interface approach has been developed to understand the onset characteristics of RBM convection in two-phase systems. Here, the two-phase system refers to a binary fluid, which poses the unique property of being partially soluble in each other based on the temperature. They exhibit complete miscibility above a critical temperature, called the upper critical solution temperature (UCST). The current approach has been applied to a wide range of parameters starting from the pure immiscible limit to the states very close to the critical point, i.e., UCST.

- We have utilised a Chebyshev-based spectral collocation procedure for spatially discretising the flow and temperature parameters. This provides an 'exponentially accurate' approach for predicting the critical parameters for the convection onset.

- In view of the thin diffuse interface region present in the domain, an adaptive Chebyshev grid formulation has been employed instead of the standard Gauss-Lobatto-Chebyshev (G-L-C) points to efficiently capture the interfacial region, thereby reducing the computational cost.

- The consistency of the formulation was verified by considering a very small value for the interfacial width ($\varepsilon/H_2 = 10^{-4}$) to mimic the behavior of the system in the immiscible (far below UCST) sharp-interface limit.

- The analysis unequivocally establishes the need for using models with diffuse interface consideration so that the behaviour of systems closer to their critical point is estimated accurately.
- The results reveal that the oscillatory window in the case of RB convection narrows down with the increase in the system's temperature. This behaviour occurs on account of the increase in the system's solubility with temperature. Hence, one can expect the property ratios to approach unity, and the combination $(\rho\beta\kappa_T)_r$ to become closer to unity.
- Even in the pure immiscible limit, the Marangoni effect plays the dual role of suppressing the oscillatory convection in some range and enhancing it elsewhere. Note that the onset characteristics of RBM convection depend on the non-dimensional number Υ in the immiscible limit. For a smaller value of $\Upsilon(=0.001)$, onset characteristics of RB and RBM convections are the same. For $\Upsilon = 0.01$, the onset of RBM convection is completely time-independent. Any increase above $\Upsilon = 0.01$, one can expect to observe oscillatory onset in the immiscible limit.
- Mathematically, the non-self-adjoint nature of the system, responsible for the manifestation of oscillatory onset, is determined by two boundary terms, one involving $\left((\rho\beta\kappa_T)_r - 1\right)$ and the other involving Υ. In the above case, the terms nullify each other at around the value of $\Upsilon = 0.01$, making the system self-adjoint and the onset stationary.
- The Marangoni effect plays a minor role when the system operates very close to the critical temperature. This is because the surface tension value is smaller, close to the critical temperature and the gradient in surface tension is even smaller.
- Further extending the result (obtained for an immiscible system) to the miscible case considerations, the time-independent behavior at the onset is observed at $r\Upsilon = 0.01$.

5.1 Scope for future extension

In the present scenario, we have assumed the value of r to be constant owing to the small temperature change in the system. This assumption will not hold well for a system where the temperature change inside the system is more than $10K$. In the future, one can attempt to develop a model to address the inhomogeneities of the r value in the system. Using the model developed in the current work, one can also attempt to perform a full non-linear fluid flow simulation, which would be relevant for many practical applications.

Appendix A

Sharp-Interface approach

A.1 Domain decomposition approach to the two-layer RB problem

The current appendix describes the procedure for predicting the onset characteristics/parameters of a two-layer Rayleigh-Bénard convection under sharp-interface considerations. The simplest way to perform the analysis is to identify the two layers to be distinct domains that have their own set of equations governing the flow and temperature evolution. A set of matching conditions are applied to the fluid-fluid interface to establish mechanical and thermal continuity between the two layers. The interface is assumed to be non-deformable, a valid consideration for predicting the onset of convection in a fluid system with large disparity in their densities. We now begin the analysis by formulating the underlying governing equations and the boundary/interfacial conditions.

A.1.1 Governing Equations

The current system consists of two non-reacting, immiscible, and incompressible fluids lying quiescently in a cavity of finite height and infinite horizontal extents. Understandably, the lighter fluid is on top of the denser one, in order to avoid Rayleigh-Taylor instability. The interface has been considered non-deformable since the present interests are to study the different scenarios of convection onset for fluids with large density disparity. Here, ρ_i, η_i, ν_i, κ_i, κ_{T_i}, and β_i represent the density, dynamic viscosity, kinematic viscosity, thermal conductivity, thermal diffusivity, and co-efficient of thermal expansion for the two fluids. Note that $i = 1$ represents the bottom fluid and $i = 2$ represents the top fluid. Hence, the ratios utilised here are reciprocal of the ratios specified in the chapters. The ratios of all the

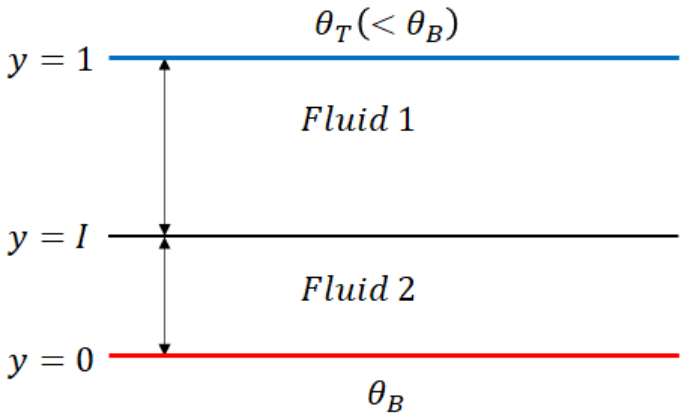

Fig. A.1 System configuration in a sharp interface limit

relevant properties form the input parameters for the problem. In fact, they give rise to the following six dimensionless parameters:

$$\rho = \frac{\rho_1}{\rho_2} \qquad \eta = \frac{\eta_1}{\eta_2} \qquad \nu = \frac{\nu_1}{\nu_2}$$
$$\kappa = \frac{\kappa_1}{\kappa_2} \qquad \kappa_T = \frac{\kappa_{T_1}}{\kappa_{T_2}} \qquad \beta = \frac{\beta_1}{\beta_2}$$

Our main aim is to investigate the flow onset behaviour in two distinct, quiescent fluid layers that are subjected to perturbations under adverse thermal gradients. The non-dimensionalised equations governing the flow and temperature evolutions are given as follows:

For fluid 1 (Top layer)

$$\frac{\partial u_{1j}}{\partial t} + \underline{u}_1 \cdot \nabla u_{1j} = -Pr_1 \nabla_j p_1 + Ra_1 Pr_1 \theta_1 \delta_{j2} + Pr_1 \nabla^2 u_{1j}$$

$$\nabla \cdot \underline{u}_1 = 0 \tag{A.1}$$

$$\frac{\partial \theta_1}{\partial t} + \underline{u}_1 \cdot \nabla \theta_1 = \nabla^2 \theta_1 \tag{A.2}$$

For fluid 2 (Bottom Layer)

$$\frac{\partial u_{2j}}{\partial t} + \underline{u}_2 \cdot \nabla u_{2j} = -\rho Pr_1 \nabla_j p_2 + \frac{Ra_1 Pr_1}{\beta} \theta_2 \delta_{j2} + \frac{Pr_1}{\nu} \nabla^2 u_{2j}$$

$$\nabla \cdot \underline{u}_2 = 0 \tag{A.3}$$

$$\frac{\partial \theta_2}{\partial t} + \underline{u}_2 \cdot \nabla \theta_2 = \frac{1}{\kappa_T} \nabla^2 \theta_2 \tag{A.4}$$

The scaling has been performed here by using the properties of the fluid 1 as follows.

$$x = \frac{x^*}{a_1} \qquad z = \frac{z^*}{a_1} \qquad t = \frac{t^* \kappa_{T_1}}{(a_1)^2}$$

$$u = \frac{u^* a_1}{\kappa_{T_1}} \qquad \theta = \frac{\theta^*}{\Delta\theta} \qquad p = \frac{p^* (a_1)^2}{\rho_1 \kappa_{T_1} \nu_1}$$

$$Ra_1 = \frac{g\beta_1 \Delta\theta^* (a_1)^3}{\nu_1 \kappa_{T_1}} \qquad Pr_1 = \frac{\nu_1}{\kappa_{T_1}}$$

Both the top and bottom plates are assumed to be rigid and are maintained at constant temperatures. The bottom plate is usually heated to generate an adverse density gradient which is responsible for onset of convection in the system. The following conditions are enforced at the material interface between two fluids.

1. Continuity of horizontal velocity: $u_1 = u_2$
2. Continuity of vertical velocity: $v_1 = v_2 = 0$ (owing to the non-deformablity of the interface)
3. Continuity of the heat flux: $\frac{\partial \theta_1}{\partial y} = \frac{1}{\kappa} \frac{\partial \theta_2}{\partial y}$
4. Continuity of temperature: $\theta_1 = \theta_2$
5. Continuity of tangential stress: $\frac{\partial u_1}{\partial y} - \frac{1}{\eta} \frac{\partial u_2}{\partial y} = Ma \frac{\partial \theta}{\partial x}$

A.1.2 Linear stability analysis

We now perform the linear stability analysis to obtain the critical Rayleigh number and the parametric space for oscillatory onset of convection. The base state profile is a pure conduction problem without any underlying flow: $\underline{U}_i^b = 0$, $\frac{\partial \Theta_i^b}{\partial y} = \Lambda_i^b$, where Λ_i^b is the vertical temperature gradient in each fluid layer i. The perturbations to the base state field variables are expanded in terms of normal modes as $(\underline{u}_i', p_i', \theta_i') = (\hat{\underline{u}}_i(y), \hat{p}_i(y), \hat{\theta}_i(y)) \exp(\lambda t + \imath k x)$.

The resultant semi-discrete linearized equations are given as follows:

For fluid 1

$$\lambda \hat{u}_{1j} = -Pr_1 \nabla_j p_1 + Ra_1 Pr_1 \hat{\theta}_1 \delta_{j2} + Pr_1 \left(\frac{d^2 \hat{u}_{1j}}{dy^2} - k^2 \hat{u}_{1j} \right)$$

$$\nabla \cdot \underline{\hat{u}}_1 = 0 \tag{A.5}$$

$$\lambda \hat{\theta}_1 = -\Lambda_1 \hat{v}_1 + \frac{d^2 \hat{\theta}_1}{dy^2} - k^2 \hat{\theta}_1 \tag{A.6}$$

Fluid 2

$$\lambda \hat{u}_{2j} = -\rho Pr_1 \nabla_j p_2 + \frac{Ra_1 Pr_1}{\beta} \hat{\theta}_2 \delta_{j2} + \frac{Pr_1}{\nu} \left(\frac{d^2 \hat{u}_{2j}}{dy^2} - k^2 \hat{u}_{2j} \right)$$

$$\nabla \cdot \underline{\hat{u}}_2 = 0 \tag{A.7}$$

$$\lambda \hat{\theta}_2 = -\Lambda_2 \hat{v}_2 + \frac{1}{\kappa_T} \left(\frac{d^2 \hat{\theta}_2}{dy^2} - k^2 \hat{\theta}_2 \right) \tag{A.8}$$

The associated boundary and interfacial conditions are

$$\underline{\hat{u}}_i = 0 \qquad \hat{\theta}_i = 0 \qquad at\ y = 0, 1 \tag{A.9}$$

$$\hat{u}_1 = \hat{u}_2 \qquad \hat{v}_1 = \hat{v}_2 = 0 \qquad \hat{\theta}_1 = \hat{\theta}_2 \qquad \kappa \frac{d\hat{\theta}_1}{dy} = \frac{d\hat{\theta}_2}{dy} \qquad \eta \frac{d\hat{u}_1}{dy} = \frac{d\hat{u}_2}{dy} \tag{A.10}$$

Once again, the spatial discretization of the variables are carried out using the chebyshev pseudo-spectral method. Any variable Ξ can be expressed as a Lagrangian interpolation of the collocation points

$$\Xi_N(y) = \sum_{i=0}^{N} h_i(y) \Xi(y_i) \tag{A.11}$$

where N is the number of collocation points along the vertical (normal to the interface) direction and the cardinal function $h_i(y)$ is defined over the collocation points, $y_i = \cos \frac{\pi N}{i}$ expressed as

$$h_i(y) = \frac{(-1)^{i+1}(1-y^2) T_N{}'(y)}{\overline{c_i} N^2 (y - y_i)} \tag{A.12}$$

where $\overline{c_i} = 2$ for the end points, 1 for all in between points and $T_N{}'(y)$ is the N-th derivative of the Chebyshev polynomial of first kind. The pressure variable alone is expanded as,

$$p_{N-2}(y) = \sum_{i=1}^{N-1} \hat{h}_i(y) p(y_i) \tag{A.13}$$

wherein, the cardinal is defined as

$$\hat{h}_i(y) = \frac{(1-y_i{}^2)}{(1-y)} h_i(y) \tag{A.14}$$

Using above polynomial expansions for different variables, the set of governing equations can be represented as a generalized eigenvalue problem of the form $A\underline{X} = \lambda B\underline{X}$. This eigenvalue problem has been solved here by using the standard QR algorithm. Solving the generalized eigenvalue problem may give rise to the spurious modes due to the sparsity of the matrix B, mainly due to the zero-valued rows corresponding to the continuity equation and the boundary conditions. The presence of these spurious modes possesses a serious threat to finding the largest eigenvalue, since these large spurious modes may be confused with the actual eigenvalues. To avoid such a scenario, we employ the reciprocal approach. Instead of finding the largest eigenvalue for $A\underline{X} = \lambda B\underline{X}$, we aim for the smallest eigenvalue for $\lambda A\underline{X} = B\underline{X}$. We check for the presence of zero-valued eigenvectors while calculating these eigenvalues and if found, we discard those from the eigenvalue calculation process. Figure A.2 shows the typical neutral curve obtained for the two layer system. The fluid properties used for this analysis and inferences from these curves have been dealt in detail in chapter 3.

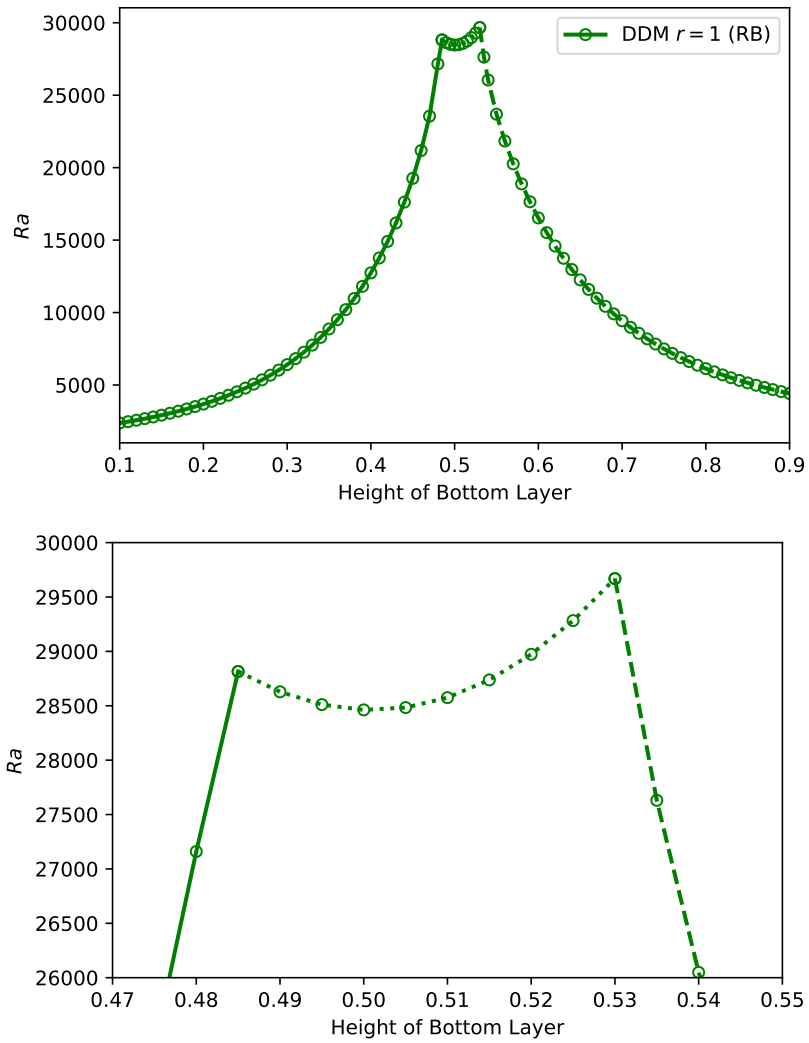

Fig. A.2 Neutral Curve obtained via Domain Decomposition Method

Appendix B

Linearization of the Cahn-Hilliard equation

The current appendix deals with linearization of Cahn-Hilliard (CH) equation in the context of Rayleigh-Bénard-Marangoni convection. In a general form, the CH equation is written as

$$\frac{\partial \phi}{\partial t} + \boldsymbol{u} \cdot \boldsymbol{\nabla} \phi = \boldsymbol{\nabla} \cdot \left[\gamma \boldsymbol{\nabla} \left\{ \Lambda \left(\frac{r^q \phi^3 - r\phi}{\varepsilon^2} - r^p \nabla^2 \phi \right) \right\} \right] \tag{B.1}$$

We now intend to incorporate the non-trivial value of surface tension gradient into the analysis. One typically represents the surface tension term via Λ, which is the magnitude of the mixing free energy. Here, we will consider the variation of interfacial tension with temperature only. Thus, Λ can no longer be considered as a constant and for the simplest case, a linear form of Λ is assumed, $\Lambda = \Lambda_0 - \Lambda_\theta \theta$. The linearized version of the CH equation is then given as

$$\frac{\partial \phi^{'}}{\partial t} + \boldsymbol{u}^{'} \cdot \boldsymbol{\nabla} \Phi^b = \boldsymbol{\nabla} \cdot \left[\gamma \boldsymbol{\nabla} \left\{ \left(\Lambda_0 - \Lambda_\theta \Theta^b \right) \left(r^q 3 (\Phi^b)^2 \phi^{'} - r\phi^{'} - \left(\frac{\varepsilon}{H_2} \right)^2 r^p \nabla^2 \phi^{'} \right) \right\} \right] \tag{B.2}$$

Assuming the mobility parameter γ to be a constant, the dimensionless CH takes the following form:

$$\frac{\partial \phi^{'}}{\partial t} + \boldsymbol{u}^{'} \cdot \boldsymbol{\nabla} \Phi^b = M \nabla^2 \left[\left(1 - \frac{Ma}{Ca} \Theta^b \right) \left(r^q 3 (\Phi^b)^2 \phi^{'} - r\phi^{'} - \left(\frac{\varepsilon}{H_2} \right)^2 r^p \nabla^2 \phi^{'} \right) \right] \tag{B.3}$$

Here, M is the dimensionless mobility which represents the ratio of the diffuse-interface diffusivity to the thermal diffusivity, $\frac{\gamma \Lambda_0}{\varepsilon^2 \kappa_{T_2}}$. $Ma (= \frac{\sigma_\theta \Delta \theta H_2}{\eta_2 \kappa_{T_2}})$ is the Marangoni number which gives the relative importance of the transport due to surface tension gradient to the diffusive

effects of the gradient, and Ca is the inverse capillary number. Note that this number is different from Γ_θ that we defined earlier, where $\Gamma_\theta = \frac{\Lambda}{\rho_2 \kappa_{T_2}^2}$. Usually Ca is defined as

$$Ca = \frac{\sigma}{\eta V} \tag{B.4}$$

where

- η : dynamic viscosity
- V : velocity scale
- σ : surface tension

We have chosen the velocity scale, V to be $\frac{\kappa_{T_2}}{H_2}$. So, the inverse capillary number becomes $Ca = \frac{\sigma H_2}{\eta \kappa_{T_2}}$.

Also note that the Marangoni number (Ma) and the Rayleigh number (Ra) are not independent.

$$\frac{Ma}{Ra} = \frac{\sigma_\theta}{g\rho_2\beta_2 H_2^2} = \Upsilon \tag{B.5}$$

Thus, the above dimensionless CH equation can be rewritten as

$$\frac{\partial \phi'}{\partial t} + \boldsymbol{u}' \cdot \boldsymbol{\nabla}\Phi^b = M\nabla^2 \left[\left(1 - \frac{\Upsilon Ra}{Ca}\Theta^b\right) \left(r^q 3(\Phi^b)^2 \phi' - r\phi' - \left(\frac{\varepsilon}{H_2}\right)^2 r^p \nabla^2 \phi' \right) \right] \tag{B.6}$$

$$\begin{aligned} \frac{\partial \phi'}{\partial t} + \boldsymbol{u}' \cdot \boldsymbol{\nabla}\Phi^b =& M\nabla^2 \left(r^q 3(\Phi^b)^2 \phi' - r\phi' - \left(\frac{\varepsilon}{H_2}\right)^2 r^p \nabla^2 \phi' \right) \\ & - M\frac{\Upsilon Ra}{Ca}\nabla^2 \left[\Theta^b \left(r^q 3(\Phi^b)^2 \phi' - r\phi' - \left(\frac{\varepsilon}{H_2}\right)^2 r^p \nabla^2 \phi' \right) \right] \end{aligned} \tag{B.7}$$

We employ the normal mode analysis to carry out the linear stability analysis.

Let us calculate the second part on RHS *i.e.*$\nabla^2\left[\Theta^b\left(r^q 3(\Phi^b)^2\phi' - r\phi' - \left(\frac{\varepsilon}{H_2}\right)^2 r^p\nabla^2\phi'\right)\right]$

$$\begin{aligned}\nabla^2\left[\Theta^b\left(r^q 3(\Phi^b)^2\phi' - r\phi' - \left(\frac{\varepsilon}{H_2}\right)^2 r^p\nabla^2\phi'\right)\right] = \Theta^b\Bigg[&3r^q\Big((\Phi^b)^2(-k^2\hat{\phi}) + 2(\frac{d\Phi^b}{dy})^2\hat{\phi} + 2(\Phi^b)\frac{d^2\Phi^b}{dy^2}\hat{\phi}\\ &+ 4(\Phi^b)\frac{d\Phi^b}{dy}\frac{d\hat{\phi}}{dy} + (\Phi^b)^2\frac{d^2\hat{\phi}}{dy^2}\Big)\\ &- r(\frac{d^2\hat{\phi}}{dy^2} - k^2\hat{\phi}) - \left(\frac{\varepsilon}{H_2}\right)^2 r^p\left(\frac{d^4\hat{\phi}}{dy^4} - 2k^2\frac{d^2\hat{\phi}}{dy^2} + k^4\hat{\phi}\right)\Bigg]\\ &+ 2\frac{d\Theta^b}{dy}\Bigg(r^q 3(\Phi^b)^2\frac{d\hat{\phi}}{dy} + r^q 6(\Phi^b)\frac{d\Phi^b}{dy}\hat{\phi} - r\frac{d\hat{\phi}}{dy}\\ &- \left(\frac{\varepsilon}{H_2}\right)^2 r^p\left(\frac{d^2}{dy^2} - k^2\right)\frac{d\hat{\phi}}{dy}\Bigg)\\ &+ \frac{d^2\Theta^b}{dy^2}\left(r^q 3(\Phi^b)^2\hat{\phi} - r\hat{\phi} - \left(\frac{\varepsilon}{H_2}\right)^2 r^p\nabla^2\hat{\phi}\right)\end{aligned} \tag{B.8}$$

Finally we can have the linearized form of the perturbed phase evolution equation

$$\begin{aligned}\lambda\hat{\phi} + \hat{v}\frac{\partial\Phi^b}{\partial y} = M\Bigg[&3r^q\Bigg(-(\Phi^b)^2k^2\hat{\phi} + 2(\frac{d\Phi^b}{dy})^2\hat{\phi} + 2\Phi^b\frac{d^2\Phi^b}{dy^2}\hat{\phi} + 4\Phi^b\frac{d\Phi^b}{dy}\frac{d\hat{\phi}}{dy} + (\Phi^b)^2\frac{d^2\hat{\phi}}{dy^2}\Bigg)\\ &- r\left(-k^2\hat{\phi} + \frac{d^2\hat{\phi}}{dy^2}\right) - \left(\frac{\varepsilon}{H_2}\right)^2 r^p\left(\frac{d^4\hat{\phi}}{dy^4} - 2k^2\frac{d^2\hat{\phi}}{dy^2} + k^4\hat{\phi}\right)\Bigg]\\ -M\left(\frac{\Upsilon Ra}{Ca}\right)\Theta^b\Bigg[&3r^q\Bigg(-(\Phi^b)^2k^2\hat{\phi} + 2(\frac{d\Phi^b}{dy})^2\hat{\phi} + 2\Phi^b\frac{d^2\Phi^b}{dy^2}\hat{\phi} + 4\Phi^b\frac{d\Phi^b}{dy}\frac{d\hat{\phi}}{dy} + (\Phi^b)^2\frac{d^2\hat{\phi}}{dy^2}\Bigg)\\ &- r\left(-k^2\hat{\phi} + \frac{d^2\hat{\phi}}{dy^2}\right) - \left(\frac{\varepsilon}{H_2}\right)^2 r^p\left(\frac{d^4\hat{\phi}}{dy^4} - 2k^2\frac{d^2\hat{\phi}}{dy^2} + k^4\hat{\phi}\right)\Bigg]\\ -2M\left(\frac{\Upsilon Ra}{Ca}\right)\frac{d\Theta^b}{dy}\Bigg[&3r^q(\Phi^b)^2\frac{d\hat{\phi}}{dy} + 6r^q(\Phi^b)\frac{d\Phi^b}{dy}\hat{\phi} - r\frac{d\hat{\phi}}{dy} - \left(\frac{\varepsilon}{H_2}\right)^2 r^p\left(\frac{d^2}{dy^2} - k^2\right)\frac{d\hat{\phi}}{dy}\Bigg]\\ -M\left(\frac{\Upsilon Ra}{Ca}\right)&\frac{d^2\Theta^b}{dy^2}\left(r^q 3(\Phi^b)^2\hat{\phi} - r\hat{\phi} - \left(\frac{\varepsilon}{H_2}\right)^2 r^p\nabla^2\hat{\phi}\right)\end{aligned} \tag{B.9}$$

Appendix C

Derivation of the interfacial stress terms

This appendix deals with derivation of the interfacial stress terms in the context of the phase-field model representing the Rayleigh-Bénard-Marangoni convection. Recall from chapter 3 that the generalized Navier-Stokes equations involve the

$$\frac{\partial \rho \boldsymbol{u}}{\partial t} + \boldsymbol{\nabla} \cdot (\rho \boldsymbol{u}\boldsymbol{u}) = -\boldsymbol{\nabla} p + \boldsymbol{\nabla} \cdot \left[\eta \left(\boldsymbol{\nabla} \boldsymbol{u} + (\boldsymbol{\nabla} \boldsymbol{u})^{+} - \frac{2}{3} \boldsymbol{\nabla} \cdot \boldsymbol{u} \boldsymbol{I} \right) \right] + \boldsymbol{\nabla} \cdot \left(\mathscr{L} \boldsymbol{I} - \boldsymbol{\nabla} \phi \frac{\partial \mathscr{L}}{\partial (\boldsymbol{\nabla} \phi)} \right) - \rho^{'} g \mathbf{1}_{y} \tag{C.1}$$

$$\mathscr{L} = \frac{\Lambda}{4\varepsilon^2} r^{q} \phi^{4} - \frac{\Lambda}{2\varepsilon^2} r \phi^{2} + \frac{\Lambda}{2} r^{p} |\boldsymbol{\nabla} \phi(x)|^{2} \tag{C.2}$$

Let us now calculate the contribution from the non-viscous stress tensor : $\boldsymbol{\nabla} \cdot \left(\mathscr{L} \boldsymbol{I} - \boldsymbol{\nabla} \phi \frac{\partial \mathscr{L}}{\partial (\boldsymbol{\nabla} \phi)} \right)$

$$\begin{aligned}\boldsymbol{\nabla}\cdot\left(\mathscr{L}\boldsymbol{I}-\boldsymbol{\nabla}\phi\frac{\partial\mathscr{L}}{\partial(\boldsymbol{\nabla}\phi)}\right)&=\boldsymbol{\nabla}\cdot\left(\left\{\frac{\Lambda}{4\varepsilon^2}r^q\phi^4-\frac{\Lambda}{2\varepsilon^2}r\phi^2+\frac{\Lambda}{2}r^p|\boldsymbol{\nabla}\phi(x)|^2\right\}\boldsymbol{I}\right.\\&\qquad\left.-\boldsymbol{\nabla}\phi\frac{\partial}{\partial(\boldsymbol{\nabla}\phi)}\left\{\frac{\Lambda}{4\varepsilon^2}r^q\phi^4-\frac{\Lambda}{2\varepsilon^2}r\phi^2+\frac{\Lambda}{2}r^p|\boldsymbol{\nabla}\phi(x)|^2\right\}\right)\\&=\frac{\partial}{\partial x_j}\left(\left\{\frac{\Lambda}{4\varepsilon^2}r^q\phi^4-\frac{\Lambda}{2\varepsilon^2}r\phi^2+\frac{\Lambda}{2}r^p|\nabla_k\phi(x)|^2\right\}\delta_{ij}\right.\\&\qquad\left.-\nabla_j\phi\frac{\partial}{\partial(\nabla_i\phi)}\left\{\frac{\Lambda}{4\varepsilon^2}r^q\phi^4-\frac{\Lambda}{2\varepsilon^2}r\phi^2+\frac{\Lambda}{2}r^p|\nabla_k\phi(x)|^2\right\}\right)\\&=\frac{\partial}{\partial x_i}\left(\frac{\Lambda}{4\varepsilon^2}r^q\phi^4-\frac{\Lambda}{2\varepsilon^2}r\phi^2+\frac{\Lambda}{2}r^p|\nabla_k\phi(x)|^2\right)\\&\qquad-\frac{\partial}{\partial x_j}\left[\nabla_j\phi\frac{\partial}{\partial(\nabla_i\phi)}\left(\frac{\Lambda}{4\varepsilon^2}r^q\phi^4-\frac{\Lambda}{2\varepsilon^2}r\phi^2+\frac{\Lambda}{2}r^p|\nabla_k\phi(x)|^2\right)\right]\end{aligned}\tag{C.3}$$

Calculating the first part of the RHS of the equation gives

$$\begin{aligned}\frac{\partial}{\partial x_i}\left(\frac{\Lambda}{4\varepsilon^2}r^q\phi^4-\frac{\Lambda}{2\varepsilon^2}r\phi^2+\frac{\Lambda}{2}r^p|\nabla_k\phi(x)|^2\right)&=\frac{\Lambda}{\varepsilon^2}\left(r^q\phi^3-r\phi\right)\nabla_i\phi+\Lambda r^p\frac{\partial}{\partial x_i}\left(\frac{1}{2}\left|\frac{\partial\phi}{\partial x_k}\right|^2\right)\\&\quad+\left(\frac{1}{4\varepsilon^2}r^q\phi^4-\frac{1}{2\varepsilon^2}r\phi^2+\frac{1}{2}r^p|\nabla_k\phi(x)|^2\right)\frac{\partial\Lambda}{\partial\theta}\nabla_i\theta\end{aligned}\tag{C.4}$$

The second part gives

$$\begin{aligned}\frac{\partial}{\partial x_j}\left[\nabla_j\phi\frac{\partial}{\partial(\nabla_i\phi)}\left(\frac{\Lambda}{4\varepsilon^2}r^q\phi^4-\frac{\Lambda}{2\varepsilon^2}r\phi^2+\frac{\Lambda}{2}r^p|\nabla_k\phi(x)|^2\right)\right]&=\nabla_j\left(\nabla_j\phi\Lambda r^p\nabla_i\phi\right)\\&=\Lambda r^p\nabla_j\left(\nabla_j\phi\nabla_i\phi\right)+r^p\nabla_j\phi\nabla_i\phi\frac{\partial\Lambda}{\partial\theta}\nabla_j\theta\\&=\Lambda r^p\left(\frac{1}{2}\nabla_i|\nabla_j\phi|^2+\nabla_j^2\phi\nabla_i\phi\right)\\&\quad+r^p\frac{\partial\Lambda}{\partial\theta}\nabla_j\phi\nabla_j\theta\nabla_i\phi\end{aligned}\tag{C.5}$$

Finally, we obtain the contribution from the non-viscous stress tensor as

$$\begin{aligned}\boldsymbol{\nabla}\cdot\left(\mathscr{L}\boldsymbol{I}-\boldsymbol{\nabla}\phi\frac{\partial\mathscr{L}}{\partial(\boldsymbol{\nabla}\phi)}\right) &= \left(\Lambda_0+\frac{\partial\Lambda}{\partial\theta}\theta\right)\left(\frac{r^q\phi^3-r\phi}{\varepsilon^2}-r^p\nabla^2\phi\right)\boldsymbol{\nabla}\phi \\ &\quad+\left(\frac{1}{4\varepsilon^2}r^q\phi^4-\frac{1}{2\varepsilon^2}r\phi^2+\frac{1}{2}r^p|\boldsymbol{\nabla}\phi|^2\right)\frac{\partial\Lambda}{\partial\theta}\boldsymbol{\nabla}\theta-r^p\frac{\partial\Lambda}{\partial\theta}(\boldsymbol{\nabla}\phi)\cdot(\boldsymbol{\nabla}\theta)\boldsymbol{\nabla}\phi \\ &= \mu\boldsymbol{\nabla}\phi+\left(\frac{1}{4\varepsilon^2}r^q\phi^4-\frac{1}{2\varepsilon^2}r\phi^2+\frac{1}{2}r^p|\boldsymbol{\nabla}\phi|^2\right)\frac{\partial\Lambda}{\partial\theta}\boldsymbol{\nabla}\theta-r^p\frac{\partial\Lambda}{\partial\theta}(\boldsymbol{\nabla}\phi)\cdot(\boldsymbol{\nabla}\theta)\boldsymbol{\nabla}\phi\end{aligned} \tag{C.6}$$

Note that if we neglect the variation of Λ with temperature *i.e.* ignore the surface tension gradient, we will obtain the form

$$\begin{aligned}\boldsymbol{\nabla}\cdot\left(\mathscr{L}\boldsymbol{I}-\boldsymbol{\nabla}\phi\frac{\partial\mathscr{L}}{\partial(\boldsymbol{\nabla}\phi)}\right) &= \Lambda_0\left(\frac{r^q\phi^3-r\phi}{\varepsilon^2}-r^p\nabla^2\phi\right)\boldsymbol{\nabla}\phi \\ &= \mu\boldsymbol{\nabla}\phi\end{aligned} \tag{C.7}$$

where $\mu=\Lambda_0\left(\frac{r^q\phi^3-r\phi}{\varepsilon^2}-r^p\nabla^2\phi\right)$

Appendix D

Energy equation

In current appendix, we derive the appropriate form of the energy equation corresponding to the phase-field formulation for Rayleigh-Bénard-Marangoni convection.

Here, the total energy of the system can be written as

$$E(\phi,\theta)=\int_{\Omega}\left[\frac{1}{2}\rho|\boldsymbol{u}|^2+\rho gy+e_0+\rho c(\theta-\theta_0)+\frac{\Lambda_0}{4\varepsilon^2}r^q\phi^4-\frac{\Lambda_0}{2\varepsilon^2}r\phi^2+\frac{\Lambda_0}{2}r^p|\boldsymbol{\nabla}\phi(x)|^2\right]d\mathbf{x} \tag{D.1}$$

Following Anderson *et al.*[4] the energy balance equation can be written as

$$\frac{\partial\rho c\theta}{\partial t}+\boldsymbol{\nabla}\cdot(\rho\boldsymbol{u}c\theta)+\left(\frac{\Lambda_0 r^q}{\varepsilon^2}\phi^3-\frac{\Lambda_0 r}{\varepsilon^2}\phi\right)\frac{D\phi}{Dt}+\left(\frac{\Lambda_0}{4\varepsilon^2}r^q\phi^4-\frac{\Lambda_0}{2\varepsilon^2}r\phi^2\right)\boldsymbol{\nabla}\cdot\boldsymbol{u}+\Lambda_0 r^p Q_G=-\boldsymbol{\nabla}\cdot\boldsymbol{q}_E+\mathscr{D} \tag{D.2}$$

The flux of energy through the boundary of the control volume is given by

$$\boldsymbol{q}_E=\tilde{\kappa}\boldsymbol{\nabla}\left(\frac{1}{\theta}\right)-\Lambda_0 r^p\boldsymbol{\nabla}\phi\frac{D\phi}{Dt} \tag{D.3}$$

hence,

$$-\boldsymbol{\nabla}\cdot\boldsymbol{q}_E=\boldsymbol{\nabla}\cdot(\kappa\boldsymbol{\nabla}\theta)+\Lambda_0 r^p\boldsymbol{\nabla}\cdot\left(\boldsymbol{\nabla}\phi\frac{D\phi}{Dt}\right) \tag{D.4}$$

where $\tilde{\kappa}=\theta^2\kappa$ [4]. κ is the thermal conductivity of the material.

Note that

$$Q_G=\boldsymbol{\nabla}\cdot\left(\boldsymbol{\nabla}\phi\frac{D\phi}{Dt}\right)-\nabla^2\phi\frac{D\phi}{Dt}-\boldsymbol{\nabla}\boldsymbol{u}:\boldsymbol{\nabla}\phi\boldsymbol{\nabla}\phi+\frac{1}{2}|\boldsymbol{\nabla}\phi|^2\boldsymbol{\nabla}\cdot\boldsymbol{u} \tag{D.5}$$

and

$$\frac{d}{dt}\int_{\Omega}\frac{1}{2}|\boldsymbol{\nabla}\phi|^2d\boldsymbol{x}=\int_{\Omega}Q_G d\boldsymbol{x} \tag{D.6}$$

Thus, we obtain

$$\frac{\partial \rho c\theta}{\partial t}+\boldsymbol{\nabla}\cdot(\rho \boldsymbol{u} c\theta)+\Lambda_0\left(\frac{r^q\phi^3-r\phi}{\varepsilon^2}-r^q\nabla^2\phi\right)\frac{D\phi}{Dt} +\left(\frac{\Lambda_0}{4\varepsilon^2}r^q\phi^4-\frac{\Lambda_0}{2\varepsilon^2}r\phi^2+\frac{\Lambda_0}{2}r^p|\boldsymbol{\nabla}\phi(x)|^2\right)\boldsymbol{\nabla}\cdot\boldsymbol{u}=\boldsymbol{\nabla}\cdot(\kappa\boldsymbol{\nabla}\theta)+\mathscr{D}+\Lambda_0 r^p\boldsymbol{\nabla}\boldsymbol{u}:\boldsymbol{\nabla}\phi\boldsymbol{\nabla}\phi \tag{D.7}$$

Now we discuss the significance of the term $\mathscr{D}$, which is given as

$$\mathscr{D}=\boldsymbol{\tau}:\boldsymbol{\nabla}\boldsymbol{u}-p\boldsymbol{\nabla}\cdot\boldsymbol{u}+\boldsymbol{\tau}^{nv}:\boldsymbol{\nabla}\boldsymbol{u} \tag{D.8}$$

where $\boldsymbol{\tau}^{nv}=\mathscr{L}\boldsymbol{I}-\boldsymbol{\nabla}\phi\frac{\partial\mathscr{L}}{\partial(\boldsymbol{\nabla}\phi)}$, and $\boldsymbol{\tau}=\mu\left(\boldsymbol{\nabla}\boldsymbol{u}+(\boldsymbol{\nabla}\boldsymbol{u})^{+}-\frac{2}{3}\boldsymbol{\nabla}\cdot\boldsymbol{u}\boldsymbol{I}\right)$.

"$\boldsymbol{\tau}:\boldsymbol{\nabla}\boldsymbol{u}$" is the viscous dissipation term. We can perform an order of magnitude analysis to find out the importance of the viscous dissipation term. The convection of internal energy $\approx\frac{\rho c\Delta\theta u_R}{L_R}$, where u_R is the reference velocity scale, L_R is the reference macroscopic scale. The viscous dissipation $\approx\eta\frac{{u_R}^2}{{L_R}^2}$. Thus, the viscous dissipation to the rate of change of the internal energy is of the order of $\frac{\eta u_R}{\rho c\Delta\theta L_R}$. For a typical liquid system $\frac{\eta}{\rho c}\approx 10^{-9}$ s K, and $\frac{u_R}{\Delta\theta L_R}$ is not very large for the current system. Thus, from the above calculations, we can conclude that the viscous dissipation will not play any significant role in the present convection problems [65, 24].

The second term on the RHS *i.e.* "$-p\boldsymbol{\nabla}\cdot\boldsymbol{u}$" represents the heating due to the compression. This is a part of the reversible work done on the system by the normal forces. For a typical liquid system, this heating is negligible at normal pressures, hence we can neglect this term [24].

The last term represents the work done due to interfacial forcing terms. "$\boldsymbol{\tau}^{nv}:\boldsymbol{\nabla}\boldsymbol{u}$" is of the order of $\frac{\Lambda_0 u_R}{\varepsilon^2 L_R}$, where as the rate storage of internal energy is of the order $\frac{\rho c\Delta\theta u_R}{L_R}$. The ratio of the reversible work to the storage term is given as $\frac{\Lambda_0}{\varepsilon^2\rho c\Delta\theta}$, which is at least $\approx\mathscr{O}(10^{-2})$ in our case. Thus, we can neglect this term in our energy equation. Like wise, we can neglect the last term on RHS of the energy equation.

Finally we obtain our energy balance equation as

$$\frac{\partial \rho c\theta}{\partial t}+\boldsymbol{\nabla}\cdot(\rho \boldsymbol{u} c\theta)+\Lambda_0\left(\frac{r^q\phi^3-r\phi}{\varepsilon^2}-r^q\nabla^2\phi\right)\frac{D\phi}{Dt} +\left(\frac{\Lambda_0}{4\varepsilon^2}r^q\phi^4-\frac{\Lambda_0}{2\varepsilon^2}r\phi^2+\frac{\Lambda_0}{2}r^p|\boldsymbol{\nabla}\phi(x)|^2\right)\boldsymbol{\nabla}\cdot\boldsymbol{u}=\boldsymbol{\nabla}\cdot(\kappa\boldsymbol{\nabla}\theta) \tag{D.9}$$

For constant value of Λ, one can write

$$\frac{\partial \rho c\theta}{\partial t} + \boldsymbol{\nabla}\cdot(\rho \boldsymbol{u} c\theta) + \mu\frac{D\phi}{Dt} + \mathscr{L}\boldsymbol{\nabla}\cdot\boldsymbol{u} = \boldsymbol{\nabla}\cdot(\kappa\boldsymbol{\nabla}\theta) \tag{D.10}$$

where $\mathscr{L} = \left(\frac{\Lambda}{4\varepsilon^2}r^q\phi^4 - \frac{\Lambda}{2\varepsilon^2}r\phi^2 + \frac{\Lambda}{2}r^p|\boldsymbol{\nabla}\phi(x)|^2\right)$ is the Lagrangian density, and $\mu = \Lambda\left(\frac{r^q\phi^3 - r\phi}{\varepsilon^2} - r^q\nabla^2\phi\right)$.

Since we have considered the volume-averaged velocity to take the advantage of solenoidal velocity field ($\boldsymbol{\nabla}\cdot\boldsymbol{u} = 0$), the energy balance equation can further be rewritten to

$$\frac{\partial \rho c\theta}{\partial t} + \boldsymbol{\nabla}\cdot(\rho \boldsymbol{u} c\theta) + \theta\frac{\partial \rho c}{\partial \phi}\boldsymbol{\nabla}\cdot\boldsymbol{j}_\phi + \Lambda_0\left(\frac{r^q\phi^3 - r\phi}{\varepsilon^2} - r^q\nabla^2\phi\right)\frac{D\phi}{Dt} = \boldsymbol{\nabla}\cdot(\kappa\boldsymbol{\nabla}\theta) \tag{D.11}$$

and for constant value of Λ, the equation gets reduced to

$$\frac{\partial \rho c\theta}{\partial t} + \boldsymbol{\nabla}\cdot(\rho \boldsymbol{u} c\theta) + \theta\frac{\partial \rho c}{\partial \phi}\boldsymbol{\nabla}\cdot\boldsymbol{j}_\phi + \mu\frac{D\phi}{Dt} = \boldsymbol{\nabla}\cdot(\kappa\boldsymbol{\nabla}\theta) \tag{D.12}$$

Appendix E

Revisiting theory to predict oscillatory onset in RBM convection

In this appendix, we will derive a single equation concerning the growth rate of the perturbation. The equation manifests information about the self-adjoint or non-self-adjoint nature of the RBM convection. We take the governing equations as defined in [54], but we consider the finite Pr case here. Stratification of the fluids (Fig (E.1)) gives six dimensionless ratios in fluid properties:

$$\rho = \frac{\rho_1}{\rho_2} \qquad \eta = \frac{\eta_1}{\eta_2} \qquad \nu = \frac{\nu_1}{\nu_2}$$
$$\kappa = \frac{\kappa_1}{\kappa_2} \qquad \kappa_T = \frac{\kappa_{T_1}}{\kappa_{T_2}} \qquad \beta = \frac{\beta_1}{\beta_2}$$

where ρ_i, η_i, ν_i, κ_i, κ_{T_i}, and β_i represent the density, dynamic viscosity, kinematic viscosity, thermal conductivity, thermal diffusivity, and co-efficient of thermal expansion of fluid i.

We have used the following scales to arrive at the dimensionless equations:

$$L_R = H_2 \qquad t_R = \frac{{H_2}^2}{\kappa_{T2}} \qquad u_R = \frac{\kappa_{T2}}{H_2} \qquad \theta_R = \theta_B - \theta_T \qquad p_R = \frac{\rho_2 \kappa_{T2} \nu_2}{{H_2}^2}$$

Following the typical normal mode expansion, i.e., the perturbations being proportional to $\exp(\lambda t + ikx)$, we get the temporal derivatives as

$$\lambda \boldsymbol{u}_1 = -Pr_2 \boldsymbol{\nabla} p_1 + Ra_2 Pr_2 \theta_1 \mathbf{1}_y + Pr_2 \nabla^2 \boldsymbol{u}_1 \tag{E.1}$$

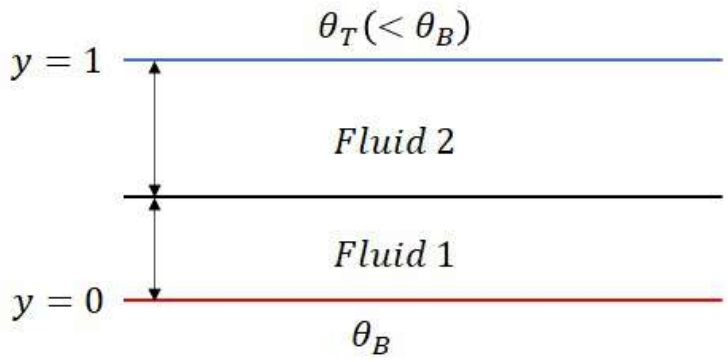

Fig. E.1 System configuration

$$\lambda \boldsymbol{u}_2 = -\rho Pr_2 \boldsymbol{\nabla} p_2 + \frac{Ra_2 Pr_2}{\beta}\theta_2 \mathbf{1}_y + \frac{Pr_2}{\nu}\nabla^2 \boldsymbol{u}_2 \tag{E.2}$$

$$\lambda \theta_1 = -v_1 \Lambda_1 + \nabla^2 \theta_1 \tag{E.3}$$

$$\lambda \theta_2 = -v_2 \Lambda_2 + \frac{1}{\kappa_T}\nabla^2 \theta_2 \tag{E.4}$$

Operating with $\mathbf{1}_y \cdot \boldsymbol{\nabla} \times \boldsymbol{\nabla}$, the momentum equations take the following forms

$$\lambda \nabla^2 v_1 = -k^2 Ra_2 Pr_2 \theta_1 + Pr_2 \nabla^4 v_1, \tag{E.5}$$

$$\lambda \nabla^2 v_2 = -k^2 \frac{Ra_2 Pr_2}{\beta}\theta_2 + \frac{Pr_2}{\nu}\nabla^4 v_2. \tag{E.6}$$

Eventually, the set of governing equations can be written as

$$\frac{\lambda}{Pr_2}\nabla^2 v_1 = -k^2 Ra_2 \theta_1 + \nabla^4 v_1 \tag{E.7}$$

$$\frac{\lambda}{Pr_2}\nabla^2 v_2 = -k^2 \frac{Ra_2}{\beta}\theta_2 + \frac{1}{\nu}\nabla^4 v_2 \tag{E.8}$$

$$\lambda \theta_1 = -v_1 \Lambda_1 + \nabla^2 \theta_1 \tag{E.9}$$

$$\lambda\theta_2 = -v_2\Lambda_2 + \frac{1}{\kappa_T}\nabla^2\theta_2 \tag{E.10}$$

Equations (E.9) and (E.10) are multiplied by $\kappa\bar{\theta}_1$ and $\kappa_T\bar{\theta}_2$ respectively. The addition of complex conjugate of the resultant equations gives

$$\begin{aligned}\bar{\lambda}\left[\int_0^I \kappa|\theta_1|^2dy + \int_I^1 \kappa_T|\theta_2|^2dy\right] &= \int_0^I \kappa\theta_1\nabla^2\bar{\theta}_1dy + \int_I^1 \kappa_T\theta_2\nabla^2\bar{\theta}_2dy \\ &\quad - \int_0^I \Lambda_2\bar{v}_1\theta_1 - \int_I^1 \kappa_T\Lambda_2\bar{v}_2\theta_2\end{aligned} \tag{E.11}$$

Equations (E.7) and (E.8) are multiplied by $\Lambda_2\bar{v}_1$ and $\kappa_T\Lambda_2\bar{v}_2$ respectively to eliminate the cross products like $\bar{v}_1\theta_1$ and $\bar{v}_2\theta_2$ from the momentum and energy equations.

Thus, the final form of the modified governing equation is given as

$$\begin{aligned}&\bar{\lambda}\left[\int_0^I \kappa|\theta_1|^2dy + \int_I^1 \kappa_T|\theta_2|^2dy\right] \\ &+ \frac{\Lambda_2}{k^2Ra_2}\frac{\lambda}{Pr_2}\left[\int_0^I \left(k^2|v_1|^2 + \left|\frac{\partial v_1}{\partial y}\right|^2\right)dy + \beta\kappa_T\int_I^1 \left(k^2|v_2|^2 + |\frac{\partial v_2}{\partial y}|^2\right)dy\right] = \\ &- \kappa\int_0^I \left(k^2|\theta_1|^2 + \left|\frac{\partial\theta_1}{\partial y}\right|^2\right)dy - \int_I^1 \left(k^2|\theta_2|^2] + \left|\frac{\partial\theta_2}{\partial y}\right|^2\right) \\ &- \frac{\Lambda_2}{k^2Ra_2}\left[\int_0^I |\nabla^2 v_1|^2dy + \int_I^1 \frac{\beta\kappa_T}{\nu}|\nabla^2 v_1|^2\right] + \frac{\Lambda_2}{k^2Ra_2}(\rho\beta\kappa_T - 1)\frac{\partial\bar{v}_1}{\partial y}\frac{\partial^2 v_1}{\partial y^2}\Big|_{y=I} \\ &+ \Lambda_2\rho\beta\kappa_T\Upsilon\theta_1\frac{\partial\bar{v}_1}{\partial y}\Big|_{y=I}\end{aligned} \tag{E.12}$$

The boundary value terms arise from integration by parts with respect to y with conditions $v_1 = v_2 = 0$ (non-deformable interface), $\frac{\partial v_1}{\partial y} = \frac{\partial v_2}{\partial y}$ (derived from continuity of velocity), $\frac{\partial^2 v_1}{\partial y^2} = \frac{1}{\eta}\frac{\partial^2 v_2}{\partial y^2} + k^2Ma\theta_1$ (continuity of shear stress), and $\kappa\frac{\partial\theta_1}{\partial y} = \frac{\partial\theta_2}{\partial y}$ (continuity of heat flux) at the interface.

References

[1] Abels, H., Garcke, H., and Grun, G. (2012). Thermodynamically consistent, frame indifferent diffuse interface models for incompressible two-phase flows with different densities. *Mathematical Models and Methods in Applied Sciences*, 22(03):1150013.

[2] Alt, H. W. and Pawlow, I. (1992). A mathematical model of dynamics of non-isothermal phase separation. *Physica D: Nonlinear Phenomena*, 59(4):389–416.

[3] Anderson, D. M., McFadden, G. B., and Wheeler, A. A. (1998). Diffuse-interface methods in fluid mechanics. *Annual Review of Fluid Mechanics*, 30(1):139–165.

[4] Anderson, D. M., McFadden, G. B., and Wheeler, A. A. (2000). A phase-field model of solidification with convection. *Physica D: Nonlinear Phenomena*, 135(1–2):175–194.

[5] Antanovskii, L. K. (1995). A phase field model of capillarity. *Physics of Fluids*, 7(4):747–753.

[6] Bénard, H. (1900). Les tourbillons cellulaires dans une nappe liquide. *Revue générale des Sciences pures et appliquées*, 11:1261–1271.

[7] Bestehorn, M., Sharma, D., Borcia, R., and Amiroudine, S. (2021). Faraday instability of binary miscible/immiscible fluids with phase field approach. *Physical Review Fluids*, 6.

[8] Besthorn, M., Sharma, D., R., B., and S., A. (2021). Faraday instability of binary miscible/immiscible fluids with phase field approach. *Physical Review Fluids*, 6:064002.

[9] Block, M. (1956). Surface tension as the cause of Bénard cells and surface deformation in a liquid film. *Nature*, 178:650–651.

[10] Borcia, R. and Bestehorn, M. (2003). Phase-field model for marangoni convection in liquid-gas systems with a deformable interface. *Phys. Rev. E*, 67:066307.

[11] Boyer, F. (2002). A theoretical and numerical model for the study of incompressible mixture flows. *Computers & Fluids*, 31:41–68.

[12] Brackbill, J., Kothe, D., and Zemach, C. (1992). A continuum method for modeling surface tension. *Journal of Computational Physics*, 100(2):335–354.

[13] Busse, F. (1981). On the aspect ratios of two-layer mantle convection. *Physics of the Earth and Planetary Interiors*, 24(4):320–324.

[14] Cahn, J. W. and Hilliard, J. E. (1958). Free energy of a nonuniform system. i. interfacial free energy. *The Journal of Chemical Physics*, 28(2):258–267.

[15] Celani, A., Mazzino, A., Muratore-Ginanneschi, P., and Vozella, L. (2009). Phase-field model for the rayleigh-taylor instability of immiscible fluids. *Journal of Fluid Mechanics*, 622:115–134.

[16] Colinet, P. and Legros, J. (1994). On the Hopf bifurcation occurring in the two-layer Rayleigh–Bénard convective instability. *Physics of Fluids*, 6:2631–2639.

[17] Daniel D. Joseph, Adam Huang, H. H. (1996). Non-solenoidal velocity effects and korteweg stresses in simple mixtures of incompressible liquids. *Physica D: Nonlinear Phenomena*, 97:104–125.

[18] Darwish, M. and Moukalled, F. (2006). Convective schemes for capturing interfaces of free-surface flows on unstructured grids. *Numerical Heat Transfer Part B-fundamentals - NUMER HEAT TRANSFER PT B-FUND*, 49.

[19] Degen, M., Colovas, P., and Andereck, C. (1998). Time-dependent patterns in the two-layer Rayleigh-Bénard system. *Physical Review E*, 57(6):6647.

[20] Ding, H., Spelt, P. D., and Shu, C. (2007). Diffuse interface model for incompressible two-phase flows with large density ratios. *Journal of Computational Physics*, 226(2):2078–2095.

[21] Diwakar, S., Das, S. K., and Sundararajan, T. (2009). A quadratic spline based interface (quasi) reconstruction algorithm for accurate tracking of two-phase flows. *Journal of Computational Physics*, 228(24):9107–9130.

[22] Diwakar, S., Tiwari, S., Das, S. K., and Sundararajan, T. (2014). Stability and resonant wave interactions of confined two-layer Rayleigh Bénard systems. *Journal of Fluid Mechanics*, 754:415–455.

[23] Diwakar, S. V., Zoueshtiagh, F., Amiroudine, S., and Narayanan, R. (2015). The faraday instability in miscible fluid systems. *Physics of Fluids*, 27(8):084111.

[24] Drazin, P. G. and Reid, W. H. (2004). *Hydrodynamic Stability*. Cambridge Mathematical Library. Cambridge University Press, 2 edition.

[25] Gada, V. and Sharma, A. (2011). On a novel dual-grid level-set method for two-phase flow simulation. *Numerical Heat Transfer*, Part B: Fundamentals:26–57.

[26] Gershuni, G. Z. and Zhukhovitskii, E. M. (1980). Instability of a system of horizontal layers of immiscible fluids heated from above. *Fluid Dynamics*, 15:816–822.

[27] Guo, Z. and Lin, P. (2015). A thermodynamically consistent phase-field model for two-phase flows with thermocapillary effects. *Journal of Fluid Mechanics*, 766:226–271.

[28] Heyns, J., Malan, A., Harms, T., and Oxtoby, O. (2013). Development of a compressive surface capturing formulation for modelling free-surface flow by using the volume-of-fluid approach. *International Journal for Numerical Methods in Fluids*, 71:788–804.

[29] Hirt, C. and Nichols, B. (1981). Volume of fluid (VOF) method for the dynamics of free boundaries. *Journal of Computational Physics*, 39(1):201–225.

[30] Inguva, V., Kenig, E., and Perot, J. (2022). A front-tracking method for two-phase flow simulation with no spurious currents. *Journal of Computational Physics*, 456:111006.

[31] Jacqmin, D. (1999). Calculation of two-phase navier–stokes flows using phase-field modeling. *Journal of Computational Physics*, 155(1):96–127.

[32] Johnson, D. and Narayanan, R. (1997). Geometric effects on convective coupling and interfacial structures in bilayer convection. *Physical Review E*, 56(5):5462–5472.

[33] Johnson, E. (1975). Liquid encapsulated floating zone melting of gaas. *Journal of Crystal Growth*, 30(2):249–256.

[34] Joseph, D. (1990). Fluid dynamics of two miscible liquids with diffusion and gradient stresses. Technical report, MINNESOTA UNIV MINNEAPOLIS DEPT OF AEROSPACE ENGINEERING AND MECHANICS.

[35] Juric, D. and Tryggvason, G. (1995). A front-tracking method for liquid-vapor phase change. *In Advances in Numerical Modeling of Free Surface and Interfacial Fluid Dynamics, ed. PE Raad, TT Huang, G Tryggvason*, 234:141–48.

[36] Juric, D. and Tryggvason, G. (1996). Direct numerical simulations of flows with phase change. *In Proceedings of the 34th Aerospace Sciences Meeting and Exhibit. Reno: American Institute of Aeronautics and Astronautics*, AIAA 96-0857.

[37] Juric, D. and Tryggvason, G. (1998). Computations of boiling flows. *International Journal of Multiphase Flow*, 24:387–410.

[38] López, J., Hernández, J., Gómez, P., and Faura, F. (2004). A volume of fluid method based on multidimensional advection and spline interface reconstruction. *Journal of Computational Physics*, 195(2):718–742.

[39] Lowengrub, J. and Truskinovsky, L. (1998). Quasi-incompressible cahn-hilliard fluids and topological transitions. *Proceedings of the Royal Society of London. Series A: Mathematical, Physical and Engineering Sciences*, 454(1978):2617–2654.

[40] Mirjalili, S., Ivey, C. B., and Mani, A. (2019). Comparison between the diffuse interface and volume of fluid methods for simulating two-phase flows. *International Journal of Multiphase Flow*, 116:221–238.

[41] Muzaferija, S. (1998). A two-fluid navier-stokes solver to simulate water entry. *Proceedings of the 22nd symposium on naval hydrodynamics, Washington, DC, 1998*.

[42] Nepomnyashchy, A. and Simanovskii, I. (2004). Influence of thermocapillary effect and interfacial heat release on convective oscillations in a two-layer system. *Physics of Fluids*, 16:1127–1139.

[43] Nield, D. (1964). Surface tension and buoyancy effects in cellular convection. *Journal of Fluid Mechanics*, 19(341):60.

[44] Nobari, M. R., Jan, Y.-J., and Tryggvason, G. (1996). Head-on collision of drops–a numerical investigation. *Physics of Fluids*, 8:29–42.

[45] Noh, W. and Woodward, P. (1976). SLIC (simple line interface calculation). In *Proceedings of the Fifth International Conference on Numerical Methods in Fluid Dynamics June 28–July 2, 1976 Twente University, Enschede*, pages 330–340. Springer.

[46] Osher, S. and Fedkiw, R. P. (2001). Level set methods: An overview and some recent results. *Journal of Computational Physics*, 169(2):463–502.

[47] Osher, S. and Sethian, J. (1988). Fronts propagating with curvature-dependent speed: algorithms based on Hamilton-Jacobi formulations. *Journal of Computational Physics*, 79:12–49.

[48] Pearson, J. (1958). On convection cells induced by surface tension. *Journal of Fluid Mechanics*, 4(05):489–500.

[49] Penrose, O. and Fife, P. C. (1990). Thermodynamically consistent models of phase-field type for the kinetic of phase transitions. *Physica D: Nonlinear Phenomena*, 43(1):44–62.

[50] Prosperetti, A. and Tryggvason, G. (2007). *Computational Methods for Multiphase Flow*. Cambridge University Press.

[51] Puckett, E., Almgren, A., Bell, J., Marcus, D., and Rider, W. (1997). A high-order projection method for tracking fluid interfaces in variable density incompressible flows. *Journal of Computational Physics*, 130(2):269–282.

[52] Rasenat, S., Busse, F., and Rehberg, I. (1989). A theoretical and experimental study of double-layer convection. *Journal of Fluid Mechanics*, 199:519–540.

[53] Rayleigh, L. (1916). On convection currents in a horizontal layer of fluid, when the higher temperature is on the under side. *Philosophical Magazine Series 6*, 32(192):529–546.

[54] Renardy, Y. (1996). Pattern formation for oscillatory bulk-mode competition in a two-layer Bénard problem. *Zeitschrift für Angewandte Mathematik und Physik (ZAMP)*, 47(4):567–590.

[55] Renardy, Y. and Joseph, D. (1985). Oscillatory instability in a Bénard problem of two fluids. *Physics of Fluids*, 28(3):788–793.

[56] Renardy, Y. and Renardy, M. (1985). Perturbation analysis of steady and oscillatory onset in a Bénard problem with two similar liquids. *Physics of Fluids*, 28:2699–2708.

[57] Renardy, Y. and Renardy, M. (2002). PROST: a parabolic reconstruction of surface tension for the volume-of-fluid method. *Journal of Computational Physics*, 183(2):400–421.

[58] Rowlinson, J. S. (1979). Translation of j. d. van der waals' "the thermodynamik theory of capillarity under the hypothesis of a continuous variation of density". *Journal of Statistical Physics*, 20:197–200.

[59] R.S., L. R. S. (1892). Xx. on the theory of surface forces.—ii. compressible fluids. *The London, Edinburgh, and Dublin Philosophical Magazine and Journal of Science*, 33(201):209–220.

[60] Scriven, L. and Sternling, C. (1964). On cellular convection driven by surface-tension gradients: effects of mean surface tension and surface viscosity. *Journal of Fluid Mechanics*, 19(03):321–340.

[61] Sethian, J. A. and Smereka, P. (2003). Level set methods for fluid interfaces. *Annual Review of Fluid Mechanics*, 35(1):341–372.

[62] Simanovskii, I. and Nepomnyashchy, A. (2006). Nonlinear development of oscillatory instability in a two-layer system under the combined action of buoyancy and thermocapillary effect. *Journal of Fluid Mechanics*, 555:177–202.

[63] Smith, K. A. (1966). On convective instability induced by surface-tension gradients. *Journal of Fluid Mechanics*, 24(2):401–414.

[64] Son, G. (2001). A numerical method for bubble motion with phase change. *Numerical Heat Transfer, Part B: Fundamentals*, 39(5):509–523.

[65] Spiegel, E. A. and Veronis, G. (1960). On the Boussinesq Approximation for a Compressible Fluid. *Astrophysical Journal*, 131:442.

[66] Sussman, M., Smereka, P., and Osher, S. (1994). A level set approach for computing solutions to incompressible two-phase flow. *Journal of Computational Physics*, 114(1):146–159.

[67] Tee, T. W. and Trefethen, L. N. (2006). A rational spectral collocation method with adaptively transformed chebyshev grid points. *SIAM Journal on Scientific Computing*, 28(5):1798–1811.

[68] Ubbink, O. and Issa, R. (1999). A method for capturing sharp fluid interfaces on arbitrary meshes. *Journal of Computational Physics*, 153(1):26–50.

[69] Unverdi, S. and G., T. (1992). A front-tracking method for viscous, incompressible, multi-fluid flows. *Journal of Computational Physics*, 100:25–37.

[70] Walters, D. and Wolgemuth, N. (2009). A new interface-capturing discretization scheme for numerical solution of the volume fraction equation in two-phase flows. *International Journal for Numerical Methods in Fluids*, 60:893 – 918.

[71] Welch, J. E., Harlow, F. H., Shannon, J. P., and Daly, B. J. (1965). The MAC method: A computing technique for solving viscous, incompressible, transient fluid-flow problems involving free surfaces. Technical report, Los Alamos National Laboratory.

[72] Wen, B., Goluskin, D., LeDuc, M., Chini, G. P., and Doering, C. R. (2020). Steady rayleigh–bénard convection between stress-free boundaries. *Journal of Fluid Mechanics*, 905:R4.

[73] Wheeler, A. A. and McFadden, G. B. (1997). On the notion of a ξ-vector and a stress tensor for a general class of anisotropic diffuse interface models. *Proceedings of the Royal Society of London. Series A: Mathematical, Physical and Engineering Sciences*, 453(1963):1611–1630.

[74] Youngs, D. (1982). Time-dependent multi-material flow with large fluid distortion. *Numerical Methods for Fluid Dynamics*, 24:273–285.

[75] YUE, P., FENG, J. J., LIU, C., and SHEN, J. (2004). A diffuse-interface method for simulating two-phase flows of complex fluids. *Journal of Fluid Mechanics*, 515:293–317.